UNIVERSITÉ DE MONTRÉAL

NUMERICAL ELECTROMAGNETIC MODELING OF HTS POWER TRANSMISSION
CABLES

MAJID SIAHRANG
DÉPARTEMENT DE GÉNIE ÉLECTRIQUE
ÉCOLE POLYTECHNIQUE DE MONTRÉAL

THÈSE PRÉSENTÉE EN VUE DE L'OBTENTION
DU DIPLÔME DE PHILOSOPHIÆ DOCTOR
(GÉNIE ÉLECTRIQUE)
DÉCEMBRE 2011

UNIVERSITÉ DE MONTRÉAL

ÉCOLE POLYTECHNIQUE DE MONTRÉAL

Cette thèse intitulée :

NUMERICAL ELECTROMAGNETIC MODELING OF HTS POWER TRANSMISSION
CABLES

présentée par : SIAHRANG, Majid
en vue de l'obtention du diplôme de : Philosophiæ Doctor
a été dûment acceptée par le jury d'examen constitué de :

M. LAURIN, Jean-Jacques, Ph.D., président.
M. SIROIS, Frédéric, Ph.D., membre et directeur de recherche.
M. MÉNARD, David, Ph.D., membre.
M. STENVALL, Antti, Ph.D., membre externe.

To my parents and my sweet sisters,
with love and gratitude. . .

ACKNOWLEDGMENTS

RÉSUMÉ

Cette thèse de doctorat est divisée en deux parties. L'objectif de la première partie était de développer un modèle numérique rapide et précis pour résoudre le problème électromagnétique de conducteurs en ruban bobinés de façon hélicoïdale. Cette méthode peut être utilisée pour trouver la distribution de courant et les pertes AC dans des applications utilisant des matériaux supraconducteurs à haute température critique (HTS) destinés aux réseaux électriques. Dans la seconde partie du projet, le modèle développé est utilisé pour réaliser des analyses paramétriques du comportement des pertes AC pour un agencement de rubans de HTS disposés sur une même couche, pour différents paramétres de conception. Le principal objectif de ces études était de minimiser les pertes AC en trouvant les paramètres optimaux pour divers agencements de rubans.

Dans la production récente de câbles de puissance HTS, les "coated tapes" sont les conducteurs privilégiés. L'épaisseur de la couche supra est d'environ 1 à 2 μm. Selon l'application, sa largeur varie de 4 à 12 mm. Dans la conception de câbles, ces rubans sont bobinés de façon hélicoïdale en simple couche ou couches multiples, sur une forme (support) cylindrique central. La géométrie complexe des rubans ainsi que la non-linéarité de la résistivité de la couche supraconductrice rendent difficiles la résolution de ce problème électromagnétique.

Dans la première partie de cette thèse, nous avons introduit une méthode numérique pour calculer la distribution du courant et du champ dans des conducteurs minces bobinés hélicoïdalement lorsqu'un ou plusieurs de ces conducteurs sont assemblés de façon symètrique. D'après les considérations symétriques associées à la géométrie du problème, et en négligeant l'épaisseur des rubans, le vrai problème 3-D peut être réduit en un problème 1-D dont le domaine se situe sur l'axe central situé à la mi-épaisseur des rubans (suivant la largeur) constituant le câble. La version basse fréquence de l'équation des courant de Foucault est discrétisée dans le domaine réduit d'étude. Pour établir une relation directe entre la densité de courant et le vecteur potentiel dans la formulation du problème, la solution de l'intégrale de Biot-Savart est utilisée pour trouver le vecteur potentiel magnétique dans les couches de courant.

En considérant la vraie géométrie 3-D des rubans dans la formulation du problème, le modèle proposé devient bien plus précis que la plupart des méthodes 2-D qui ne prennent pas en compte la configuration hélicoïdale des rubans. Par ailleurs, grâce à la symétrie utilisée pour réduire le domaine d'étude, la méthode développée est très efficace en terme de temps de calcul. Afin de vérifier la validité de la méthode proposée, nous avons réalisé des mesures expérimentales de pertes AC dans des échantillons YBCO. Les résultats trouvés concordent

parfaitement avec ceux trouvés en simulation. Dans le cas d'un conducteur prototype à une couche et bobiné de façon solénoïdale, les résultats trouvés concordent parfaitement avec ceux trouvés en simulation.

Dans la seconde partie de cette thèse, nous avons utilisé la technique numérique développée dans la partie précédente pour étudier le comportement des pertes AC de câbles HTS à couche unique. Tel que prévu par les études antérieures, les simulations ont montré que les principales causes de pertes dans ces câbles proviennent de la présence séparations ("gaps") entre rubans adjacents. Ces petits séparations perturbent la distribution du champ près des bords des rubans de sorte que dans ces régions le champ magnétique auquel les rubans sont soumis présente une importante composante orthogonale à la surface des rubans. Avec des séparations plus petits, les câbles présentent moins de pertes AC. Toutefois, à cause de considérations mécaniques inévitables, il existe toujours une séparation minimale.

Afin de réduire l'effet des séparation nous avons étudié le comportement AC de trois conceptions de câbles à couche unique, dans lesquelles les séparation sont recouverts par un chevauchement des rubans adjacents en insérant des rubans étroits en-dessous des rubans principaux. Les résultats des simulations montrent que ces concepts sont très efficace dans la réduction des pertes AC des câbles HTS de puissance.

ABSTRACT

This Ph.D. thesis consists of two successive phases. The objective of the first phase was to develop a fast and accurate numerical model to solve the electromagnetic problem of helically wound thin tape conductors. This method must be applicable to find current distribution and AC losses in High Temperature Superconducting (HTS) power transmission cables made of coated tapes. In the second phase of the project, the developed model was used to perform parametric analysis of the AC loss behavior of single layer HTS cables with different design schemes and design parameters. The main objective of this phase was focused on the minimization of AC losses in HTS cables either by searching for optimal designs parameters or alternative design schemes.

In the latest generation of HTS power cables, superconducting coated tapes are the conductors of choice. The thickness of the superconducting layer of these tapes is around 1 to 2 μm, and depending on the application, their width varies from 4 to 12 mm. In the cable design, such tapes are helically wound around cylindrical formers in single or multi-layer arrangements. The complicated geometry of the tapes as well as the non-linear resistivity of their superconducting layer make the accurate solution of the electromagnetic problem of HTS cables quite challenging.

During the first phase of this thesis, we introduced a numerical method to compute current and field distribution in helically wound thin tape conductors when one or many of them are arranged in a symmetrical manner. According to the symmetry arguments associated with the geometry of the problem, and neglecting the thickness of the tapes, the real 3-D problem of helically wound tapes could be reduced to a computationally small 1-D problem whose domain lies along the half-width of any of the constituting tapes. The low frequency version of the eddy current equation, as the governing equation of the problem, is discretized over this reduced dimension study domain. To establish a direct relationship between the current density and the vector potential in the problem formulation, the solution of the Biot-Savart integral to find the magnetic vector potential of helically wound current sheets is used.

As a consequence of considering the real 3-D geometry of the tapes in problem formulation, the proposed model is more accurate than many previous 2-D methods that cannot take into account the helical configuration of the tapes. On the other hand, because of using symmetry arguments to reduce the size of the study domain, the method is very efficient in terms of computational time. To verify the validity of the proposed method, we performed experimental measurements of AC losses in solenoid-type cables made of a sample of YBCO-coated conductor tape. Excellent agreement was observed between the experimental data

and the simulation results.

In the second phase of this thesis work, we used the numerical technique developed in the previous phase to study the AC loss behavior of single layer HTS cables. In accordance with previous studies, simulation results revealed that, the main loss mechanism in these cables arises from the presence of gaps between the adjacent tapes. These small gaps disturb the field distribution near the edges of the tapes so that in these region the magnetic field experienced by the tapes has large components perpendicular to the wide face of the tapes. With smaller gaps, cables show lower AC losses. But due to inevitable mechanical considerations, there is always a minimum limit for the gap size.

Aimed at undermining the gap effects, we investigated the AC loss behavior of three different design schemes for single layer HTS cables, in which the gap regions are covered by the overlap of the adjacent tapes or by inserting narrow tapes below the main tapes. Simulation results showed that these designs are quite effective in reducing AC losses of HTS power cables.

CONTENTS

xii

LIST OF TABLES

LIST OF FIGURES

LIST OF APPENDIXES

LIST OF ACRONYMS AND ABBREVIATIONS

HTS   High Temperature Superconductor (or Superconducting)

YBCO   Yttrium Barium Copper Oxide

SMES   Superconducting Magnetic Energy storage

SFCL   Superconducting Fault Current Limiter

IBAD   Ion Beam Assisted Deposition

RABiT   Rolling Assisted Biaxially Textured Substrates

FEM   Finite Elements Method

IM   Integral Method

MMEV   Minimum Magnetic Energy Variation

CHAPTER 1

INTRODUCTION

High temperature superconducting (HTS) power transmission cables are one of the most promising applications of superconductivity, which have potentials to be the power transmission technology of choice in some commercial applications. Reduced losses, reduced dimensions and weight, and increased environmental compatibility are the major advantages of the HTS cables over their conventional counterparts.

Despite their advantages, there are some standing obstacles in the way of the industrial usage of HTS power cables. Similar to other superconducting-based technologies, the capital cost of HTS cables is still higher than that of comparable conventional cables and transmission lines. Apart from the high cost of manufacturing HTS wires, the need for efficient and large scale cryogenic systems, which are essential to provide the low working temperature of superconductors, contributes to the high cost of superconducting-based equipment.

In AC applications, the conductivity of superconductors are not perfect and they exhibit a (very small) resistivity to AC currents. This resistivity causes losses which are called AC losses. In the HTS cables, the cryogenic system must work all along the cable length to keep the temperature of the HTS wires below the boiling temperature of liquid Nitrogen, i.e 77 K. To avoid temperature rise, any amount of heat produced inside the cable chamber must be disposed. Because of the large difference between the conductors temperature and ambient temperature, such a heat removal task causes costly loads for the cable cryogenic system.

AC losses are the main heat source inside the cable chamber. Thus, reducing these losses results in load reduction for the cryogenic system of HTS cables. In addition, with lower AC loss levels, the complexity of the cable cryogenic system can be relieved. Therefore, reduction of AC losses is an important issue to reduce the capital and the operational costs of HTS power cables.

The AC loss minimization in HTS cables, requires a comprehensive understanding of the electromagnetic behavior of HTS conductors in cable configurations. In the latest generation of HTS power cables, HTS coated tapes are the conductors of choice. The thickness of the superconducting layer of this generation of HTS tapes is in order of a few micrometer. In cable applications, such thin conductors are helically wound in single or multi-layer arrangements. The complicated twisted geometry of the tapes, and on the other hand, the highly non-linear resistivity of their HTS layers make the AC loss analysis of HTS cables a challenging problem.

Developing a numerical model to find field and current distribution and AC losses inside

the tapes of single layer HTS cables is the main objective of this thesis. In this thesis work, the developed model is used to perform parametric analysis on the AC loss behavior of single layer cables designed with different parameters and design schemes.

This thesis is presented with the help of the journal articles we have published on the subject. In this case, these articles are inserted as chapters in the body of thesis. The organization of the chapters is as follows :

Chapter 1 starts with a brief introduction to the main concepts of superconductivity from a phenomenological point of view. In the second section of this chapter, the main applications of superconductivity in power systems are briefly introduced. Since the main subject of this thesis is dealing with HTS power cables, they are discussed in more details. The last section of this chapter deals with AC losses in HTS power cables. In that section, previous work on modeling AC losses in HTS cables are reviewed and alternative design schemes proposed to reduce the AC losses in HTS cables made of coated tapes are introduced.

In Chapter 3, the hypothesis and the selected methodology to achieve the objectives of the research work are explained. The numerical computation of current distribution and AC losses in single-layer HTS power cables made of helically wound coated conductors is the objective of the irst phase. Full details about the proposed method including its hypothetical and methodological developments and the results are of its validation through experiments are provided in Chapter 4.

The objective of the second phase of this thesis (which is defined in Chapter 3) is the assessment of the effectiveness of the proposed design schemes (introduced in Chapter 2) in reducing AC losses of HTS cables. To do achieve this objective, the numerical model developed in the first phase of the project is used to perform extensive parametric studies on the AC loss behavior of these new designs. The details of this study were published in articles which are inserted as Chapter 5 and Chapter 6.

In Chapter 7 the general objectives of the thesis are briefly discussed and some potential research objectives are suggested as future work on the subject. Finally, in Chapter 8 the results of the work are summarized as conclusions.

It is worth mentioning that, all along this thesis and in the attached articles, the term HTS power cables refers to the HTS power cables made of coated conductors.

CHAPTER 2

BASIC CONCEPTS AND LITERATURE REVIEW

2.1 Superconductivity

Similar to many other discoveries in human history, the discovery of superconductivity was a fortuitous result of an unexpected observation in a series of laboratory test. In 1911, a Dutch physicist named *Heike Kamerlingh Onnes* tried to measure the electric resistivity of a sample of mercury against DC currents at very low temperatures near the absolute zero. Performing such an experiment was possible by virtue of the success he had achieved three years earlier in liquefying helium, which allowed him to reach temperatures as low as 1 K [1].

The motivation behind this experiment was to examine two theories that existed at the time for the resistivity of conductors at very low temperatures. By then, some scientists believed that when the temperature is decreased, the resistivity of conductors must decrease and tends to a minimum value caused by the presence of imperfections and impurities in their lattice. On the other hand, according to the picture that everything, including carrier electrons, will be frozen at sufficiently low temperatures, many other physicists expected that any conductor must become an insulator at sufficiently low temperatures.

Surprisingly, Onnes's observations rejected both of these predictions. What he observed was the sudden collapse of the resistivity of the sample to immeasurable levels while the temperature was below 4.2 K [1, 2]. He named this surprising behavior superconductivity. In the years to follow, Onnes and others observed the similar behavior in some other elements and it became clear that superconductivity is a state of matter that occurs at low temperatures in most metallic elements.

2.1.1 Perfect conductivity

Figure 2.1.1 shows the DC resistivity of typical superconductors as a function of temperature. As presented in this figure, below a sufficiently low temperature, the resistivity of superconductors abruptly disappears. The temperature at which the transition to superconducting state occurs is called the *critical temperature* or *transient temperature* and is referred to as T_c. The critical temperature is an inherent characteristic of the material and varies from one material to the other. Niobium (Nb) with a T_c of 9.3 K has the highest critical temperature among the elements.

Almost one year after the discovery of superconductivity, Onnes observed that, T_c is a
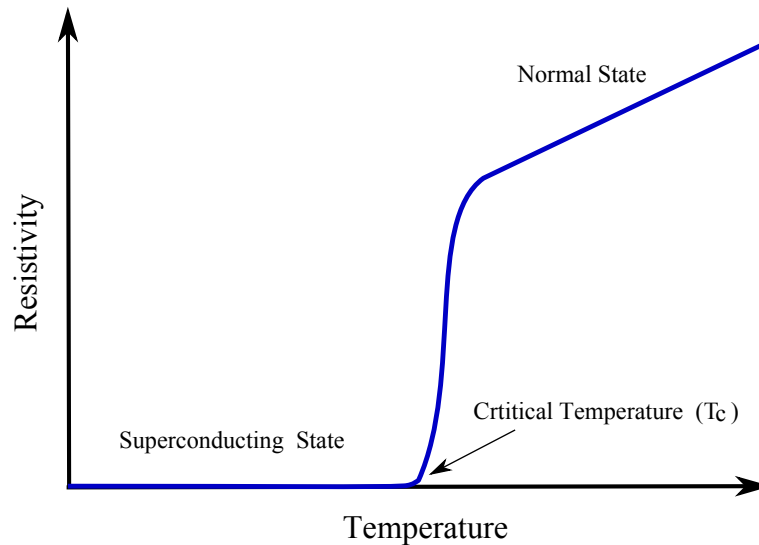
Figure 2.1 The resistivity of a typical superconductor as a function of its temperature. Below a sufficiently low temperature, i.e. T_c, transition to the superconducting state occurs. In the superconducting state the resistivity of the superconductor is such a low that cannot be measured even with most sensitive ohmmeters.

function of the experienced magnetic field by the sample, so that with stronger magnetic fields, it must be kept below a lower temperature to retain the zero resistivity. This magnetic field can be either externally applied to the superconductor or can be the self-field produced by its own current. The latter implies that being in the superconducting state is also a function of the current flowing in the superconductor, i.e. its transport current.

Figure 2.2 represents the boundaries of the superconducting state for a typical superconducting material as function of its temperature, experienced magnetic field and density of the transport current. The magnetic field above which superconductors go back to the normal state is referred to as the *critical field* (H_c), and in a similar way the current density at which the same thing happens is termed the *critical current density* (J_c).

2.1.2 Magnetic behavior of superconductors

In 1930, namely nineteen years after the discovery of superconductivity, *Meissner* and *Ochenfeld* discovered that, in the superconducting state superconductors prevent magnetic flux from penetrating inside them [3]. In other words, superconductors expel out magnetic flux due to any externally applied magnetic field not stronger than their H_c. This effect is called the *Meissner effect* and implies that superconductivity is not only perfect conductivity but also perfect diamagnetism.

Today we know that, perfect diamagnetism is not necessarily a feature of all superconduc-
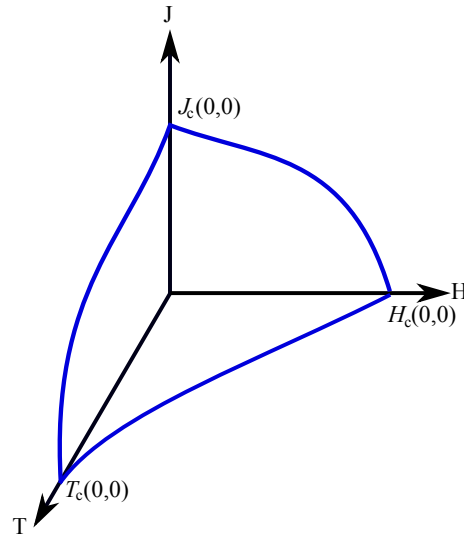
Figure 2.2 Boundaries of the superconducting state which are function of temperature, applied magnetic field and current density. T_c, H_c and J_c are inherent characteristics of the material and are mutually dependent.

tors. According to their behavior to applied magnetic fields, superconductors are classified into two types. Type-I superconductors exhibit perfect diamagnetism and zero resistivity as long as they are in the superconducting state. On the other hand, there exists type-II superconductors, which can still preserve their zero resistivity while magnetic flux is partially allowed to penetrate inside them.

For the superconductors of type-II, two critical fields are defined. As shown in figure 2.3, H_{c1} is the magnetic field below which a type-II superconductor is in the *Meissner state*, i.e. there is no magnetic flux inside it. H_{c2} corresponds to the magnetic field above which transition to the normal state state occurs. Between H_{c1} and H_{c2}, a type-II superconductor is in the mixed state, in which it exhibits perfect conductivity, but only partial diamagnetism.

2.1.3 Theory of superconductivity

Since the discovery of superconductivity, many brilliant physicist have devoted their career to explain and theorize this phenomenon. So far 20 Nobel prizes have been awarded for these efforts. Nevertheless, superconductivity is not yet fully understood and it seems that more Nobel prizes should be on the way until its complete understanding. In this section, in a very brief way, three useful theories proposed to explain superconductivity are introduced.
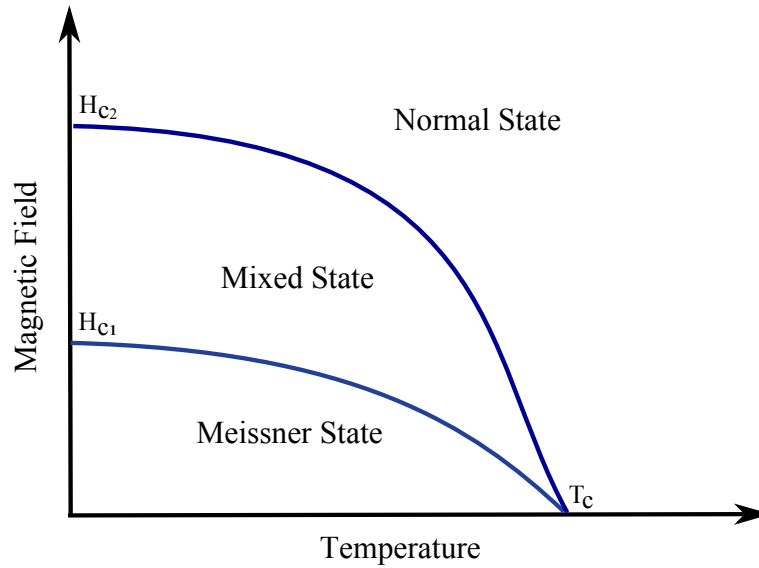
Figure 2.3 Critical fields of type-II superconductors as a function of temperature. Below H_{c1}, superconductors are in the Meissner state at which they exhibit both prefect conductivity and perfect diamagnetism. Above H_{c1} and below H_{c2}, a type-II superconductor is in the mixed state. In the mixed state, the magnetic field partially penetrates inside the superconductor, while it still preserves the property of perfect conductivity.

London theory

In 1934, by proposing a complementary constraint to the Maxwell equations, the *London* brothers developed a mathematical model for diamagnetic properties of superconductors [4]. In their theory, which is called the *London theory*, in a quite empirical way it is assumed that there is a linear relationship between the vectors of the magnetic flux density and its laplacian inside superconductors, i.e. $\nabla^2 B \propto B$. This simple assumption mathematically models that magnetic flux cannot penetrate deeper than a short depth inside superconductors. There is no formal proof for the London theory, and it was accepted because it could model the Meissner effect in superconductors.

Ginzburg-Landau theory

One of the most useful theories proposed to examine the macroscopic properties of super-conductivity is the Ginzburg-Landau theory [5]. In this theory based on quantum mechanics and classical thermodynamic arguments, the behavior of the superconducting electrons is explained by an effective wave function.

One of the useful aspect of the Ginzburg-Landau theory is the way that it explains the field penetration inside type-II superconductors. According to this theory, in the mixed state,

field penetration occurs by forming quantized and symmetrically distributed flux tubes, called *vortex*, inside type-II superconductors. Collection of the vortices inside the superconductors forms a vortex lattice, where the vortices are aligned with the applied magnetic field.

BCS theory

In 1957, *Bardeen*, *Cooper* and *Schrieffer* formulated the general microscopic theory of superconductivity [6]. This theory, which is based on quantum mechanics, is called the BCS theory. According to this theory, below the transient temperature, superconductors experience a phase transition and each of their free electrons gets coupled with another electron forming electron pairs, also called Cooper pairs. Cooper pairs can flow through superconductor without collisions, and therefore current can flow without any dissipation. Based on the available theories the emitted elastic waves by the crystal lattice are responsible for the attractive force between the electrons of a Cooper pair (called *binding force*). The binding force is weak and thermal energy of the electrons can easily break Cooper pairs. Therefore, superconductivity is observed at low temperature where the thermal energy of the electrons is not sufficient enough to break Cooper pairs. The binding force can be also overcome by the interaction between the electrons and strong enough magnetic fields, and this is the reason that above H_c, a transition to the normal state occurs.

2.1.4 The critical state model and the power law model

The resistivity of normal conductors at a given temperature is almost a constant defined by the Ohm's law as the slope of their $E - J$ characteristic. In the case of superconductors, the resistivity is highly non-linear and is a function of the current density and the applied magnetic field.

The simplest way to model $E - J$ characteristic of superconductors is the *Bean* model [7, 8](see figure 2.4). In this model, which is also referred to as the *critical state model* (CSM), it is assumed that the magnitude of the current density inside a superconductor is either zero or equal to its critical current density, i.e. J_c. In this model, the critical current density is assumed to be independent of the applied magnetic field. Figure 2.4 shows the E-J characteristic according to the Bean model.

Despite its simplicity, the CSM is accurate enough to represent the nonlinear resistivity of superconductors with sharp transition to normal state, as is the case with low T_c superconductors. But In the case of high T_c superconductors, which exhibit a smoother transition between the normal and the superconducting state, CSM can just provide a rough picture of the $E - J$ characteristic. Based on the experimental measurements, the $E - J$ characteristic
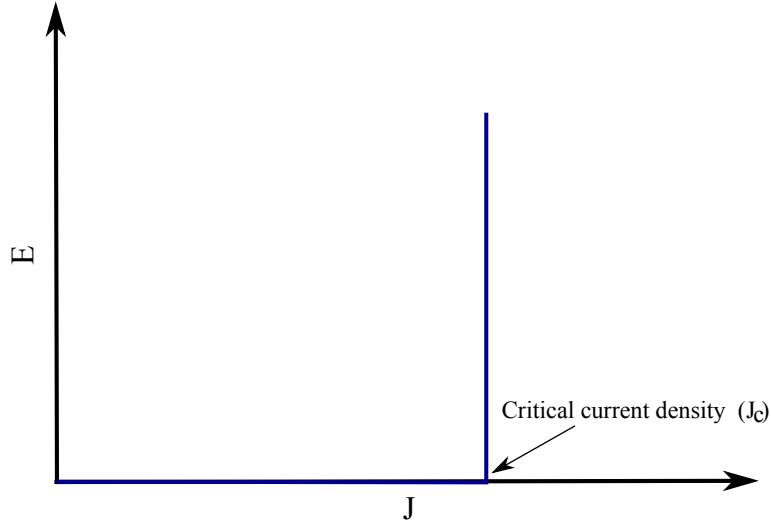
Figure 2.4 The $E - J$ characteristic corresponding to the Bean model, also called critical state model (CSM)

of this class of superconductors is similar to what is presented in figure 2.1.4. Comparing the $E - J$ characteristic shown in figure 2.1.4 with one presented in figure 2.4, it is observed that, as opposed to the CSM, J_c is not a well defined parameter anymore. Normally, J_c is defined as the current density at which an electric field of 0.1 mV/m appears across the superconductor. Therefore, E_o in figure 2.1.4, which is referred to as the electric field criterion (or sometimes the critical electric field) is 0.1 mV/m, and the current density at which this electric field is measured is defined as the critical current density of the superconductor (J_c).

This $E - J$ characteristic can be fitted by a classical power law function, i.e.

$$E = aJ^n \tag{2.1}$$

where, a and n are power law parameters which are used to model the $E - J$ characteristic obtained by experiments.

Equation (2.1) can be expressed in the classic form of the constitutive equation relating E and J, i.e. $E = \rho J$ as

$$E = a \left| J \right|^{n-1} J \tag{2.2}$$

Commonly, (2.2) is expressed as

$$E = \frac{E_c}{J_c} \left| \frac{J}{J_c} \right|^{n-1} J \tag{2.3}$$

From (2.3), the specific resistivity of a superconductors is mathematically defined as
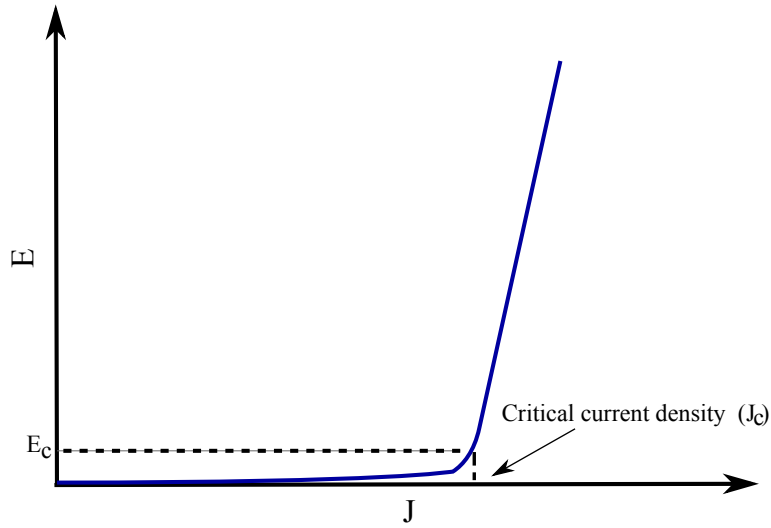
Figure 2.5 The $E-J$ characteristic of high T_c superconductors. This curve is sketched to show the measured voltage drop across superconducting samples when a DC current is imposed.

$$\rho = \frac{E_c}{J_c}\left|\frac{J}{J_c}\right|^{n-1} \tag{2.4}$$

In fact, (2.4) represents the resistivity in a general form, i.e. depending on the value of n it can describe the resistivity of normal conductors ($n = 1$), the resistivity of high T_c superconductors ($30 < n < 50$), or the resistivity of low T_c superconductor ($n >> 50$)[9].

Using the power law model is a very common way to introduce the resistivity of superconductors in the numerical analysis of the electromagnetic behavior of superconductors. On the other hand, the CSM is easier to handle and is the preferred choice for the analytic approaches.

2.1.5   Dissipative mechanisms and AC losses

According to the Ginzburg-Landau theory, in the mixed state, magnetic fields partially penetrate into type-II superconductors in the form of regularly distributed quantized flux lines or vortices. The vortices formed by the self-field are generally perpendicular to the transport current. As a consequence of the interaction with the transport current, each vortex experiences a Lorentz force which is perpendicular to the transport current and vortex lattice. This force put the vortices in movement, which in turn results in energy losses.

The dissipation of vortices in motion is prevented by fixing the position of vortices through a mechanism called flux pinning. The pinning is done by creating some energetically favorable zones in the material by different techniques. As long as, the Lorentz force between the vortices

and the transport current is lower than the maximum pinning force, they do not move and no dissipation occurs.

Although the pinning force prevents the dissipation mechanism arising from the movement of vortices, it results in the irreversibility of the magnetic properties of type-II superconductors. As a results of this irreversibility, in the case of AC transport currents (and/or AC magnetic field), the vortex are redistributed each cycle in a different geometrical equilibrium. This redistribution takes energy from the field and/or current source and is a dissipative mechanism. The losses associated with the redistribution of vortices, due to the time variation of the applied field and/or the transport current, are called AC losses.

To establish a simple and intuitive insight into the AC losses in superconductors, here we use the Bean model to find the field and current profiles inside a superconducting slab due to an externally applied magnetic field. As sketched in figure 2.6, the slab dimensions in two directions (for instance, here y and z) are infinite. The applied magnetic field is uniform and parallel to the wide face of the slab along the y direction.

Figure 2.7 shows the current and field distributions along the thickness of the slab (along the x axis). To find the field and current profiles we start with Amper's law

$$\nabla \times H = J \tag{2.5}$$

For the case of the semi-infinite slab, H has only the y-directional component. Then, according to (2.5) and the limitation of values that J can hold (CSM), $\frac{dH_y}{dx}$ can only have values $-J_c$, 0 or J_c. Therefore, the H profile inside the slab is in the form of straight lines with the slope of $\pm J_c$.

When the applied magnetic field is zero, there is no field and current inside the slab. As the magnitude of the applied magnetic field starts to increase, screening currents are induced (near the edges) to prevent field penetration inside the slab (see figure 2.7(a)). As the magnitude of the applied field increases, the current will further penetrate until it reaches the middle of the slab. In this case, as shown in figure 2.7(b), the applied field is equal to the *penetration field* (H_p). In this situation, half of the slab carries $-J_c$ and the other half carries $+J_c$.

If the magnitude of the applied field is increased again, current distribution remains unchanged, but the field profile must shift up to satisfy both (2.5) and the continuity of the field at the side faces of the slab (see figure 2.7(c)).

At this point, if the magnitude of the applied filed starts to decreases, the induced currents near the edges of the slab will change of sign to oppose the field variation, while in the middle parts of the slab the current profile remains unchanged (see figure 2.7(d)).

As shown in figure 2.7(e), when the magnitude of the applied field is reduced to zero,

there are still induced currents and trapped field inside the slab. This indicates the history dependent behavior of the magnetization characteristic of superconductors (type-II). If we increase the magnitude of the applied field, this time in the opposite direction (i.e. $-y$), the reversed current profiles penetrate up to the center of the slab (figure 2.7(f)).

The shown magnetic behavior of the superconductors, which as mentioned is a consequence of vortex pinning, is responsible for the hysteretic AC losses in type-II superconductors.

2.1.6 High temperature superconductors

Until the middle of 1980's, superconductivity had been observed in most of metallic elements and their alloys. Among these metallic superconductors, MgB_2 with $T_c = 39$ K, has the record of the highest transient temperature [10]. This class of superconductors, has low critical temperatures, which can be achieved only in liquid helium (or in some cases with liquid hydrogen).

In 1986, superconductivity was observed in some ceramic materials at much higher temperatures, higher than the boiling temperature of liquid nitrogen (77 K). This class of materials, which are of type-II, are called High Temperature Superconductors (HTS). On the other hand, the class of materials whose T_c is lower than the critical temperature of liquid nitrogen are called Low Temperature Superconductors (LTS).

One of the major obstacles in the way of the practical applications of LTS material was (and still is) the expensive capital and operational costs associated with the cryogenic systems required to keep their temperature below T_c. The only choice for the coolant material for these class of superconductors was liquid helium. Apart from the fact that liquid helium is expensive in itself, the cost associated with helium-based cryogenic system is also very high. On the other hand, nitrogen is the most abundant element on earth and liquefying it is much easier than helium and can be done at quite lower expenses. Besides, since the boiling temperature of liquid nitrogen is more than 70 K closer to the ambient temperature than that of liquid helium, the capital and the operational cost of nitrogen-based cryogenic system are much lower (around 50 times) than those of helium-based systems [11]. Therefore, the discovery of HTS materials, whose high critical temperatures can be reached by liquid nitrogen, prompted the interest in practical application of superconductors and was a very important step towards the commercial applications of superconductivity.

In March 2011, *superconductors.org* reported the observation of superconductivity at $18°$ C in a copper oxide compound ($Tl_5Pb_2Ba_2MgCu_{10}O_{17+}$). This promising claim means that superconductivity is likely to exist at room temperature. Room temperature superconductors would not need to be kept cool down to low temperatures and this would remove
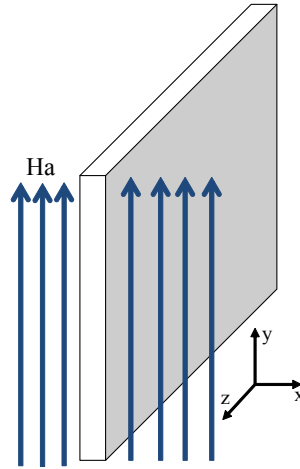
Figure 2.6 A semi-infinite slab subjected to a magnetic field parallel to its wide faces. The dimensions of the slab in the z and y directions are infinite.
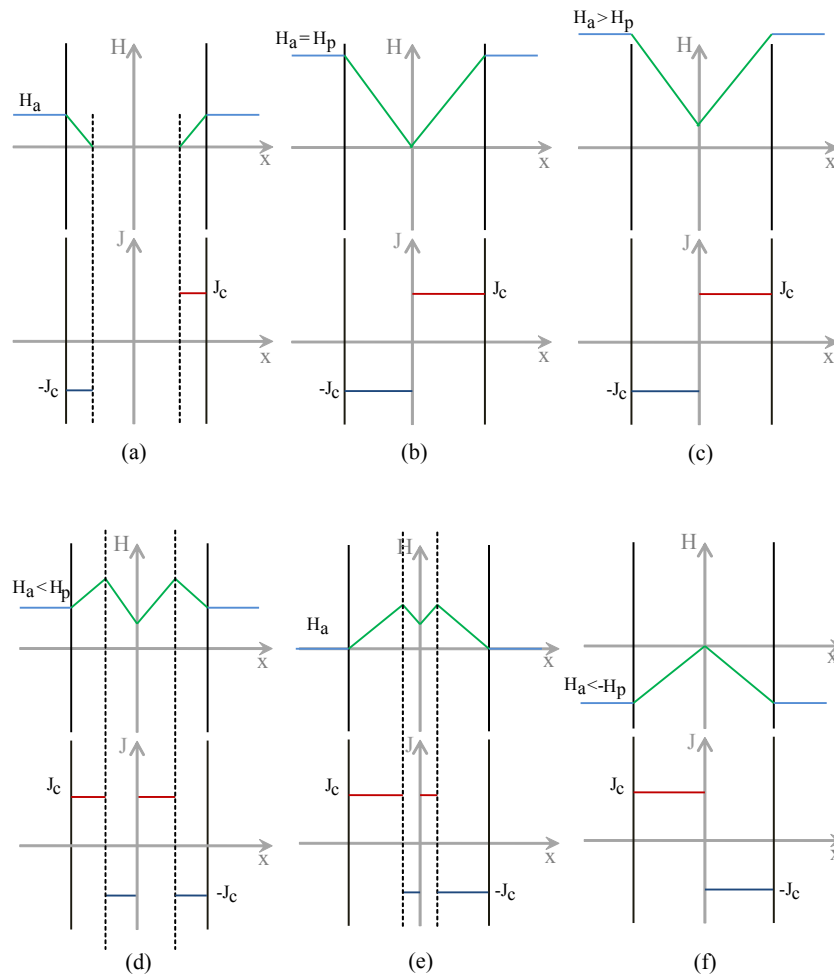
Figure 2.7 Field and current distributions inside the semi-infinite slab due to the time variation of the applied field (H_a).

the need for the cryogenic system, which now is an essential (and one of the most costly) component of superconducting devices. The discovery of room temperature superconductors would be a giant step, not only in the history of superconductivity but also in the history of science and engineering and would substantially change the architecture of many engineering system and devices. Maybe the 21th century be the witness of the revolutionary discovery of room temperature superconductors.

2.2 Power application of superconductors

Since the early years after the discovery of superconductivity, its application in power electric systems attracted huge attention. Thanks to their high current carrying capacity and low transport losses, superconductors can be used to devise more efficient electric power equipment at lower weights and smaller size as compared to existing systems which are based on the technology of conventional conductors. In power applications, due to the large amount of energy involved, even slight improvements in the efficiency can be translated to huge money savings. On the other hand, most of power electric equipment, especially at high power ratings, have large dimensions and heavy weight, so reducing their volume and weight is highly desirable.

The discovery of HTS materials in 1986 prompted renewed interest in the application of superconductors in power systems. At the moment, there are several ongoing and installed projects on superconducting electric equipment worldwide [12]. With the further developments in the technology of fabricating HTS conductors, superconducting power electric equipment will become more economically competitive with respect to their conventional counterparts. In this section, we briefly introduce most important applications of superconductivity in power engineering. Since HTS power transmission cables are the main subject of this thesis, we start with them and they are discussed in more details.

2.2.1 HTS Power Transmission Cables

One of the most brilliant features of electric energy is the fact that it can be transferred more easily and more efficiently than any other forms of energy. However, power transmission is still one of the most important and challenging issues in power systems. Power is transferred from power plants to the consumers through the transmission and distribution networks by overhead lines and power cables.

Although overhead lines are cheaper and easier to install, power cables have some exclusive advantages over them. In power cables conductors are covered by layers of insulators, therefore they can be laid in underground tunnels or below the water surface (sea, rivers). This feature

makes them more reliable in the case of natural disasters such as earthquakes, thunderstorms, and tsunamis. In some cases, power cables are the only viable options to transfer electricity, e.g. when the power must be transmitted to off shore sites, or when in the heart of cities there is no way to use overhead systems.

In power cables, conductors at different voltage levels (phase and ground) are packed close to each other, while in the overhead lines because of insulation considerations lines are positioned relatively far from each other. Therefore, the inductances of the conductors (self and mutual) in power cables are quite lower than the inductances of the overhead lines, and consequently they exhibit better electrical performances in terms of voltage regulation, system stability and so on.

Power transmission cables are one of the most promising commercial applications for superconductors. The idea of using superconductors to make power cables goes back to the early 80's, before the discovery of high temperature superconductors. A notable effort was a project on a high voltage 200-m-long AC cable at the Brookhaven National Laboratory, Long island, NY, in 1986 [13]. Projects on LTS superconducting power cables never resulted in any site installation. The main reason could be the high costs associated with their helium-based cryogenic system. After the discovery of HTS material, similar to many other application of superconductors, new projects on superconducting power cables started, this time using high temperature superconducting wires as the conductors and liquid nitrogen as the coolant of the cryogenic system. The development of HTS power cables has significantly improved over the last decade so that today there are many installed and ongoing projects on this application throughout the world [12, 14].

Design

In the latest design of HTS power transmission cables, the second generation of HTS tapes (2G) are the conductors of choice. These tapes are manufactured by coating a thin layer of YBCO[1] as the HTS conductor on layers of buffer materials and substrates through advanced deposition techniques [15]. The architecture of 2G tapes is sketched in figure 3.1. In addition to the buffer and substrate layers (which are required for the deposition of the YBCO layer), there exist two or more metallic (silver or copper) layers, called stabilization layers. The main task of the stabilization layers is to provide alternative paths for the transport current in case the HTS layer quenches (i.e. suddenly becomes normal). In such situations, the conductivity of the superconducting layer abruptly decreases, and the transport current will flow in the stabilization layers.

---

1. An HTS material composed of Yttirum, Barium and Copper Oxide
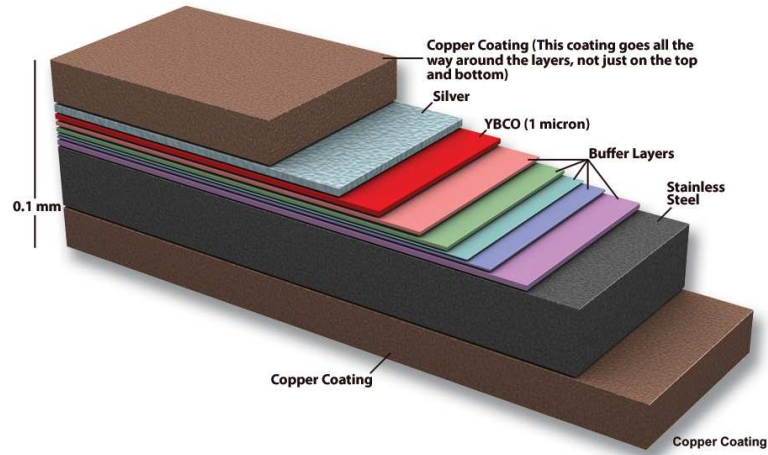
Figure 2.8 The architecture of the second generation of HTS tapes (2G tapes). The stacking shown in this figure is not to scale. According to the dimensions shown in the figure, the overall tape thickness is dominated by the substrate and the stabilization layers.

In the typical design of HTS power cables, HTS tapes are helically wound around cylindrical formers in single or multi-layer arrangements. Similar to conventional cables, insulation layers are used to prevent electric contact between conducting layers. Also, shielding layers are included to confine the magnetic field (produced by the transport current) inside the cable. Figure 3.2 shows a schematic view of a single-layer HTS cable.

The helical configuration of the tapes is beneficial in terms of mechanical and electrical considerations. With this configuration, the cable is mechanically more stable and flexible. In adition, the mutual inductance between the conducting layers are highly dependent on their winding angle. Therefore, by choosing proper winding angles the transport current of the cable can be divided between the layers in an optimized way.

In a design called the *Triad* design, three single phase cables are put together in a common
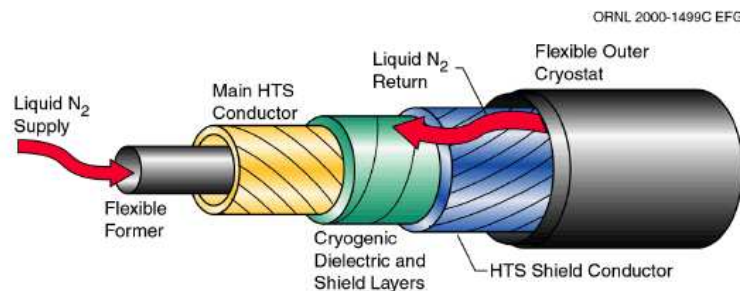
Figure 2.9 A single-layer HTS cable

cryostat to build a three phase cable (see figure 3.3). Since each phase assembly is shielded from the other phases, from the electromagnetic point of view there is no difference between the Triad design and the single phase design.

In another design scheme, which is referred to as the *Tri-Axial* design, conductors of all the three phases are arranged concentrically in a single cryostat. Figure 3.4 shows a three phase HTS cable with the Tri-Axial design.

Since with the Tri-Axial design the magnetic field of all the three phases cancel out each others, there is no need to have a HTS shield layer to confine the magnetic field of the cable. As a direct consequence, with the Tri-Axial design, the required amount of HTS tapes to transport the same level of energy is almost reduced by a factor of 2 as compared with the Triad design [16]. In addition, with the Tri-Axial design, the cross-section of the cable is reduced as compared with the Triad design, which results in reducing the size of the cable and increases the efficiency of the cryogenic system.

HTS cables versus conventional cables

HTS power cables have number of advantages over their conventional counterparts as follows :

– **Reduced dimensions** : Thanks to the high current capacity of HTS coated tapes, for the same transport currents, HTS cables occupy 9 to 10 times less space than conventional copper-based cables. This feature is very important, when due to various constraints the available space for the power transmission purpose is limited.

– **Higher efficiency** : In the case of DC currents, HTS cables are almost lossless, and in the case of AC currents, the amount of AC losses in the HTS cables is quite lower than that of conventional power cables.

Source : The website of SuperPower Inc. http://www.superpower-inc.com

Figure 2.10 An HTS cable with the Triad design. In this design, three identical single phase cables are put together in a common cryostat.

Source : `http://www.supercable.com`
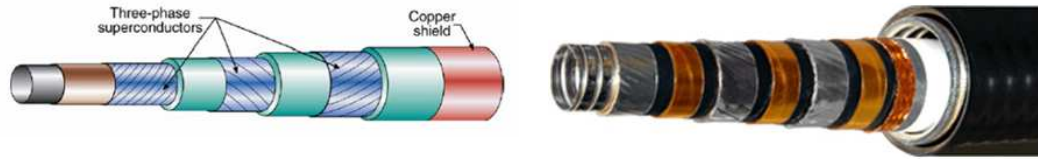
Figure 2.11 Multi-layer HTS cable

– **More environmental compatibility** : Because of the superconducting shield layer, the magnetic field due to the transport current of the cable is confined inside the cable. Therefore, HTS cables do not produce stray magnetic fields and do not cause any electromagnetic interference problem with any other neighboring systems.

– **Extended operational time** : Since the working temperature of HTS power cable is kept fixed at quite low temperatures, i.e. 77 K, they are not subjected to the physical aging caused by thermal stresses. Therefore, it is expected that their insulation system will have a longer life time compared with that of conventional cables.

– **Possibility of transmission of power at lower voltages** : Again thanks to the high current carrying capacity of HTS materials, HTS cables can transfer energy at higher currents and lower voltage levels, while on the other hand, due to the limited current capacity and Ohmic losses, conventional cables exhibit lower efficiencies in low voltage systems.

Despite all the mentioned advantages, HTS power cables are still more expensive than conventional cables. The high costs associated with the manufacturing of HTS tapes and required cryogenic systems contribute to the high capital cost of HTS power cables. On the other hand, the technology of conventional power cables is commercially quite mature. Hundreds of kilometers of these cables have been installed around the world and in average each year 75 km new cable lines are installed [17]. Although the competition with such an efficient technology is quite difficult, with the continued reduction in the price of superconductors and the improvements in the performances of HTS wires, HTS cables are economically getting more competitive against conventional cables in certain applications.

2.2.2 Superconducting Fault Current Limiters SFCL

During fault conditions, power systems and their components are subjected to fault currents, which can be up to 50 times their nominal current. To prevent damages to the components of the power system, the fault current must be limited below a safe level. To limit the fault current, power systems need protective components which should be invisible to the

network in the normal operation mode and very fast must exhibit large impedances to limit fault currents. Fuses and recloser switches are known to be the simplest and most effective devices to do this task. But such components cannot operate at high voltage levels so that in the transmission level there is not any industrialized fault current limiting devices [13, 18].

The very sharp transition between the superconducting and normal states makes superconductors very suitable material to be used as smart switches. Superconducting fault current limiters (SFCL) are current limiting devices which are connected to the power network in series. Under healthy conditions, when the current levels in the protected network is within the safety limits, SFCLs act almost as a short circuit and are invisible to the network. As soon as the protected current exceeds the safety level, the superconducting component of SFCLs switches to the normal state and provides a large enough impedance to limit the fault current.

There are two kinds of SFCLs, *resistive* and *inductive*. In the resistive type, a short length of superconducting wire is connected in series with the power line. The critical current of the superconducting element determines the maximum permitted current level. The length of the superconducting wire must be sufficient to withstand the voltage of the network and the power that must be dissipated during fault conditions.

Inductive type SFCLs are mostly of *shielded core* type, which is similar in design to a transformer whose secondary winding is replaced with a superconducting hollow cylinder (or recently a short-circuited coil made of coated conductors). This superconducting cylinder is placed between a winding made of copper wires and a magnetic core. Under the normal operation of the network, the SFCL is designed so that circulating currents in the superconducting cylinder shield the magnetic core against magnetic flux lines produced by the primary winding, connected in series with the power line. Therefore, because of the shield effect, the flux generated by the primary winding is limited to the leakage flux in the space between the primary coil and the HTS hollow cylinder, which makes the SFCL almost invisible to the power network. As soon as the network current exceeds the threshold level, the current induced in the superconducting cylinder exceeds its critical current and the superconducting core transits to the normal state and provides no more shielding for the magnetic core. Therefore, during fault conditions, the magnetic core with its high permeability becomes visible to the winding of the SFCL, and as a consequence, the inductance of the SFCL abruptly increases and limits the fault current.

SFCLs are among those applications of superconductors which do not have conventional counterparts. They are very fast, as fast as transition between the normal and superconducting states. An exclusive feature of SFCLs is this fact that the action of detecting and limiting the fault current are done by the same component almost instantaneously in a fully passive

manner. Therefore, SFCLs do not need any relay to detect fault current and do not need any control circuit to provide open and close actions signals. Although circuit breakers must still cut the short-circuit current eventually, but since the latter is reduced by the limiter, the required breakers can be chosen smaller. SFCLs, especially resistive types, are very promising application of superconductivity which are predicted to be introduced in power networks in a near future.

2.2.3 HTS Transformers

Since superconductors have quite higher current carrying capacity than that of copper, they can be used for the windings in a transformer, which leads to a reduction in the weight and size of the windings. With the reduction in winding dimensions, the size of the magnetic core is also reduced. Therefore, by using HTS wires, the overall weight and size of transformers can be reduced.

The amount of AC losses in the winding of HTS transformers is lower than the Ohmic losses in the winding of conventional transformers. In addition, because of the reduced size of the iron core, HTS transformers have lower iron losses compared with their conventional competitors. Therefore, the efficiency of HTS transformers is higher than that of conventional ones.

Liquid nitrogen happens to be a good insulator, therefore in HTS transformers it is used both as the coolant and the insulator. Replacing toxic and flammable transformer oils with liquid nitrogen, which is an environmental friendly gas, makes HTS transformers appealing in terms of environmental impacts.

Since the working temperature of HTS transformers is quite lower than that of conventional transformers, the ageing phenomena associated with thermal stresses do not affect their operational life and they are expected to have longer life times. In addition, superconducting transformers can exhibit better overload capabilities.

The idea of fault current limiting characteristics of superconducting materials can be merged with HTS transformers. High Temperature Superconducting Fault Current Limiting Transformers (SFCLT) are superconducting transformers that exhibit the fault current limiting capability [19, 20]. This exclusive characteristic is very important to increase the chance of superconducting transformers to compete with conventional transformers.

2.2.4 HTS Motors and Generators

In large synchronous electric machines, the required magneto motive force (mmf) is produced by passing DC currents through excitation coils, which are wound of many turns

of copper wires. The number of turns and the current of the exciting coils determine the strength of the mmf of the machines. Working at higher mmf increases the power density of the machine and in turn reduces its size for a given power rating [21].

By using HTS wires as the conductors of the exciting circuit of synchronous motors and generators, more mmf can be generated with quite lower losses as compared with copper-based exciting coils. With strong enough mmf, there is no need for low reluctance paths for the magnetic flux, and the iron core can be eliminated from the structure of the machine. Therefore, the operating flux density of the machine can be improved without any limitation imposed by the saturation of the magnetic core.

Compared with conventional machines, the elimination of the iron core results in reductions of weight, and working at higher flux density leads to reductions in size. Therefore, HTS motors and generators are smaller and more compact than their conventional counterparts. In addition, the efficiency of HTS motors/generators are higher than that of comparable conventional copper/iron based machines. The reason for the higher efficiency of the HTS machines mostly comes from the elimination of the iron losses.

Another advantage for HTS generators, which again comes from the elimination of the iron core, is their small synchronous reactance, i.e. X_d. A smaller X_d permits generators to work at smaller load angles, and in consequence results in improved performances in terms of dynamic response, stability, voltage regulation, overload capability and reactive power compensation [22, 23]. It is worth mentioning that the transient and sub-transient reactance of a HTS generator are in the range of similar conventional units [24]. Therefore, in case of replacing a conventional generator with a HTS one, the previous monitoring and protection systems can still be used.

2.2.5 Supercondutig Magnetic Energy Storage (SMES)

The idea of a SMES can be simply explained as a very large inductor with zero resistance. If a DC current circulates in such a short-circuited inductor, the energy can be stored in its magnetic field permanently without decay.

A SMES system consists of four main components as follows :

– **Superconducting coil** : This component is a large coil made of superconducting wires. Energy is stored in the magnetic field produced by a DC current circulating in the coil. The amount of the energy that can be stored in the coil is determined by its inductance and its current level. Since the energy stored in an inductance is proportional to the square of the magnetic field, increasing the operating field results in higher storage capacity. LTS material can remain in superconducting state with higher magnetic fields compared with HTS materials. Therefore, so far, in most practical units, wires made of

LTS materials have been used to wind SMES coils [13].

- **Cryogenic system** : Similar to the other superconducting-based equipment, an elaborate cryogenic system is necessary to provide the low working temperature for the superconducting wires used in the SMES units. Because of using LTS wires, liquid helium is used as the coolant in the cryogenic system of SMES units.

- **AC/DC power converters** : As electric storage systems, SMES units interact with AC networks during charge and discharge periods. Therefore, in SMES units, AC/DC converters are needed for interfacing with the power network.

- **Control circuit** : The task of the control circuit is to provide the required signals for managing the components of the system.

The efficiency of the SMES units depends on their capacity. For large scale units, the efficiency can go up to 95% (considering the AC/DC converters and the cooling system). SMES units can be built at different capacities. In large and medium capacities, they can be used in utility power system as a short term storage station for power quality and stability purposes. At smaller capacities, SMES systems can be used as uninterrupted power supply units (UPS) for special purposes. Due to the fast dynamic response of SMES systems, they have been proposed for applications where very fast power pulses are required, e.g. shipboard electric systems and some military applications [12, 13].

2.3   AC losses in superconducting power cables

One of the most challenging issues in the development of HTS power cables (in AC applications) is the reduction of AC losses occurring in their tapes. Although these losses are quite lower than the classical Ohmic losses in conventional cables, they cause a costly load for the cryogenic system of the cable. The temperature of the cable chamber must be kept cool (below the boiling point of liquid nitrogen), therefore any produced heat due to AC losses must be removed from the cable. Because of the large difference between the ambient temperature and conductor's temperature, this heat removal is a costly and challenging task for the cryostat of the cable, so that each Watt of AC losses act like as 10 Watt load for a cryogenic system with the cryogen of liquid nitrogen [11]. The long length, which is the nature of the cables, adds more difficulty to the cable cryogenic system and makes it more challenging compared with the cooling system of other applications of superconductors. Therefore, reduction of AC losses is one of the key factors in determining the operational and capital cost of HTS power cables, and consequently it is a very important factor to determine the level of the commercial application of HTS power cables in the future of the power transmission industry.

In general, AC losses in HTS cables include all the losses that occur in the conductors of the cable. These losses can be divided into two categories; classical electromagnetic losses and superconducting losses. Classical electromagnetic losses in the conductors of HTS power cables made of coated conductors include the Ohmic and eddy current losses in the stabilizer layer (copper and/or silver) of the tapes and the ferromagnetic losses occurring in the substrate layers. Ferromagnetic losses exist only when the substrate layer of the tapes is made of ferromagnetic materials, as in the case of RABiTS[2] tapes. If these magnetic substrates are exposed to AC magnetic fields, the ferromagnetic losses will correspond to the area of the hysteresis loop of the substrate $B - H$ curve. Under normal working conditions, Ohmic and eddy current losses are quite negligible compared to the total AC losses. On the other hand, in HTS cables the ferromagnetic losses dominate at low transport currents (below $40 - 50$ % of the critical current of the cable) and at higher transport currents these losses become less important compared to the total AC losses of the cable [25, 26].

As explained in earlier, the mechanism through which losses occur in HTS materials is quite different from classical electric and ferromagnetic losses. The superconducting losses occur when HTS materials carry time varying currents or are exposed to time varying magnetic fields, e.g. AC currents and fields. These losses are derived from the magnetic field distribution inside and on the surface boundaries of the conductors. Therefore, the geometry of the conductors (e.g. tapes in the case of HTS power cables) and their relative positioning change the field distribution and consequently affect the AC losses.

The edge effect is the loss mechanism which dominantly contributes to the AC losses in the tapes of single-layer HTS cables. The associated losses with the edge effects arise from the presence of a gap between adjacent tapes, which disturbs the field distribution near the edges of the tapes. Because of these gaps, the magnetic field presents high perpendicular components near the gap region, which results in large field penetration from the edges of the tapes. As a direct consequence this field penetrations, tapes carry more current near their edges and this results in higher losses.

Another loss mechanism which is considered in most of AC loss analysis of HTS power cable comes from the polygonal configuration of the tapes in the 2D cross-section of a cable (see figure 2.12). Such a polygonal configuration disturbs the circumferential magnetic field along the width of the tapes and contributes to magnifying the perpendicular components of the magnetic field within the tapes.

Since in HTS power cables, tapes are helically wound around cylindrical formers, the wide face of the tapes must be conformed to the former. So as an inevitable consequence of their helical configuration, as shown in figure 2.13 tapes must have bent shapes conformed to the

---

2. Rolling Assisted Biaxially Textured Substrates
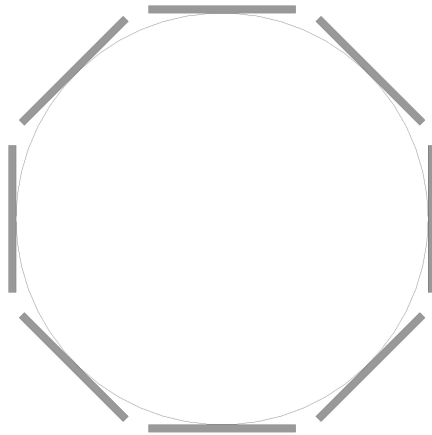
Figure 2.12 Polygonal arrangement of the tape in the 2-D cross-section of the cable, when tapes are not conformed to the cable former

former in the 2-D cross-section of the cable. Therefore, we believed that there must be no loss associated to the polygonal configuration of the tape. Therefore considering losses associated with the polygonal configuration of the tapes results in the overestimation of the AC losses. This in turn could lead to wrong conclusions for the AC loss reduction in HTS cables. For example, in some research work [27–29], it is concluded that, by increasing the number of the tapes,and due this fact that the contribution of the polygonal losses is decreased, the AC losses of the cable are reduced. But since the real configuration of the tapes in the cross-section of the cable is more similar to that presented in figure 2.13 (rather than figure 2.12), increasing the number of tapes does not reduce the AC losses. On the other hand, with increasing the number of tapes the number of gaps is automatically increased and in turn the contribution of the edge effect to the AC losses is increased.

AC loss mechanisms in HTS power cables made of coated tapes are discussed in more details in Chapter 6.

2.3.1 Computation of current distribution and AC losses in HTS power cables

For the optimal design of superconducting cables, the precise prediction of their AC losses is an important issue. AC losses can be measured experimentally, or can be calculated by analytical or numerical methods. The accurate measurement of AC losses in many practical applications, including power cables, is a challenging issue which requires elaborate techniques and instruments [30]. On the other hand, the extremely non-linear resistivity of superconducting materials and the sensitivity of their characteristics to external magnetic fields narrow the availability of analytical solutions down to a few simple geometries. In this context, nu-
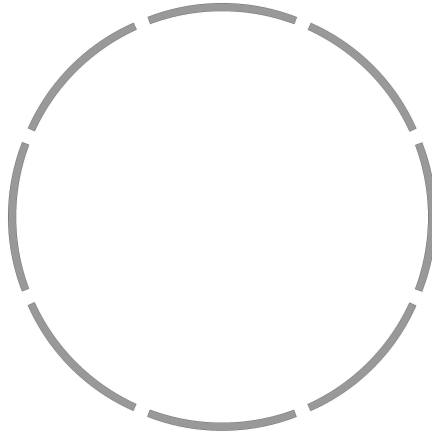
Figure 2.13 Cross-sectional view of a single-layer HTS cable (typical design), when tapes are conformed to the cable former

merical techniques are of utmost interest as efficient tools to predict current distributions and AC losses inside superconducting wires in various applications. Numerical techniques can be used to study the electromagnetic behavior of superconducting materials and help researchers and design engineers to get a better understanding of the electromagnetic behavior of superconducting materials in different applications.

2.3.2 Literature review

Analytical approaches

Due to the non-linear resistivity of superconducting materials, even for simple geometries, analytical computation of their AC losses is rarely possible. Most of the proposed analytical approaches to find AC losses of HTS cables are based on Norris' work [31, 32]. Norris calculated analytically the AC losses for a few simple geometries such as : infinite slabs, infinite thin strips and round wires.

Norris used his developments for the AC loss calculation inside infinitely thin strips to find the AC losses in HTS power cables made of superconducting tapes. In his models, the helical configuration of the tapes is neglected and the problem is considered as a 2-D one. In Norris' model, the superconducting characteristic of the tapes is introduced by the Bean model, and losses are scaled as the square of the gap and the fourth power of the applied field.

The main drawbacks of such analytical approaches are as follows. First of all, coupling losses due to the electromagnetic interaction between the tapes of different layers is not considered. Therefore, this model is applicable only for single-layer cables. Second, similar to other

2-D approaches, the helical configuration of the tapes is neglected and they are considered as straight conductors forming a polygonal configuration in the cross-section of the cable. Since in such polygonal configuration tapes experience larger perpendicular components of the magnetic field, these approaches result in the overestimation of AC losses. Recently, Mawatari et al. [33] have extended the Norris model for the cases in which the cross-section of the tapes has a bent shape conformed with the former cylinder of the cable.

Neglecting the gap between the tapes and considering each layer of the cable as a super-conducting hollow cylinder, Vellego and Metra [34] proposed an analytic approach to find AC losses of HTS cables, which is referred to as the *Monoblock model*. With this model, the magnetic field is assumed to be purely tangential to the tapes, and the only considered loss mechanism is the penetration of the magnetic field from the wide face of the tapes.

The current distribution between the layers of the superconducting multi-layer cable has been widely analyzed by electric circuit models. The idea is to use a simple electrical model based on the self and mutual inductances of densely wound helical coils. In such approaches, the cable is described from a macroscopic point of view. Since the internal structure of the HTS tapes is not taken into account, these models cannot be used directly for computing the AC losses. In many proposed models, the idea of such equivalent circuits has been combined with the analytical approach for the AC losses in infinite slabs, developed by Norris or Carr [35], to find AC losses in HTS cables [36–48]. The main drawback of these models is the fact that AC loss calculation is done regardless of the current distribution inside the tapes. In such approaches the solution of the magnetic field is obtained by the classical expressions for the magnetic field of densely wound helical coils, i.e. the non-linear behavior of the HTS tapes and the adjacent gaps between them is not considered in the solution of the magnetic field (or in the estimation of elements of the equivalent circuit of the cable).

Numerical approaches

Based on various numerical techniques, many numerical models have been proposed to address the problem of finding AC losses and current distributions in the conductors of HTS cables. Many of these models are based on the Finite Element Method (FEM), which is known to be a powerful numerical technique to tackle problems with complicated geometries. However, with the currently available technology of computers, it seems that it is still quite difficult to model the real geometry of HTS power cables with FEM, as modeling thin tapes in helical configurations leads to very large number of degrees of freedoms. Therefore solving the electromagnetic problem of HTS cables, faithful to their real geometry, requires ultra fast computers with an enormous amount of memory.

Up to now all the FEM based model proposed to simulate the HTS power cables have

come with major simplification of the real geometry of the problem. Neglecting the helical configuration of the tapes and converting the problem to a 2-D one, many researchers have used FEM models, either on home-made [49–52] or commercial codes [53–55], to simulate the electromagnetic problem of HTS cables. One of the successful FEM model to find 2-D field and current distributions in superconductors is based on the first-order edge element formulation [56, 57]. This model has been widely used in the electromagnetic modeling and the AC loss analysis of HTS materials [58–60]. Another notable example of FEM approaches for AC loss analysis of HTS cables is the model developed by Amemiya et al. [51, 61]. In this model, the thickness of the HTS tapes is neglected and only the perpendicular component of the magnetic field to the wide face of the tapes is considered.

By neglecting the gap between the tapes of each layer of the cables and considering the whole tapes of each layer in the form of very thin hollow cylinder, Honjo et al. [62] proposed a 3-D FEM model to simulate the electromagnetic behavior of multi-layer HTS power cables. In this approach, the helical configuration of the tape is physically introduced by defining an anisotropic conductivity for each layer. In such approaches, existing gaps between superconducting tapes of each layer are neglected. These gaps cause the increase of inductance which, in turn, affects the balanced current distribution among the layers. The gaps also produce magnetic fields perpendicular to the tape surfaces, which results in an important contribution to the AC losses of the cable. Therefore, using this method leads to underestimation of the AC losses.

The electromagnetic solution of HTS cables has been approached also with other numerical techniques. Based on an integral-type model proposed by Brandt [63] to solve the electromagnetic problems involving superconducting materials, some numerical models have been developed for the simulation of HTS power cables. In these models, with the help of the direct relationship between the current density and the magnetic vector potential (obtaining from the Biot-Savart integral), the eddy current equation is formulated in terms of current density over the conducting regions of the problem. Since the problem is solved directly to find the current density, as opposed to FEM approaches, there is no need to mesh the air region around the tapes and it is enough to just discretize the problem over the conducting regions. This feature reduces the number of degrees of freedom of the problem and makes it more efficient in terms of computational time and memory requirements (when the number of degrees of freedom is below a certain value [64]). Fukui et al. [27, 65] have used this method to find the AC losses of HTS power cables when the helical configuration of tapes is neglected. In their approach, similar to many other 2-D approaches, the tapes of the cable form a polygonal configuration in the cross-section of the cable, which leads to the overestimation of the AC losses as discussed earlier.

Using an analytic expression in the form of infinite series for the mutual and self inductances of helically wound thin conductors to formulate the circuit equation, a numerical model has been introduced in [66] to find current distribution and AC losses in single-layer HTS cables. However, as mentioned by the author, this method is very slow and needs to be improved for practical cases.

The Minimum Magnetic Energy Variation (MMEV) method is another numerical approach based on CSM to find current distribution in thin superconducting tapes. In this method, current distribution is found by searching for solution which results in minimization of the stored magnetic energy. The idea is to find new CSM type current distribution which leads to smallest change in magnetic energy and satisfies certain constraints (such as applied field and/or net imposed current). This method has been used in the AC loss study of superconducting coils with $2 - D$ (plane and axial symmetry) [67, 68].

2.3.3 Reduction of AC losses in HTS power transmission cables

Reduction of AC losses is a key technical issue in the development of HTS power cables. With lower AC losses, the initial and the operational costs of HTS power cables are remarkably reduced and this allows them to be in a better position to compete with conventional power cables. Therefore, the reduction of AC losses is one of the most important factors for the commercial application of HTS power cables in the future of the power transmission industry.

AC losses can be reduced in two different ways. One approach, which is the task of material scientists rather than engineers, is to produce HTS conductors with improved superconducting performances, i.e. higher critical current, higher critical field and higher critical temperature. In addition, for a given superconducting characteristics of the tapes, AC losses in HTS cables can be minimized by choosing optimal design parameters or by proposing alternative design schemes, other than the typical designs.

2.3.4 Alternative design schemes to reduce the AC losses in HTS cables

According to the arguments that ideally no loss due to the polygonal configuration contributes to the AC losses of HTS cables, the edge effect is the most important loss mechanism to determine the AC losses in single-layer HTS cables made of non-ferromagnetic substrates. With smaller gaps between the tapes, the edge effect is undermined so that when these gaps are close AC losses are minimized. But due to the mechanical consideration (the winding process and the mechanical flexibility of the cable), there is a minimum size for the gap ($\sim$ $0.6 - 0.8$ mm) in the typical design of HTS power cables [33].

Through experimental trials to reduce the AC losses in HTS coils and as an attempt to further close the gap, engineers of SuperPower observed that when the adjacent tapes overlap each other, the AC losses of the HTS coils are reduced. Based on their experimental observations, they proposed two overlapped design schemes for reducing AC losses in HTS coils and cables which have been registered as an US patent [69].

In one of these designs, which we called *cyclic overlapped design*, the adjacent tapes of the cable periodically overlap each other up to a certain distance ($\sim 1 - 2$ mm). Figure 2.14 shows the cross-section of a cable whose tapes periodically overlap each other.

In another design, shown in figure 2.15, the adjacent tapes can be alternatively arranged so that both edges of one tape overlap the adjacent tapes and therefore the edges of the next tape are overlapped by the edges of the two adjacent tapes. We called this design scheme *anticyclic overlapped design*.
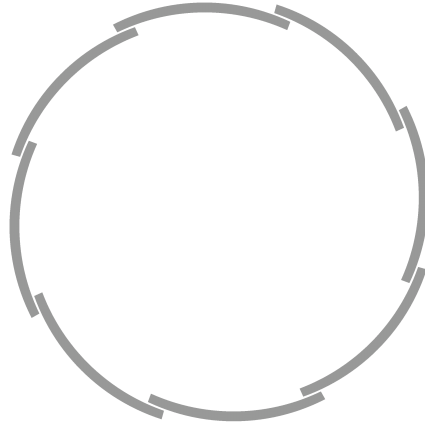
Figure 2.14 Cross-section view of a HTS cable when tapes are arranged according to the cyclic overlapped design; with this design the adjacent tapes periodically overlap each other up to a certain distance $(1 - 2 \text{ mm})$
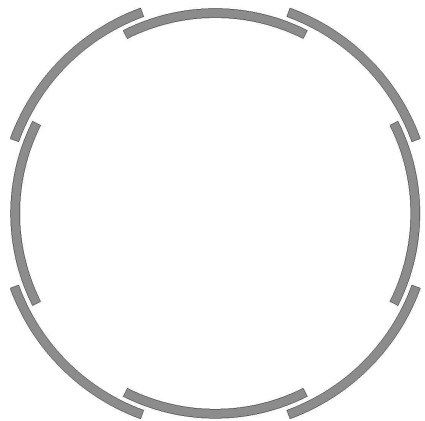
Figure 2.15 Cross-section view of a HTS cable when tapes are arranged according to the anticyclic overlapped design; with this design both edges of one tape overlap the adjacent tapes and the edges of the next tape are overlapped by the edges of its two adjacent tapes

CHAPTER 3

RESEARCH OBJECTIVES AND METHODOLOGY

3.1 First phase

3.1.1 Research objective

The objective of the first phase of this thesis work is to develop a fast numerical method for the accurate computation of the current distribution and AC losses in single-layer assembly of helically wound thin tape conductors. The exact helical configuration of the tapes must be considered, and the non-linear resistivity of HTS materials must also be taken into account. Since the model is supposed to be used to perform parametric simulations, it should be efficient in terms of computational time.

3.1.2 Hypotheses

The proposed approach to reach the objective of the thesis is based on the following hypotheses :

1. As shown in figure 3.1, even if the tapes are not identical (physically or geometrically), when they are wound with the same winding angle their relative position (with respect to each other) remains unchanged along the length of the cable. Therefore, thanks to the geometrical symmetry associated with the helical configurations of the problem, as long as all the tapes are wound with the same winding angle, the governing equations of the full 3-D problem can be formulated over a 2-D cross-section of the cable.

2. The numerical method of choice is an integral-type method, which is similar to the Brandt method. In this case, the governing equations of the problem are established to solve directly for the current density inside the conductors. Therefore, the problem formulation is done just over the conducting regions in the cross-section of the cable.

3. Since in HTS cables, all the tapes (of each layer) are identical and are arranged in a symmetrical way, the study domain can be reduced to the half width of one of them (see figure 3.2).

4. The thickness of the superconducting layer of the HTS tapes is between 0.5 to 2 μm, while in the cable application tapes width varies from 4 to 10 mm. Therefore, the aspect ratio of the tapes are in the order of thousands. Because of the high aspect ratio of the tapes, their thickness can be neglected and tapes are treated as helically wound current
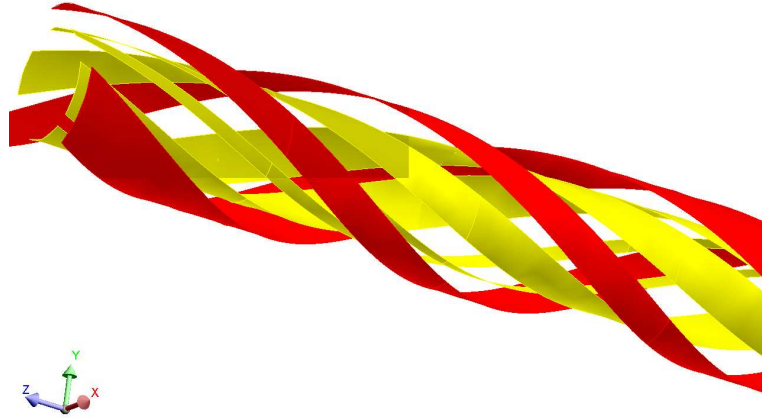
Figure 3.1 As long as tapes have the same wining angle, their relative position (with respect to each other) does not change along the cable length. This symmetrical argument implies that the problem can be formulated in the cross-section of the cable.

sheets. Therefore, the final study domain of the problem is a 1-D line defined along the cross-section of one of the tapes of the cable.

5. The resistivity of the non-superconducting layers of the HTS tapes is much larger than the AC resistivity of the superconducting layer of the tapes. Therefore in this model, just the superconducting layer of the tapes is considered. This assumption is highly accurate in the case of HTS tapes with non-ferromagnetic substrates (such as IBAD tapes), but not in the case of tapes with ferromagnetic substrates (such as RABiTS tapes). Therefore, this hypothesis limits the application of the method to HTS tapes with non-ferromagnetic substrates. In the Chapter 5, the validity of this assumption is examined and it is shown that the losses in the non-superconducting layer are quite negligible compared with the AC losses in the superconducting layer of the tapes.

6. As a consequence of the current sheet assumption, and due to this fact that all the tapes are wound with the same winding angle, the current can flow only in the direction of the helical trajectory of the tape (deviation of the current from the helical trajectory of the tape violates the symmetry arguments associated with the geometry of the problem).

7. The non-linear resistivity of the HTS layer of the tapes is introduced in the form of the power law model (see Chapter 1 equation (2.4)).
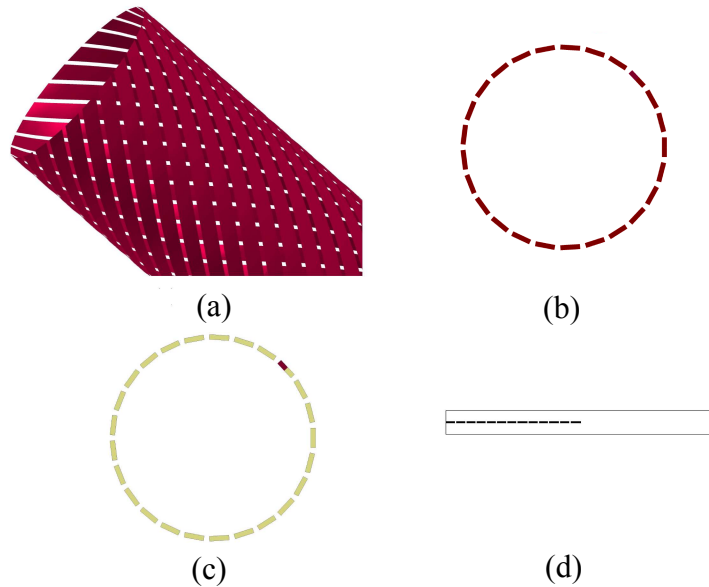
Figure 3.2 Successive reduction of the study domain in the proposed hypothesis (tapes dimensions not drawn to scale). (a) Real 3D geometry, (b) 2D cross-section of the tapes, (c) Reduction of study domain to half of a tape, (d) Final study domain in the form of discretized interconnected 1D strips (straight lines) along half width of one tape.

3.1.3   Method limitations

As one of the main hypotheses of the model, it is assumed that the vector of the current density in all the elements of the study domain has only one component aligned with the helical trajectory of the tapes. This assumption is true, as long as all the tapes are wound with the same winding angle. Therefore, the proposed model is applicable to solve the electromagnetic problem of helically wound tapes as long as they have the same winding angle. This means that the model can be extended to multi-layer cables, only when all the layers are wound with the same winding angle.

In our model, we just consider the HTS layer of the tapes, and all the other layers are neglected. In the case of HTS tapes with non-ferromagnetic substrates, this assumption is highly accurate. But, for the case of HTS tapes with ferromagnetic substrates, the problem formulation must be extended to cover these layers. In this case, the effect of the magnetization (induced by the transport current of the HTS layer) must be considered in the problem formulation. In addition, ferromagnetic losses occurring at the substrate layer must be considered in the AC loss computation.

3.1.4   Methodology

Mathematical formulation

In the proposed approach the governing equation of the problem is the eddy current equation, i.e.

$$\vec{E} = -\frac{\partial \vec{A}}{\partial t} - \vec{\nabla} V \tag{3.1}$$

where, $\vec{E}$, $\vec{A}$ and $\vec{\nabla} V$ are respectively the electric field, magnetic potential and electric potential gradient.

The eddy current equation is derived from the combination of the differential form of Faraday's law, i.e.

$$\nabla \times \vec{E} = -\frac{\partial \vec{B}}{\partial t} \tag{3.2}$$

and, the definition of the magnetic vector potential, i.e.

$$\nabla \times \vec{A} = \vec{B}. \tag{3.3}$$

Replacing $\vec{B}$ with (3.3) on the right-hand side of (3.2), we have

$$\nabla \times \vec{E} = -\frac{\partial (\nabla \times \vec{A})}{\partial t} \tag{3.4}$$

or

$$\nabla \times (\vec{E} + \frac{\partial \vec{A}}{\partial t}) = 0. \tag{3.5}$$

We know that a curl free vector can be expressed as the gradient of a scalar, therefore the argument of the curl operator in (3.5) can be expressed as the gradient of a scalar field. This scalar field can be chosen to be the same scalar electric potential defined in electrostatic. Therefore, we have

$$\vec{E} + \frac{\partial \vec{A}}{\partial t} = -\vec{\nabla} V, \tag{3.6}$$

which is equivalent to (3.1).

As explained in the previous section, due to the symmetry of the problem and considering the tapes as infinitely thin current sheets, it is assumed that $\vec{E}$ has only components aligned with the helical trajectory of the tapes. Therefore, (3.1) can revert to a scalar form as

$$E_h = -\frac{\partial A_h}{\partial t} - \nabla V_h \tag{3.7}$$

where E_h, A_h and ∇V_h are the components of $\vec{E}$, $\vec{A}$, and $\vec{\nabla} V$ aligned with the helical trajectory of the tapes. For the sake of simplicity, in what follows, we omit their index notation.

To prepare (3.7) to be solved directly for the current density (J), E and A must be expressed in terms of J. To do so, first E in the left side of (3.7) is replaced with the $E - J$ constitutive equation, i.e.

$$E = \rho J \tag{3.8}$$

where, ρ represents the intrinsic resistivity of the tapes. In its general case, ρ can be a function of other electromagnetic variables, such as J and B (magnetic flux density) as is the case with superconductors. In our approach ρ is defined in the form of the power law expression (see (2.4)).

On the right-hand side of (3.7), A also must be expressed in terms of J. The relationship between A and J is obtained from the Biot-Savart potential integral, i. e.

$$\mathbf{A} = \frac{\mu_0}{4\pi} \int \frac{\mathbf{J}}{|\mathbf{r} - \mathbf{r}'|} d\Omega \tag{3.9}$$

where here Ω represents the surface occupied by the tape in a 3-D space, and $\mathbf{r}$ and $\mathbf{r}'$, are the position vectors of the observation and source points, respectively. The solution of this equation for helically wound current sheets is used to establish a direct relationship between A and J in all the elements of the study domain in a matrix form as

$$[\mathbf{A}]_{k \times 1} = [\mathbf{M_A}]_{k \times k} [\mathbf{J}]_{k \times 1} \tag{3.10}$$

where, k is the number of the discretized elements, and $[\mathbf{A}]$ and $[\mathbf{J}]$ contain the magnetic potential and the current density of each element of the study domain. $[\mathbf{M_A}]$ is a k by k matrix which relates A in each element to the J of all the elements.

In its final form, the problem is formulated as

$$\mathbf{diag}[\rho(J_i)]_{k \times k} [\mathbf{J}]_k = -\frac{\partial}{\partial t} ([\mathbf{M_A}]_{k \times k} [\mathbf{J}]_{k \times 1}) - [\nabla \mathbf{V}]_{k \times 1} \tag{3.11}$$

where $\mathrm{diag}[\rho(J_i)]$ represents a k by k matrix whose diagonal entries correspond to the resistivity of each element i, obtained by the power law model. All the entries of $[\nabla V]$, which represent the voltage per unit length of the tape, are identical. When a voltage is applied across the cable, ∇V is known and J in all the elements constitute the k unknowns of the

problem. In the case of imposing a known current to the tapes, ∇V is unknown. In this case, as the $(k+1)^{th}$ equation, we use a current constraint equation, i.e.

$$I = s \sum_{i=1}^{k} J_i \tag{3.12}$$

where, I is the injected current into the tape and s is the area of each element.

At this stage, by using a proper time transient integration algorithm, (3.11) is solved for [**J**]. Once the values of J in all the elements of the study domain are known, the AC losses of the cable (expressed in Watts per meter of tape) are obtained through

$$Q = 2N \int\limits_{0}^{1/f} dt \int\limits_{0}^{w/2} \rho J^2 dl \tag{3.13}$$

where, f is the frequency of the applied current, w is the width of the tapes and N is the number of tapes.

Since with this approach we solve for J, we do not automatically have access to the solution of the magnetic field. But the magnetic field at given observation points can be computed by establishing suitable matrices (with the help of the Biot-Savart field formula), which relate the components of the magnetic field at those points to the current density of all the elements of the study domain. Therefore, if the solution of the magnetic field is of interest, the field at given observation points can be computed as a postprocessing step.

Method validation

In the absence of any other available model to compute the AC losses of helically wound HTS tapes (to establish a benchmark), the only feasible way to assess the validity of the proposed model was comparing its prediction of AC losses with the results of experimental measurements. Since performing AC loss measurements requires elaborate instruments which at the time were not available in our laboratory, the experimental measurements to verify the validity of the model were done by our collaborators (Dr. Doan N. Nguyen and Dr. Stepen P. Ashworth) in the Superconductivity Technology Center (STC) of the Los Alamos National Laboratory.

Excellent agreements were observed between the numerical prediction and the results of the experimental measurements for AC losses of a helically wound HTS coated tapes with different geometrical parameters. Full details about the method, including its mathematics and hypothetical developments and the results of the experimental verification have been publish in [70]. This paper is inserted as Chapter 4 of this thesis.

We used this method to perform a parametric study on the AC losses of single-layer HTS cables with different geometrical parameters. Among the simulation results it was observed that, for a fixed former radius and a given number of tapes, tapes twisted with smaller pitches show lower AC losses per unit length of the cable. The results of this parametric study were published in [71] which is inserted as Appendix C of this thesis.

3.2 Second phase

3.2.1 Research objective

Since there were no quantitative data and detailed analysis available about the loss reduction in HTS cables by the overlapped designs, the objective of the second phase of this thesis was defined to assess the effectiveness of these designs in reducing AC losses in single-layer HTS power cables.

3.2.2 Methodology

We started with the cyclic overlapped design, and through an extensive parametric simulation we compared the AC loss behavior of this design against the typical design of HTS cables. At this stage, we neglected the helical configuration of the tapes. A 2-D version of the integral-type method developed in the first phase of this thesis was employed to perform the simulations. Through the simulation results AC losses and the field and current distribution inside the tapes of a single-layer HTS cable, were compared for both the cyclic overlapped design and the typical design. The accuracy of the simulation results were verified with the help of 2-D FEM simulations. Simulation results revealed that, by overlapping the tapes AC losses can be reduced up to 5 times compared with the minimum AC losses that can be achieved with the optimum typical design. The detailed results of this study were published in [72], which is inserted Chapter 5 of this thesis.

As the next step, we used the 3-D version of our developed method to investigate the effect of the helical configuration on the performance of the overlapped designs. In this step, through parametric numerical simulations, the AC loss behavior of the cyclic and anticyclic overlapped designs were compared against the typical design for different geometrical parameters, including the winding angle of the tapes.

In addition to the overlapped designs proposed by SuperPower, we investigated the idea of putting narrow HTS tapes bellow the main tapes under the gap regions (see figure 3.3). The motivation behind this idea is to use the magnetic field produced by the narrow tapes to undermine the edge effect in the main tapes. It is expected that the current flowing in the narrow tapes shield the flux lines so they cannot enter in the gap region.
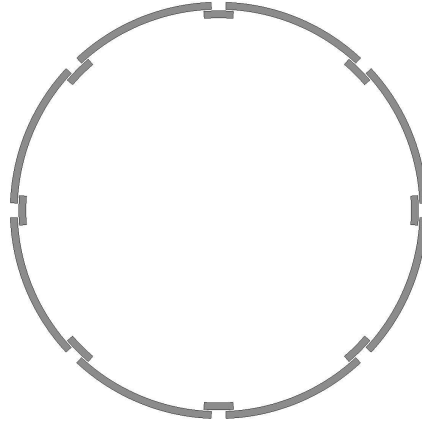
Figure 3.3 Cross-section view of a cable when narrow tapes are symmetrically placed below the gap region

The detailed results about the AC loss behavior of the overlapped designs, and the effectiveness of the idea of inserting narrow tapes have been published in [73], which is inserted Chapter 6 of this thesis work. According to the results of this study, the idea of overlapping the tapes and putting narrow tapes under the gap regions are quite effective in reducing AC losses of single-layer HTS cables made of coated tapes, so that with realistic design parameters AC losses can be reduced up to 70%.

CHAPTER 4

FAST NUMERICAL COMPUTATION OF CURRENT DISTRIBUTION AND AC LOSSES IN HELICALLY WOUND THIN TAPE CONDUCTORS : SINGLE-LAYER COAXIAL ARRANGEMENT

Majid Siahrang[*], Frédéric Sirois[*], Doan N. Nguyen[+], Slobodan Babic[*], and Stephen P. Ashworth[+]

[*]École Polytechnique de Montréal
[+]Superconductivity Technology Center, Los Alamos National Laboratory

Abstract

In this paper, we introduce a very fast method to compute the current distribution in helically wound thin conductors, when one or many of them are arranged in a symmetrical manner to form a single-layer power cable. The method relies on two different approaches to find the magnetic vector potential due to helically wound current sheets. By invoking relevant symmetry arguments associated with the geometry of the problem, and neglecting the thickness of the tape conductors, we show that this 3-D problem can be reduced to a computationally small 1-D problem, whose domain lies along the half-width of any of the constituting conductor. As a consequence, the proposed method is very efficient in terms of computational time, and it is more accurate than many previous 2-D methods that cannot take into account the twist pitch. Since the non-linear resistivity of superconducting material can easily be treated with this method, it can be used to find current and field distributions, as well as AC losses in HTS coils and cables made of coated tapes. To verify the validity of the proposed method, we performed experimental measurements of AC losses in two configurations of solenoid-type cables made of a sample of YBCO coated conductor tape. Excellent agreement was observed between the experimental data and simulation results.

4.1 Introduction

To make High Temperature Superconductor (HTS) coils and cables economically more competitive, computational tools that make it possible to predict the current distribution and power AC losses in helically wound thin conductors is of ultimate importance. With such tools, the analysis and design stages could be coupled with optimization tools to achieve the best possible configurations for given technical requirements.

The conductors of choice in the latest generation of HTS power transmission cables are YBCO coated tapes. The thickness of the superconducting layer in these tapes is about 1 μm, while the typical width varies from 4 to 12 mm. Many such tapes are helically wound in coaxial arrangements to constitute HTS power cables, due to both mechanical and electrical considerations. This results in a fairly complicated geometry to model, and numerically speaking, the problem is highly challenging to tackle with conventional approaches. Even the Finite Element Method (FEM), which is recognized as one of the most powerful techniques for dealing with complicated geometries, requires an enormous amount of memory to mesh this kind of geometry, where such thin conductors are involved. In addition, the highly non-linear resistivity of the HTS materials adds another level of complexity to this already challenging problem.

To circumvent the geometric modeling challenge, most of the previous approaches for solving cable problems simplified the real geometry using various approximations. In most cases, the first simplification is to neglect the twisted configuration of the tapes so thatthey can be considered as straight parallel conductors [27, 50, 51, 65]. While providing useful information, these approaches cannot be used to optimize cable designs, since the twist angle is actually a very important parameter. In other proposed approaches, the cable layers are considered as thin hollow tubular conductors. In these methods, the current can be forced to flow along the helical trajectory of the tapes by defining the conductivity of the cylinder as an anisotropic tensor [62, 74, 75]. Although this approach partially takes into account the twisted configuration of the tapes, the tape-to-tape gaps are neglected, whereas they are shown here to play a dominant role in determining AC losses. It has been reported that this approximation leads to a significant underestimation of AC losses [62]. Using an analytic expression in the form of infinite series for mutual and self inductance of helically wound thin conductors to formulate the circuit equation, another method has been recently introduced in [66] to solve this problem. However as mentioned by the author, this method is very slow and needs to be improved for practical cases.

To find current distribution and AC losses in single-layer HTS cables, in this paper we propose a fast and accurate numerical technique that is applicable to the twisted configuration

of each individual tape. The method avoids meshing the whole cable domain by using an integral formulation, and exploits both the helical symmetry of the problem and the very small thickness of the tapes to reduce it to a computationally small 1-D problem, involving only a few hundred of unknowns. The electromagnetic problem is solved in terms of J, the current density, which is itself related to the vector potential (and field components, if necessary) through Biot-Savart integrals evaluated on the real helical trajectory of the tapes. The results are obtained in a significantly reduced time as compared with all previous methods, while being much closer to the reality. No magnetic materials are considered at this stage, such as when superconducting layers are deposited on a ferromagnetic substrate.

This paper is organized as follows : First, two methods to solve the Biot-Savart potential integrals for helical current sheets are presented. Second, using these methods together with symmetry arguments, the governing equations of the problem are formulated over a properly defined study domain. Finally, the accuracy of the method is confirmed by comparing the simulation results to AC loss experimental data.

4.2 Magnetic potential due to helical current sheets

In this section, we introduce two different methods to find the magnetic potential associated with current carrying helical sheets. Both of these methods are based on the solution of Biot-Savart potential integrals. In the first method, the integrals are solved numerically, whereas in the second method, we use a semianalytic approach.

4.2.1 Reduced dimension numerical integration

This first approach constitutes an important part of the novelty proposed in this paper, and it is the basic building block entering the mathematical formulation of the problem. In the forthcoming developments, we assume that the HTS tapes have a negligible thickness, and therefore behave as infinitely thin current sheets. We also assume that the cross-section of each twisted tape can be approximated by a straight line (parallel to the $\hat{\mathbf{v}}$ axis, see figure 4.1). Although this is not exactly true (the tapes are actually slightly curved on the former), it becomes a very good approximation when we subdivide the real tape into many narrow sub-tapes. Therefore, each tape is modeled by extruding this straight line along a helical trajectory, which is defined by :

$$\vec{\mathbf{c}} = R\cos\left(2\pi u + \phi_0\right)\hat{\mathbf{x}} + R\sin\left(2\pi u + \phi_0\right)\hat{\mathbf{y}} + Lu\,\hat{\mathbf{z}}\,, \tag{4.1}$$

where, R, L and u, are respectively the radius, the pitch length and parameter of the helix, and ϕ_0 is an offset angle that determines position of the tape around the former (see
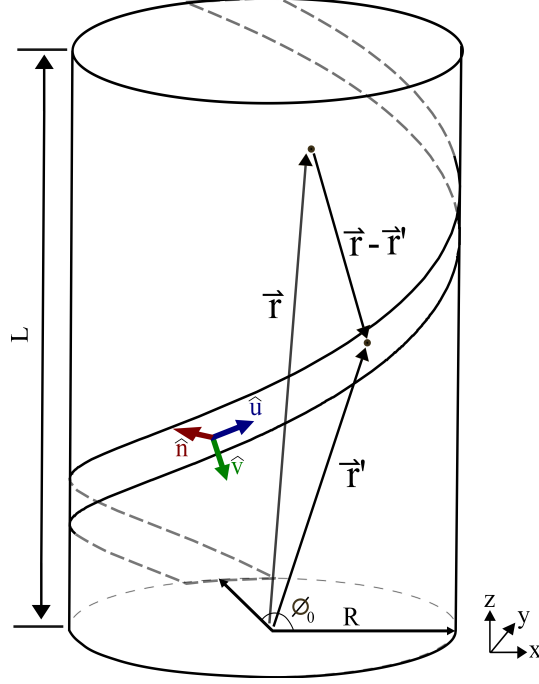
Figure 4.1 Helically wound thin conductor geometry and associated notations considered in this paper.

figure 4.1). In what follows, we restrict our developments to a single reference tape of width $2a$, whose center line passes through $(0, 0, 0)$; thus we can set $\phi_0 = 0$. We can determine the vector potential $\vec{\mathbf{A}}$ associated to a sheet current density $\vec{\mathbf{j}}$ flowing into this tape at any point $\vec{\mathbf{r}} = (x, y, z)$ in space from the the Biot-Savart law, i.e.

$$\vec{\mathbf{A}}(\vec{\mathbf{r}}) = \frac{\mu_0}{4\pi} \int\limits_{\Omega} \frac{\vec{\mathbf{j}}}{|\vec{\mathbf{r}} - \vec{\mathbf{r}}'|} \, \mathrm{d}\Omega \, , \tag{4.2}$$

where Ω represents the surface occupied by the tape in a 3-D space, as shown in figure 4.1. When considering the actual tape width $(2a)$, and supposing that the sheet current density $|\vec{\mathbf{j}}| = j$ A/m is uniform and flows along the helical path only, we obtain the following integral (see Appendix A for the detailed procedure) :

$$\vec{\mathbf{A}}(x, y, z) = \frac{\mu_0 a \ell j}{4\pi} \int\limits_{-n_p/2}^{n_p/2} \mathrm{d}u \, \hat{\mathbf{u}} \int\limits_{-1}^{1} \frac{\mathrm{d}v}{\sqrt{d_x^2 + d_y^2 + d_z^2}} \, , \tag{4.3}$$

where n_p is the number of twisted pitches considered in the integral, i.e. $-n_p/2 < u < n_p/2$ (half of the number of pitches above and below the plane $z = 0$), v is a parameter used to define the strip width, and the remaining notations are defined as follows :

$$\ell = \sqrt{(2\pi R)^2 + L^2}\,,$$

$$\hat{\mathbf{u}} = \frac{2\pi R}{\ell}\left[-\sin\left(2\pi u\right)\hat{\mathbf{x}} + \cos\left(2\pi u\right)\hat{\mathbf{y}} + \frac{L}{2\pi R}\,\hat{\mathbf{z}}\right],$$

$$d_x = x - R\cos\left(2\pi u\right) - \frac{avL}{\ell}\sin\left(2\pi u\right),$$

$$d_y = y - R\sin\left(2\pi u\right) + \frac{avL}{\ell}\cos\left(2\pi u\right),$$

$$d_z = z - Lu - \frac{2\pi avR}{\ell}\,. \tag{4.4}$$

Defining B and K as

$$B = -\frac{2}{a\ell}\Big\{L\big[x\sin(2\pi u) - y\cos(2\pi u)\big] + 2\pi R(z - Lu)\Big\},$$

$$K = \frac{1}{a^2}\Big\{\big[x - R\cos(2\pi u)\big]^2 + \big[y - R\sin(2\pi u)\big]^2$$

$$+ \big[z - Lu\big]^2\Big\}, \tag{4.5}$$

one can rewrite (4.3) as

$$\vec{\mathbf{A}} = \frac{\mu_0 \ell j}{4\pi}\int\limits_{-n_p/2}^{n_p/2} \mathrm{d}u\,\hat{\mathbf{u}}\int\limits_{-1}^{1}\frac{\mathrm{d}v}{\sqrt{v^2 + Bv + K}}\,, \tag{4.6}$$

where the rightmost integration in (4.6) can be solved analytically. The result is

$$I_0 = \int\limits_{-1}^{1}\frac{\mathrm{d}v}{\sqrt{v^2 + Bv + K}} = \ln\left(\frac{B + 2 + 2\sqrt{1 + B + K}}{B - 2 + 2\sqrt{1 - B + K}}\right). \tag{4.7}$$

Despite the compact notation, one must not forget that I_0 is a function of u. By inserting this analytic solution in (4.6), the order of integrations to find $\vec{\mathbf{A}}$ is reduced to one. Therefore, after substituting $\hat{\mathbf{u}}$ from (4.4), $\vec{\mathbf{A}}$ can be decomposed into its components, in the Cartesian

coordinate system, as three simple integrals, i.e.,

$$A_x = \frac{\mu_0 R j}{2} \int_{-n_p/2}^{n_p/2} \sin(2\pi u) I_0(u) \, \mathrm{d}u \,,$$

$$A_y = \frac{\mu_0 R j}{2} \int_{-n_p/2}^{n_p/2} \cos(2\pi u) I_0(u) \, \mathrm{d}u \,,$$

$$A_z = \frac{\mu_0 L j}{4\pi} \int_{-n_p/2}^{n_p/2} I_0(u) \, \mathrm{d}u \,. \tag{4.8}$$

These 1-D integrals, although not analytically tractable, can numerically be solved much faster and more easily than the 2-D version shown in (4.6). However, some care must be taken since potential integrals diverge when the observation point $\vec{\mathbf{r}} = (x, y, z)$ lies in the integration domain, namely, the tape surface. In this case, I_0 diverges at $\vec{\mathbf{r}}' = \vec{\mathbf{r}}$, although the integral does not. In principle, this can be addressed by using special quadrature integration techniques, but these are not easy at all to implement in a robust way. Another approach that avoid dealing with singularities is to revert to analytical approximations in this part of the integral, as shown in next section.

4.2.2 Semianalytic approach

In this approach, the helical current sheet is assumed to be constructed by the interconnection of tiny rectangular elements, as shown in figure 4.2. By doing this, the geometry is no longer the exact geometry (presence of a discontinuity between each element), but it makes it possible to develop analytic expressions for the vector potential.

Figure 4.3 shows one of these elements in a local coordinate system (x, y, z). In this figure, w and h are the width and height of the element, respectively. For the sake of simplicity, we consider that the z axis of the local coordinate system is aligned with the helical path $\vec{\mathbf{c}}$, as defined in (4.1), whereas the y axis is normal to the surface of the tape. Therefore, when the current flows along the helical trajectory of the tape, a sheet current of j (in amper per meter) flows in the element along the z axis (still in the local coordinate system). Under these conditions, the contribution to the vector potential at any desired observation point $\vec{\mathbf{r}} = (x, y, z)$ of the local coordinate system has a unique component oriented along z (colinear with the sheet current) that can be determined from the following potential integral :

Figure 4.2 Thin helical conductor constructed by interconnection of tiny rectangular elements.

$$A_z(x, y, z) = \frac{\mu_0 j}{4\pi} \int\limits_{\frac{-w}{2}}^{\frac{w}{2}} \int\limits_{\frac{-h}{2}}^{\frac{h}{2}} \frac{\mathrm{d}z' \mathrm{d}x'}{P} \,, \tag{4.9}$$

where $P = \sqrt{X^2 + y^2 + Z^2}$ (always positive), $X = x - x'$ and $Z = z - z'$. An analytic result is easily found for this double integral, i.e.,

$$A_z = \frac{\mu_0 j}{4\pi} \Bigg\{ z' + y \left[\arctan\left(\frac{Z}{y}\right) - \arctan\left(\frac{ZX}{yP}\right) \right] + Z \ln(X + P) + X \ln(Z + P) \Bigg\} \Bigg|_{x'=-\frac{w}{2}}^{x'=\frac{w}{2}} \Bigg|_{z'=-\frac{h}{2}}^{z'=\frac{h}{2}} \tag{4.10}$$

where arctan terms return a value between $-\pi/2$ and $\pi/2$.

The total vector potential at any observation point is obtained by superimposing the contribution of all the rectangular current sheets in a global coordinate system, which requires applying a different rotation matrix to each element. The minimum number of elements required to achieve a given accuracy depends on the radius and pitch length of the helix, and can be determined after a few manual iterations.

4.2.3   Comparison between numerical and semianalytic methods

From the point of view of computational performances, numerical integration is faster than the presented semianalytic method. On the other hand, the semi-analytic approach handles the singularities of the potential integrals much more easily than the numerical approach. To
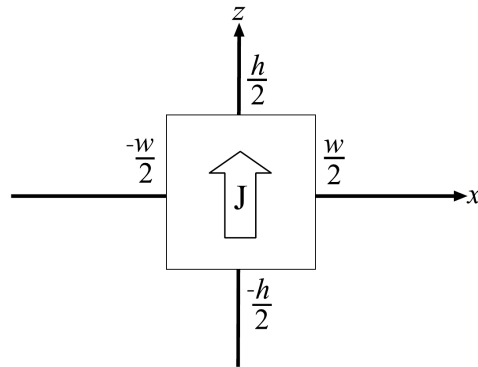
Figure 4.3 An elementary rectangular current sheet in its local coordinate system (x, y, z).

exploit the advantages of both methods, we did use numerical integration as often as possible, except for singular cases, which we treated with the semianalytic method. This explains why we introduced the two methods in detail in this paper.

4.3 Formulation of the electromagnetic problem

4.3.1 Assumptions

As shown in figure 4.4, we assumed a symmetrical arrangement of tapes helically wound around a cylindrical former, so they all have the same twist pitch. In the rest of this paper, this configuration is referred to as "single-layer cable" or simply "cable." In addition the term "tape" is used to refer to each of its constituting thin conductors.

On the modeling side, the only geometrical approximation used for the cable was to consider the tapes as infinitely thin conductors (current sheet approximation) to be consistent with the formulas previously derived.

In addition, from the preceding assumptions, one can deduce the following statements :
– As long as the cable length is long enough, the current distribution along the cross-section of any tapes is the same at any position along the length of the cable.
– As long as all tapes are identical (geometrically and physically) and symmetrically positioned, their current distributions are identical.
– The current in each tape always flows along its helical trajectory and the current density vector (i.e., $\vec{J}$) is always tangential to this path.
– The current distribution in the tapes must necessarily exhibit an even symmetry along their width.

Based on the preceding statements and in the absence of any magnetic material, the formulation of the problem to find $\vec{J}$ can be established over a 1-D study domain defined along the
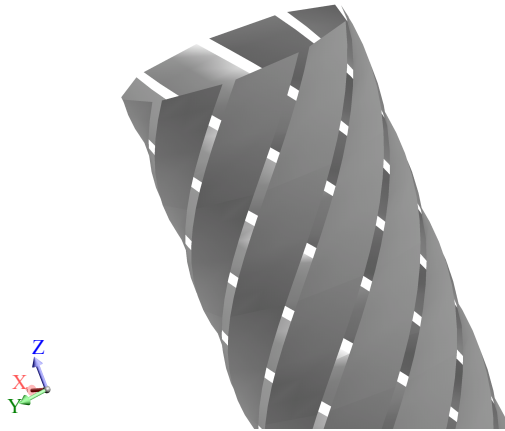
Figure 4.4 Helically wound thin conductors in single-layer coaxial arrangement.

half-width of one tape. This line domain, which is actually a bent line tangential to the tape wide face and normal to its edge, is shown in figure 4.5.

A particular feature of this model is that finding $\vec{\mathbf{J}}$ along this 1-D domain is sufficient to find the current distribution and power dissipation in the whole cable. In addition, we already know from symmetry considerations, that $\vec{\mathbf{J}}$ only has a component oriented along the helical path of the tape, i.e., $\vec{\mathbf{J}} = J\,\hat{\mathbf{h}}$ (see figure 4.5). Therefore, in the rest of the paper, we will drop the vector notation and use J to express the unknowns of our problem, knowing that J actually corresponds to the helical component of the current density in the tapes.

To solve for J, the 1-D study domain has to be discretized first. This is done by redefining this slightly curved domain as a set of interconnected straight lines. From figure 4.5, each of these straight lines is parallel to $\hat{\mathbf{t}}$. These straight lines constitute the discretized "elements" of the numerical problem. To each of these elements, we associate an unknown helical current density J, as previously mentioned. Therefore, the total number of unknowns (or "degrees of freedom") of the problem will be simply equal to the number of elements used in the discretized study domain.

4.3.2 Matrix formulation of the electromagnetic problem

To find the distribution of the helical current density J, we start from the electric field $\vec{\mathbf{E}}$ equation expressed in its local form, in the low frequency approximation, i.e.,

$$\vec{\mathbf{E}} = -\frac{\partial \vec{\mathbf{A}}}{\partial t} - \nabla\phi\,,\tag{4.11}$$

where, $\vec{\mathbf{E}}$, $\vec{\mathbf{A}}$ and $\nabla\phi$ are, respectively, the electric field, the magnetic vector potential and
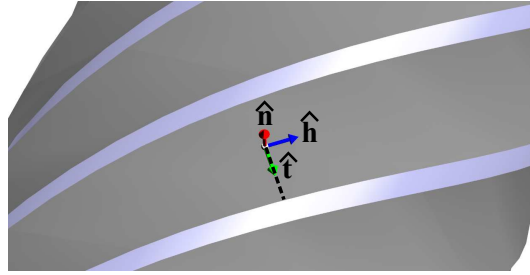
Figure 4.5 One-dimensional study domain defined over the cross-section of one tape, shown with the local coordinate system of one of its elements ($\hat{\mathbf{t}}$: vector tangential to tape surface and parallel to cross-section, $\hat{\mathbf{h}}$: helical vector, also tangential to tape surface, $\hat{\mathbf{n}}$: vector normal to tape surface).

the electric potential gradient. This equation directly relates each component of $\vec{\mathbf{E}}$ with those of $\vec{\mathbf{A}}$ and $\nabla\phi$. Since we only need to compute the helical component of J, we can revert to the scalar form of (4.11), i.e.,

$$E_h = -\frac{\partial A_h}{\partial t} - \nabla V \,, \tag{4.12}$$

where E_h and A_h are the helical components of $\vec{\mathbf{E}}$ and $\vec{\mathbf{A}}$, and ∇V is a constant representing the voltage per unit length of tape, which drives the desired helical current in each tape. One should note that ∇V is different from $\nabla\phi$ since the former has only a helical component, whereas the later may also have a transverse component, which we do not need to evaluate explicitly. In what follows, we drop the "h" index denoting the helical components.

To obtain an equation in terms of J, we first use the classical $E - J$ constitutive equation (in its scalar form), i.e.,

$$E = \rho J \,, \tag{4.13}$$

where, ρ represents the intrinsic resistivity of the tapes. In its general case, ρ can be a constant (i.e. metallic conductors) or a function of other electromagnetic variables, such as $\vec{\mathbf{J}}$ or $\vec{\mathbf{B}}$ (the magnetic flux density), such as in superconductors.

Inserting (4.13) into (4.12), and applying a simple point collocation technique to obtain a discrete set of equations in which the helical current density J_i and the resistivity $\rho(J_i)$ are assumed piecewise constant by element (but not necessarily linear), we obtain

$$E_i = \rho(J_i)J_i = -\frac{\partial A_i}{\partial t} - \nabla V \,, \tag{4.14}$$

where, i corresponds to the i_{th} element ($1 < i < n$), and n denotes the total number ele-

ments in the discretized domain. For convenience, we assume that all J_i and A_i are evaluated at the center point of each element.

The above equations are now expressed in matrix form, i.e.,

$$\mathbf{diag}[\rho(J_i)]_{n \times n}[\mathbf{J}]_{\mathbf{n}} = -\frac{\partial}{\partial t}[\mathbf{A}]_{n \times 1} - [\nabla \mathbf{V}]_{n \times 1} \,, \tag{4.15}$$

where $\mathbf{diag}[\rho(J_i)]$ represents an n by n matrix whose diagonal entries corresponds to the resistivity of each element i. In addition, $[\mathbf{J}]$ and $[\mathbf{A}]$ are respectively the column vector representation of the helical components of the current density and magnetic potential in all elements of the problem, i.e., the components tangential to the helical trajectory of the tapes. Finally, we emphasize that all n entries of $[\nabla \mathbf{V}]$ are identical, since ∇V is a constant when all tapes are identical, symmetrically arranged and carry the same transport current.

As a last step towards an equation expressed only in terms of $[\mathbf{J}]$, results of the second section of this paper are employed to provide a direct relationship between $[\mathbf{A}]$ and $[\mathbf{J}]$, i.e.,

$$[\mathbf{A}]_{n \times 1} = [\mathbf{M_A}]_{n \times n}[\mathbf{J}]_{n \times 1} \,, \tag{4.16}$$

where the each helical sheet current densities j required in (4.8) or (4.10) is related to the preceding J through $j_i = d\,J_i$, where d is the actual thickness of the tapes. Within this paper, we used a combination of both methods proposed in the second section to determine these coefficients, i.e., the semianalytic approach was used to find the helical component of $\vec{\mathbf{A}}$ when the observation point was located within or close to the source element, (singular or nearly singular points), and the numerical integration was used otherwise. Although this procedure proved to be relatively fast, it could further be optimized. To model a long cable, the contribution of each twisted strip has to be considered over a sufficient number of pitches (n_p). An adequate figure seems to be around $n_p \gtrsim 20L/R$.

In the general case, the generation of the $[\mathbf{M_A}]$ matrix takes a long time. However, due to the particular helical symmetry encountered here, and since we assume the same current distribution in each tape, $[\mathbf{M_A}]$ can be fully generated with the computation of its first row only, by using a cyclic permutation of the coefficients. In addition, since the determination of $[\mathbf{M_A}]$ depends only on the geometrical data of the problem, it can be generated only once for a given geometry and reused multiple times to perform parametric analysis involving other non-geometric parameters, such as varying the transport current, the resistivity, and so on.

To obtain our final equation, we insert (4.16) into (4.15), which results in the following equation :

$$\mathbf{diag}[\rho(J_i)]_{n \times n}[\mathbf{J}]_n = -\frac{\partial}{\partial t}([\mathbf{M_A}]_{n \times n}[\mathbf{J}]_{n \times 1}) - [\nabla \mathbf{V}]_{n \times 1} \,. \tag{4.17}$$

To obtain our final equation, we insert (4.16) into (4.15), which results in the following equation :

$$\mathbf{diag}[\rho(J_i)]_{n\times n}[\mathbf{J}]_n = -\frac{\partial}{\partial t}([\mathbf{M_A}]_{n\times n}[\mathbf{J}]_{n\times 1}) - [\nabla\mathbf{V}]_{n\times 1}\,. \tag{4.18}$$

This equation can be used to solve both voltage driven or current driven problems. In the first case, ∇V is supposed as known, and correspond to a voltage source expressed per unit length. In the second case, ∇V is unknown, and one must write an additional equation to impose a given transport current in one tape. The way to do this was already described in details in [76], so it is not repeated here.

Regarding the time derivative appearing in (4.18), it can be dealt with differently depending on the nature of the resistivity. If the later is linear and the excitation is periodic, a simple time-harmonic solution can be used (J and ∇V are then complex) and yield to solutions quickly. However, if the resistivity is non-linear, such as with superconductors, one need a full solution to the time transient problem, and a proper time integration algorithm must be used (e.g. Euler, Runge-Kutta, etc.). To improve the convergence of the solution process, it is highly recommended to use adaptive time transient solvers, such as "ode45" or "ode15s" available in *Matlab* [77], or even more sophisticated solvers such as "DASSL" or "DASPK" [78, 79], available in various public code distributions, such as the *Sundials* solver suite [80], which was used here. Further details about how we formulated the final equations in order to use *Sundials* can be found in [64].

Finally, since we solve for J, we do not automatically have access to the magnetic field or flux density components. If these quantities are of interest, they can be computed with the help of the analytic formulas proposed in [81] for thin rectangular current sheets (see Appendix B), in a similar way to the semi-analytic method proposed in the second section of this paper. Unless the resistivity of the tapes depends on $\vec{\mathbf{B}}$, these computations can be done only as a post-processing step. Indeed, if one wishes to know the field at given observation points (say m points), suffices to evaluate the following matrix-vector products for obtaining either the helical ($\hat{\mathbf{h}}$), tangential ($\hat{\mathbf{t}}$) or normal ($\hat{\mathbf{n}}$) component of $\vec{\mathbf{B}}$ (see figure 4.5), i.e.

$$[\mathbf{B_h}]_{m\times 1} = [\mathbf{M_{B_h}}]_{m\times n}[\mathbf{J}]_{n\times 1}\,,$$
$$[\mathbf{B_t}]_{m\times 1} = [\mathbf{M_{B_t}}]_{m\times n}[\mathbf{J}]_{n\times 1}\,,$$
$$[\mathbf{B_n}]_{m\times 1} = [\mathbf{M_{B_n}}]_{m\times n}[\mathbf{J}]_{n\times 1}\,. \tag{4.19}$$

If we choose to compute the field at the center of each element, we have $m = n$, and we also end up with a significant economy in computation time, since by symmetry, only the first row of $[\mathbf{M_B}]$ needs to be computed (similarly to the case of $[\mathbf{M_A}]$).

4.4   Validation of the numerical method

4.4.1   Experimental benchmark

To assess the validity of the method previously presented, we performed experimental measurements on samples made of HTS tapes. We chose HTS tapes for two major reasons. First, the main purpose of the method is to determine the current distribution and AC losses in HTS coils and cables. Second, although the current distribution cannot be measured experimentally, we can measure the AC losses under a sinusoidal transport current. Due to the mechanism by which these losses occur, the value of the AC losses is very sensitive to the field and current distributions inside the superconducting sample. Therefore, obtaining a good prediction of AC losses under various experimental conditions (different transport currents and helical configurations of the HTS tapes) should be a sufficient condition to consider the numerical results as valid.

The selected HTS conductor used to perform the experiments was an IBAD (Ion Beam Assisted Deposition) YBCO coated conductor tape, manufactured by *SuperPower*. The tape width was 12 mm, and the thickness of its superconducting YBCO layer was 1 μm. To assess the reliability of the numerical method for a diversified range of geometrical parameter, simulation and experimental results were compared when the tape is not twisted (isolated straight tape) and when the tape is helically wound with two different twist pitches (solenoid-type cable). The solenoidal configuration has the advantage of ensuring that the total current is the same in every tape section, a condition that would be difficult to satisfy experimentally for short cable samples made of multiple tapes.

In our cable samples, the 12 mm tape was wound around a cylindrical former of 11.26 mm of radius. The two pitch lengths chosen were of 15.4 mm and 13.3 mm, resulting in respective gaps of 3 mm and 1 mm between two adjacent turns of the coil. To ensure that the prototypes
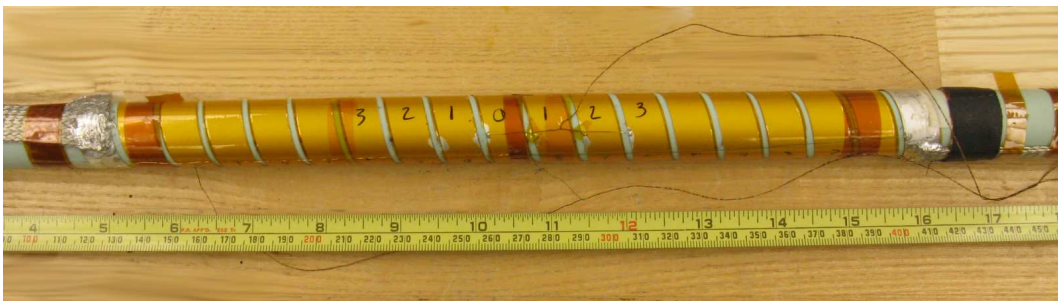
Figure 4.6 Solenoid-type cable made of 12 mm wide HTS YBCO tape helically wound on a former of 11.26 mm of radius. This cable was used to obtain experimental AC loss values, required to validate the numerical method introduced in this paper.

behave as "long" cables, the tape was wound over $n_p = 16$ pitches. Figure 4.6 shows the first solenoidal cable prototype, i.e., the one with a pitch length of 15.4 mm and a gap of 3 mm.

In all three experimental scenarios considered, a series of 50 Hz sinusoidal transport currents were imposed in the tape. The peak value of the imposed current was progressively increased from $\approx 15\%$ to 90% of the critical current of the tape ($I_c = 320$ A), whereas the losses were measured over the 2 middle turns. The results are presented in the next section.

4.4.2 Numerical simulations

In the numerical simulations, the tape was discretized into 150 elements along its half-width. The non-linear resistivity of the YBCO tape was modeled with a classical power law characteristic, which is known to be quite representative of the HTS behavior when J is in the range of J_c, i.e.,

$$\rho = \frac{E_c}{J_c} \left| \frac{J}{J_c} \right|^{p-1} \tag{4.20}$$

where E_c is the electric field criterion ($E_c = 10^{-4}$ V/m), p is the power law exponent ($p = 50$), and J_c is the local critical current density. In what follows, J_c was chosen as to be non-uniform across the width of the sample, i.e. $J_c = f(x)$, where $f(x)$ is shown in figure 4.7. This choice follows from good fits obtained between simulation and experimental results published previously for the same type of HTS tape [82]. In this paper, we used a value of $J_{c0} = 2.8 \times 10^6$ A/cm^2, corresponding the critical current value of $I_c = 320$ A mentioned previously.

The $[\mathbf{M_A}]$ matrices required for each simulation case (straight tape, and two helical cables with different twist pitches) were generated in less than 40 s. They were generated only once, and re-used for each simulation scenario. Regarding the simulation times themselves, for each transport current imposed in the tape, the solver converged and provided the AC loss results within a few seconds (most often less than 10 s). This is a significant reduction in computation time if we compare to the closest procedure found in literature, where simulation times in the range of hours or even days were reported [66].
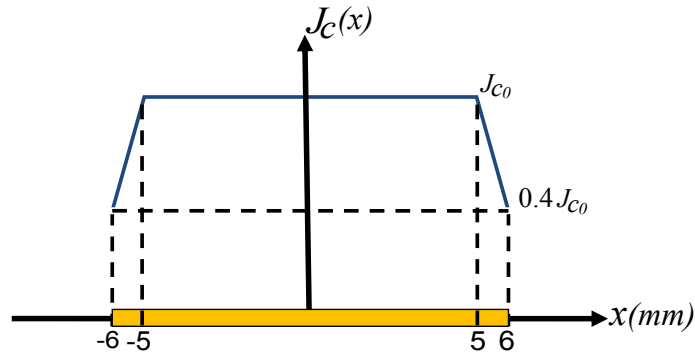
Figure 4.7 Model of the critical current distribution in the YBCO tape used in the prototype cable. This $J_c(x)$ function was taken from [82], where it was shown to fit well with experimental measurements.

4.4.3 Comparison of numerical and experimental results

The AC losses can be computed from the J profiles obtained by numerical simulation with the help of the following formula :

$$Q = 2 \int\limits_0^{1/f} dt \int\limits_0^{w/2} \rho J^2 dl \,. \tag{4.21}$$

One should note that this formula gives the AC losses per unit length of tape, not per unit length of cable. The AC losses per meter of tape provide a better comparison of the intrinsic losses, especially in this case, since all cable samples were made with a single tape.

The AC loss results obtained by simulation are shown in figure 4.8, together with the experimental values, for the three cases considered in this paper. As expected, the losses decrease as the gap size decreases (highest losses for the isolated tape). In all cases, we observe an excellent agreement between the predicted values and the measured ones, which supports the validity of the numerical simulations.

In figure 4.9, the field and current distributions along the cross-section of the helical tape are shown for the two twisted cables above, corresponding to gaps of 1 mm and 3 mm respectively. The profiles shown correspond to the maximum of a peak transport current of 220 A, i.e. $\approx 0.7 I_c$. Although the current distribution was obtained directly from the numerical computations, the field components were obtained as post-processed quantities derived with the help of (4.19). Still, in figure 4.9, we observe that the normal component of the field (B_n) is higher near the edges of the tape and penetrates further towards its center when the gap is larger. We also observe that the tangential component of the field (B_t) is in the same range of values as B_n (even slightly higher near the edges), and even increases
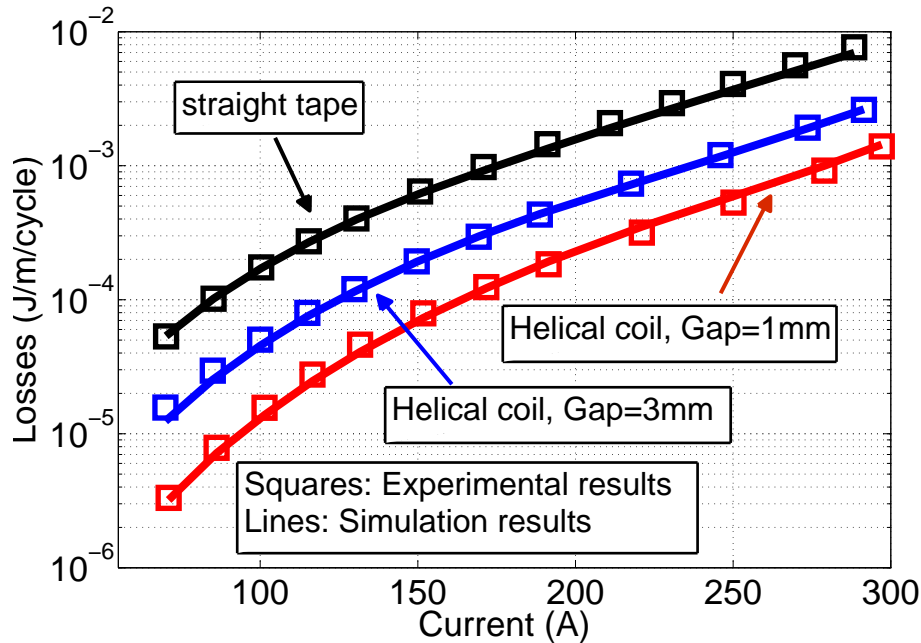
Figure 4.8 Measurements (squares) and simulations (lines) of AC losses per unit length of tape for a straight and helically wound HTS tape as a function of the transport current. The same 12 mm wide tape sample was used for all three experiments.

at the center when the gap is larger. The helical field component (B_h), corresponding to the component parallel to J, is the smallest one (roughly 5 times less than B_n). It decreases as the gap size increases, and is nearly independent of the position along the tape width. This was intuitively predictable since this component must tend towards zero as the gap size increases, meaning that the solenoid-type cable tends to be a straight tape. As a consequence of these field distributions, it is observed that, for small gaps, the current tends to distribute itself more uniformly within the tape, with reduced peaks near the edges, and thus reduced losses.

Although relatively convincing, these simulations did not allow us to clearly identify the important parameters for optimizing AC losses in HTS cables made of multiple conductors. This important question is more complicated than it appears at first sight. For instance, one could reasonably suppose that the AC losses are dominated by the penetration of the magnetic field at the edges of the tapes, which is itself strongly related to the gap size. Therefore, we might think that a simple 2-D simulation of the cable cross-section could in principle be sufficient to get quantitative data about the impact of the gap size. However, for a given combination of twist pitch, tape width and gap size, the former radius is automatically fixed. A 2-D analysis (no twist pitch) using the same parameters therefore implies that the former radius must change, and then the problem is no longer the same as before. One could

think about adding tapes to keep the former radius constant, but then the total current carrying capability of the cable increases, increasing the magnitude of the field components, and consequently the AC losses. Therefore, it does not seem possible to neglect the twist pitch and simply use 2-D simulations for the purpose of properly optimizing a cable design, and this issue will inevitably get more complicated for multi-layer cables.

A comprehensive parametric analysis of single-layer cable layouts requires a different methodology than what was presented here, it will be addressed in a separate publication.

4.5   Conclusion

In this paper, we have presented a new numerical approach to finding the current distribution and the field components in helically wound thin conductors, such as HTS YBCO tapes. The method is particularly well suited for solving problems where one or many of such thin conductors are symmetrically positioned with respect to each other, in a coaxial arrangement. The method does consider the real helical configuration of the tapes, and approximates their geometry as infinitely thin strips. The approach relies on symmetry arguments to formulate the discrete problem with a minimum number of degrees of freedoms. Since the non-linear resistivity of the HTS material can be easily inserted in the model, the method can be applied to analyze single layer power cables made of twisted HTS coated conductors. The accuracy of the method was verified by comparing the AC losses obtained by simulation with experimental results. An excellent agreement was found for the three different cases considered in this paper. The typical computation time required to solve a problem is in the range of seconds, which is a significant improvement over existing methods. This method could be used to determine the optimal geometric parameters to devise low-loss HTS power cables.
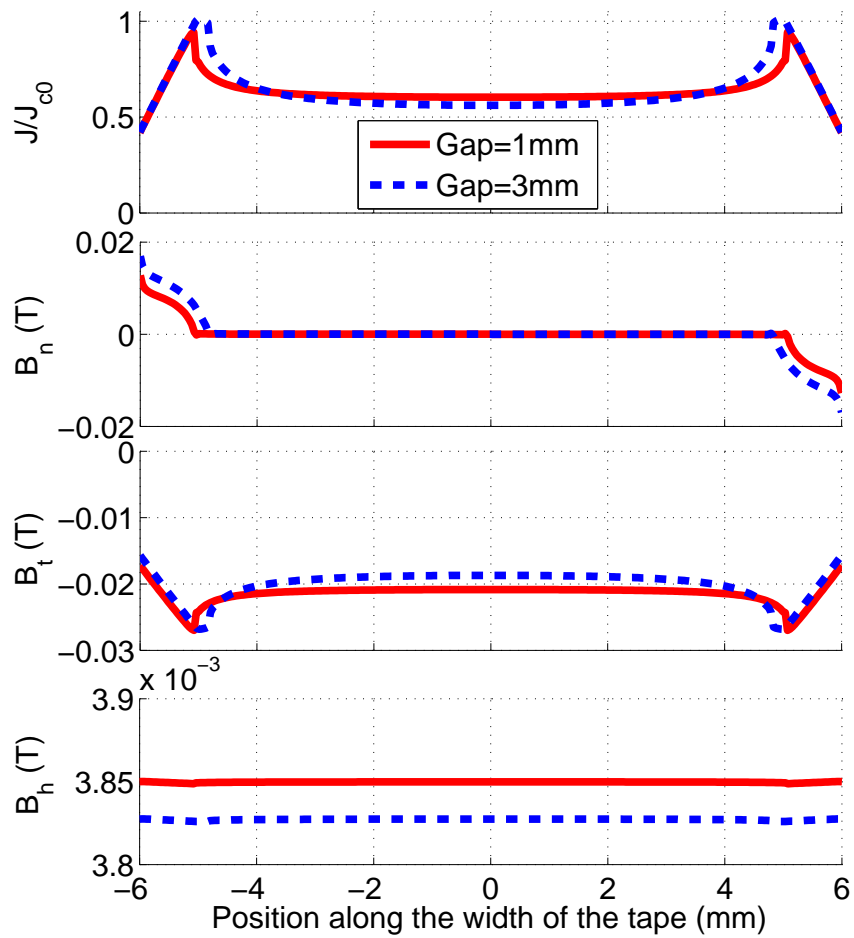
Figure 4.9 Simulation results for the current density (normalized) and for the components of the magnetic flux density along the width of the helically wound HTS tape at a peak transport current of 220 A, corresponding to $\approx 0.7 I_c$.

CHAPTER 5

REDUCTION OF AC LOSSES IN HTS POWER TRANSMISSION CABLES MADE OF COATED CONDUCTORS BY OVERLAPPING THE TAPES

Majid Siahrang and Frédéric Sirois

École Polytechnique de Montréal

Abstract

In this paper, we investigate the effectiveness of an alternative design scheme to reduce the AC losses in HTS power transmission cables made of non-ferromagnetic HTS coated conductors. With this design, the adjacent tapes of each layer of the cable overlap each other up to a certain distance from their edges, typically 1 or 2 mm. Using two different numerical methods, an integral technique and a finite element method, we performed a parametric investigation of the idea of overlapping the tapes in the case of a single-layer HTS power cable. Through the simulation results, we show that overlapping the tape leads to an important reduction in the AC losses of the cable (typically two to five times), mostly due to an advantageous redistribution of the current in tapes.

5.1 Introduction

Transmission of power through High Temperature Superconducting (HTS) cables is one of the most promising industrial application of HTS materials for commercialization in the near future. The reduction of electric power dissipation due to alternating current flow in HTS conductors, commonly called AC losses, is a key technical issue in the development of HTS cables. Although these losses are relatively small as compared to the range of power dissipated in copper cables, the generated heat must be extracted from the cryostat to the ambient environment in order to keep the temperature of the superconductor below the critical temperature. Because of the large difference between the conductor's temperature and the ambient temperature, heat removal requires a bulk and costly cryogenic system.

Reduction of the AC losses therefore contributes to a significant reduction in the capital and operational costs of HTS cables and makes them more competitive with respect to other technologies.

In the latest generation of HTS power cables, YBCO coated tapes are the conductors of choice. In the typical design of HTS power transmission cables, these tapes are helically wound around cylindrical formers in single or multi-layer coaxial arrangements. Figure 5.1 shows a cross-sectional view of a single-layer HTS power cable made of eight coated conductors. Due to the helical configuration, the wide face of the tapes are curved along the surface of the cylindrical former around which the tapes are wound. With this design scheme, small gaps separate the adjacent tapes of each layer. From a pure electromagnetic point of view, the most favorable design to achieve minimum losses occurs when these gaps are completely closed [33, 70, 71]. But the minimum size of the gap is inevitably limited by the need for mechanical flexibility and by the winding process of the cable. In the current design of HTS cables, the minimum size of the gap is limited to ≈ 0.6 to 0.8 mm [33].

In this paper, we investigate a new design scheme for HTS power transmission cables made of coated tapes. This design has been already suggested in a patent by Superpower [69], but there are no quantitative effectiveness data and detailed analysis of the electromagnetic behavior for this design in literature. In this design, the adjacent tapes of a given layer overlap each other over a certain distance from their edges. Through simulation results, we show that this design leads to a considerable reduction in AC losses in HTS power transmission cables. In addition, this design seems realizable in practice and would not prevent the cable from being bent, as required in a field installation.

This paper is organized as follows : firstly, we introduce the new design in more details. Secondly, we introduce two different numerical models that were used to perform parametric simulations to assess the effectiveness of the new design on AC loss reduction in the case of a single-layer, untwisted HTS power cable. Finally, we discuss the reasons for the reduced AC losses obtained with this design.

5.2 Overlapped design

In the proposed overlapped design, the constituting tapes of each layer of the cable are symmetrically positioned around a cylindrical former, similar to the typical design. However, instead of having a gap between the tapes, the adjacent tapes of each layer periodically overlap each other over a certain distance from their edges, as shown in figure 5.2.

To mathematically define the overlapped design in the 2-D cross-section of the cable, we assumed that, unlike in the typical design, the edges of the constituting tapes are located at
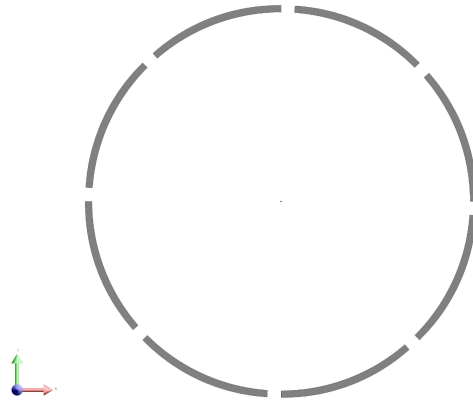
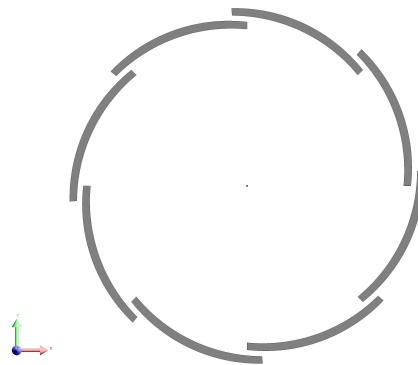Figure 5.1 Cross-sectional view of a single-layer HTS cable (typical design).

Figure 5.2 Cross-sectional view of a single-layer HTS cable (Overlapped design)

two different distances from the center of the former. As shown in figure 5.3, let us consider R_1 as the radius of this cylinder. If, for instances, the rightmost edge of each tape is located on the former circumference, the leftmost edge must be positioned at a distance of R_2 meter from the center point of the former. To complete the definition of the overlapped design without any ambiguity about the positioning of the tapes, we assume that the wide face of the tape is conformed with a cylinder of radius of R_3 (illustrated by the dashed lines in figure 5.3), where R_3 is the average of R_1 and R_2 (i.e. $R_3 = (R_1 + R_2)/2$).

As shown in figure 5.4, in the overlapped design, two geometric parameters are introduced :
- The *vertical gap*, which is defined as the vertical distance between the bottom of the adjacent tapes.
- The *overlap distance*, which is the distance along which the adjacent tapes overlap each other.

5.3   Overlapped design vs typical design

5.3.1   Numerical methods

To assess the effectiveness of the overlapped design, we used two different numerical methods to perform a parametric study on the AC loss behavior of a single-layer HTS cable made of coated conductors. Since these methods are quite different in nature, they were used to validate each other. In both of these methods, the helical configuration of the tapes was neglected. Therefore, due to the invariance of the physical quantity along the length of the cable, the problem could be formulated in the 2-D cross-section of the cable.

Integral method (IM)

In this method, we used a point collocation method (Brandt-type formulation) for solving the electric field equation at low frequency [63, 76], on a 2-D cross-section of the cable, i.e.

$$E = -\frac{\partial A}{\partial t} - \nabla V \tag{5.1}$$

where E, A and ∇V are the z components of the vectors of the electric field, magnetic potential and potential gradient, respectively. Since we consider each tape identical, the electromagnetic problem can be entirely solved over a domain consisting in a single tape.

In this model, we considered only the superconducting layer of the tapes, and no magnetic material is involved. To obtain a discrete system of equations from (5.1), the HTS layer of the tape was discretized into many interconnected line elements along its width. In order to consider the current distribution across the thickness of the tapes, the discretization is done
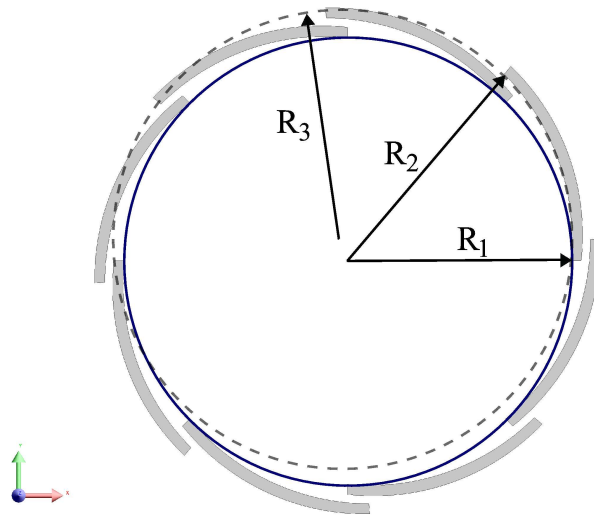
Figure 5.3 Mathematical introduction of the overlapped design
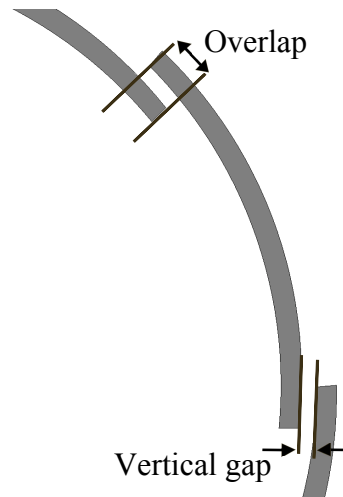
Figure 5.4 Geometrical parameters of the overlapped design

along three parallel 1-D domains, which divide the tape into three identical sub-domains as shown in figure 5.5.

Since we are interested in solving (5.1) to obtain J in each element, where J is the z component of the current density vector inside the tapes, we have to rewrite A and E in (5.1) in term of J.

To establish a relationship between J and A in (5.1) for all the elements of the study domain, we used the analytical solution of the Biot-Savart potential integral for an infinitely long straight current sheet of j A/m (shown in 5.3.1). This analytical solution is

$$A_z(x, y) = \frac{\mu_0 j}{8\pi} \left\{ 8a + 4y \left(\arctan\left(\frac{D}{2y}\right) + \arctan\left(\frac{C}{2y}\right) \right) \right.$$
$$\left. + D \ln\left(y^2 + \frac{D^2}{4}\right) + C \ln\left(y^2 + \frac{C^2}{4}\right) \right\}, \tag{5.2}$$

where $C = 2(a - x)$, $D = 2(a + x)$, $2a$ is the width of the current sheet, and (x, y) is the coordinate of the observation point.

Using (5.2) we introduce an n by n matrix $[M_A]$, which provides a direct relationship between J and A in all the n elements of the study domain, i.e.

$$[A]_{n\times 1} = [M_A]_{n\times n}[J]_{n\times 1}. \tag{5.3}$$

To find the entries of $[M_A]$, we inject a sheet current density of $j = 1$ A/m into each element of the study domain and compute A at the middle point of all the elements with the help of (5.2). The computed values of A must be divided by the thickness of each line element, i.e. one third of the thickness of the HTS layer, to obtain dimensionally correct entries in $[M_A]$. It is worth mentioning that, although the problem is formulated inside only one tape, the contribution of all the other constituting tapes must also be taken into account to set up the $[M_A]$.

In order to write E in the left side of (5.1) in term of J, we use the $E - J$ constitutive equation, i.e. :

Figure 5.5 Discretization of the superconducting layer of one tape into magnetically coupled line elements in the IM model. Although it is pictured as a straight line, the domain is actually curved.
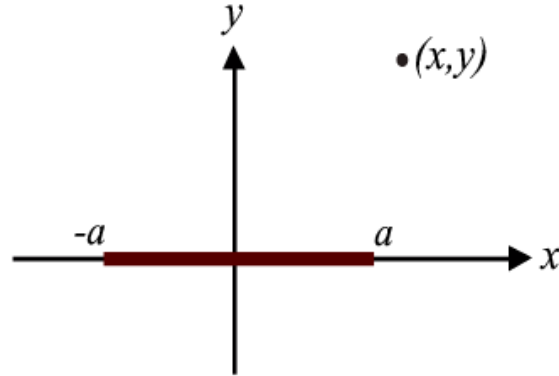
Figure 5.6 2-D cross-section of an infinitely long current sheet of width $2a$.

$$E = \rho J, \tag{5.4}$$

where, ρ represents the intrinsic resistivity of the conductor. To introduce the non-linear resistivity of the HTS layer of the tapes in (5.4), we used the classical power law model, i.e. :

$$\rho = \frac{E_c}{J_c} \left| \frac{J}{J_c} \right|^{k-1}, \tag{5.5}$$

where, E_c is the electric field criterion $(1 \times 10^{-4}$ V/m$)$, J_c is the critical current density of the HTS material, and k is the power law index.

With the help of (5.2), (5.4) and (5.5) to eliminate A and E, (5.1) can be expressed in term of J as :

$$\text{diag}[\rho(J_i)]_{n \times n}[J]_n = -\frac{\partial}{\partial t}([M_A]_{n \times n}[J]_{n \times 1}) - [\nabla V]_{n \times 1}, \tag{5.6}$$

where $\text{diag}[\rho(J_i)]$ represents an n by n matrix whose diagonal entries correspond to the resistivity of each element i, obtained by (5.5). All the entries of $[\nabla V]$, which represent the voltage per unit length of the tape, are identical. When a voltage is applied across the cable, ∇V is known and J in all the elements constitute the n unknowns of the problem. In the case of imposing a known current to the tapes, ∇V is unknown. In this case, as the $(n+1)^{th}$ equation, we use a current constraint equation, i.e.

$$I = s \sum_{i=1}^{n} J_i \tag{5.7}$$

where, I is the injected current into the tape and s is the area of each element.

Due to the strongly non-linear resistivity of HTS materials, a proper time integration

algorithm must be used (e.g. Euler, Runge-Kutta, etc.) (5.6). In order to speed up the solution process, we used the DASPK algorithm [78, 79] which is available in various public code distributions, such as the *Sundials* solver suite [80]. More details about the problem formulation and using *Sundials* to solve it can be found in [76].

To solve (5.6) we assume that J is constant within each element. When the J values in all the elements of the study domain are known, the AC losses (expressed in W/m/tape) are obtained through

$$Q = \frac{s}{n_{pc}} \sum_{i=1}^{n_{pc}} \sum_{j=1}^{n} \rho_{i,j} \, J_{i,j}^2, \tag{5.8}$$

where n_{pc} is the number of points per cycle in the solution vector, and s is the cross-section of each element (assumed uniform over the domain).

Finite element method with edge element formulation

This method is a finite element method (FEM) which is based on the first-order edge element formulation [57]. This model has been widely used in electromagnetic modeling and AC loss analysis of HTS materials [56, 71, 82].

As shown in figure 6, thanks to the symmetry, the study domain of the problem can be defined inside a triangular area, while cyclic periodic boundary conditions must be applied to edges OA and OB, and a regular Neumann boundary condition is used on edge AB (i.e. the normal flux is zero on the outer boundary). Since this method is based on the numerical solution of partial differential equations, we have to mesh the surrounding air region in addition to the tape domains, as opposed to the IM method introduced previously. As a consequence, the number of degrees of freedom of the FEM model is much larger than that of the IM model. Although this could be seen as a disadvantage, we will take
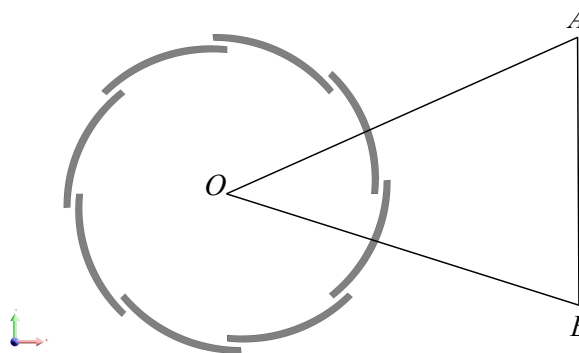

Figure 5.7 Illustration of the study domain in the FEM model

it as an opportunity to model all the constituting layers of the IBAD coated conductors considered in this investigation (shown in figure 5.8). However, in order to be able to mesh all the constituting layers of the HTS tape with a reasonable number of elements, we used a "mapped mesh" (i.e. quadrilateral elements), which allowed us to mesh the YBCO layer to its real thickness of 1 μm (no scaling of the geometry, as in most work found in literature).

In this paper, we used the IM model for all parametric analysis, because it was much faster, and we restricted the use of the FEM model for the field analysis and verifying the results obtained with the IM model for some specific cases only.

5.3.2   Simulation scenarios

The HTS cable model considered in this paper consisted of eight identical 10 mm wide YBCO coated conductors (IBAD-type, no ferromagnetic substrate). These two parameters were kept constant throughout all simulations, as well as the critical current density per tape, which means that the current rating of the cable remained the same in all the simulated cases.

We started the simulations by considering the typical cable design. The size of the gap was gradually reduced from 1 mm until it was completely closed (gap=0). Then, for the overlapped design, we considered two different vertical gaps (0.15 and 0.25 mm), and we gradually overlapped the adjacent tapes up to 2 mm from their edges. Since the number of the tapes and their width were kept constant throughout all simulations, the radius of the cable followed directly from the choice of parameters, i.e. it was a function of the gap in the typical design, and a function of both the vertical gap and the overlap distance in the overlapped design.

Regarding the critical current density of the tapes, we considered both of the following cases :

   – A critical current density (J_c) that is uniformly distributed along the width of the tapes

   – A non-uniform J_c, which is lower near the edges of the tapes and uniform in the middle
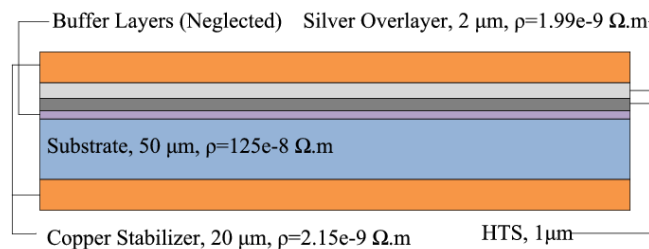

Figure 5.8 Layers of IBAD YBCO coated conductors considered in the FEM model (IBAD : Ion Bean Assisted Deposition). The electrical properties at 77 K were taken in [83].

part (resulting from the slitting process)

In all cases, the critical current of each tape was 270 A. This means $J_c = 2.7e10$ A/m² when the critical current density is uniform. In the non-uniform case, we used the $J_c(x)$ pattern presented in figure 5.9, resulting in $J_{c0} = 2.87e10$ A/m². This pattern has been used in previous work and has shown a good agreement between the experimental and simulation results in [82] and it has been verified again in [70]. In all the above cases, a 50 Hz sinusoidal transport current with an amplitude of 190 A ($0.7I_c$) was injected into each tape, and the AC loss per tape was computed as a function of the geometrical parameters.

In addition to this, we also investigated the AC losses resulting from the overlapped design over a wide range of transport currents, i.e. $0.1I_c < I < I_c$, with an overlap distance of 0.5 mm and a vertical gap of 0.15 mm. For the same range of transport currents, these results were compared with the AC losses resulting from a typical cable design, considering that the gap had the optimistic size of 0.5 mm.

To verify the accuracy of the results obtained with the IM method, we employed the FEM model to obtain the AC losses in one of the simulated cases. To do so, we chose the overlapped design when the vertical gap and the overlap distance were 0.15 mm and 1 mm, respectively. Figure 5.10 shows the meshed geometry used for the FEM simulations.

The simulation parameters used with both the IM and the FEM models are presented in table 5.1.

5.3.3 Simulation results

Figure 5.11 and 5.12 show the AC losses (per unit length of tape) in one tape of the cable as a function of the gap size (typical cable design), and for two different vertical gaps as a function of the overlap distance (overlapped cable design). Figure 5.11 shows the case with uniform J_c, and figure 5.12 corresponds to the $J_c(x)$ pattern illustrated in figure 5.9.

Table 5.1 Simulation patameters used in numerical simulations

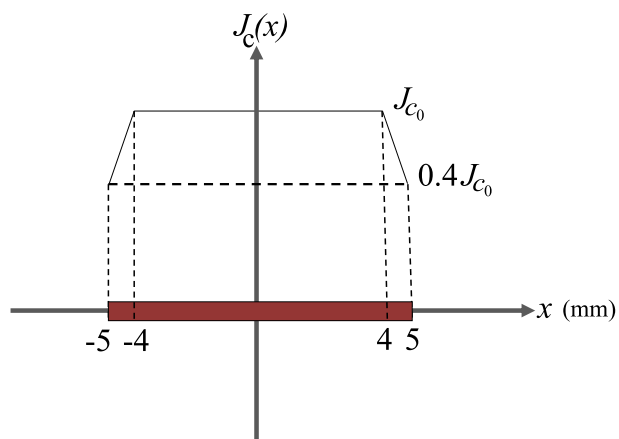| Parameter	IM model	FEM model
Critical current of the tape (A)	270	270
Peak of the imposed current (A)	190	190
Power law index (k)	50	50
Frequency (Hz)	50	50
Gap (typical design)	0 :0.05 :1	-
Overlap distance (mm)	0 :0.05 :2	1
Vertical gap (mm)	0.15 and 0.25	0.15
Number of degrees of freedom	3×300	21059

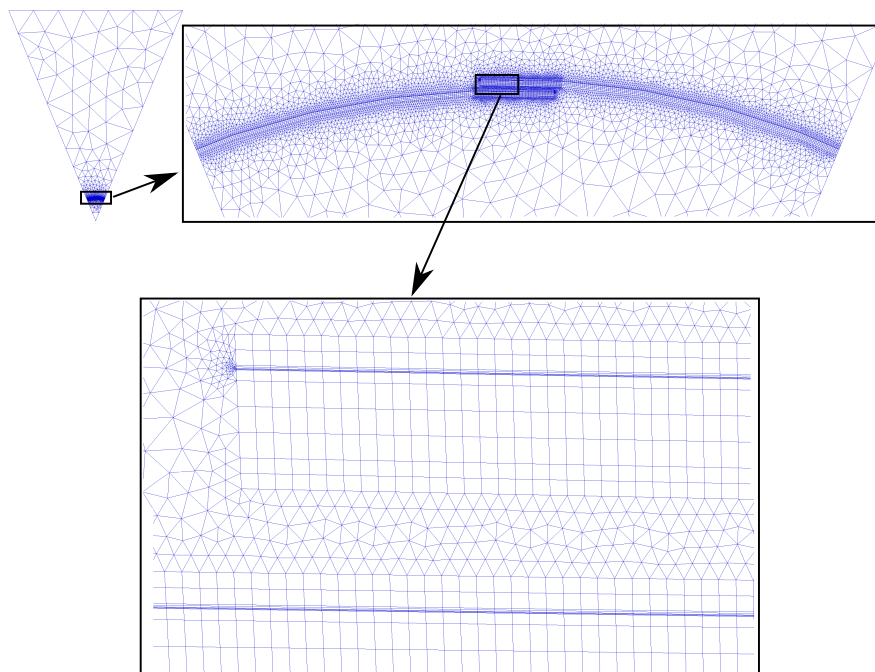Figure 5.9 Pattern used to define the non-uniform distribution of J_c in IBAD YBCO tapes.

Figure 5.10 Meshed geometry in the FEM model

We can observe in figure 5.11 and 5.12 that, for the typical design, when the size of the gap decreases, the AC losses decrease and reach the minimum value when the gap is completely closed. However, as mentioned previously, due to practical considerations, the lower limit of the gap can not be much smaller than $0.6 - 0.8$ mm. As an optimistic reference case, we took the case corresponding to a gap size of 0.5 mm as a comparison threshold with the overlapped design, shown as dashed lines in figures 5.11 and 5.12. In these two figures, one can see that the overlapped design can provide lower losses than the minimum possible losses achievable with a typical practical design. In particular, if we consider the case of a non-uniform J_c (figure 5.12), we observe that the overlapped design provide lower losses than the typical design even if the gap is completely closed in the typical design. That is to say that the lower J_c at the edge of the tapes acts as a "virtual gap" that cannot be closed mechanically, unless we accept to overlap the tapes.

Still in figures 5.11 and 5.12, one can see that the AC loss behavior of the overlapped design is very sensitive to the vertical gap size. As can be observed, the smaller the vertical gap is, the lower are the AC losses. However, similarly as for the gap size in the typical design, there might be a lower limit for the vertical gap in the overlapped design.

In figures 5.13 and 5.14, the AC loss behavior of the overlapped design (vertical gap of 0.15 mm ; overlap distance of 0.5 mm) is compared with the typical design (gap of 0.5 mm) as a function of the transport current. In figure 5.13, J_c is assumed to be uniform, while in figure 5.14, we considered the $J_c(x)$ distribution shown in figure 5.9. In figure 5.13, it is observed that, unless the amplitude of the imposed current is very close to the critical current of the tapes, lower AC losses can be achieved with the overlapped design. Figure 5.14 shows that the overlapped design always provides lower losses as compared with the typical design, regardless of the amplitude of the transport current. The best improvement is observed near $I/I_c = 0.9$, where we have a reduction of AC losses by a factor of 7.

In order to verify the simulation results, we used the FEM model to simulate a cable with the overlapped design when the vertical gap and the overlap distance were 0.15 mm and 1 mm respectively. Figures 5.15 and 5.16 show the instantaneous losses obtained with the IM and FEM methods, respectively, for the second cycle of the sinusoidal transport current, for uniform and non-uniform J_c distributions. In these figures, very good agreements are observed between the results obtained with both methods.

Since in the FEM model we considered all the constituting layers of the tapes (see figure 5.8), it was possible to determine the losses in each of these layers. As an example, the AC losses in all the constituting layers of one tape of the cable are presented in table 5.2, corresponding to the case of a vertical gap and an overlap distance of 0.15 and 1 mm respectively. As expected, the losses in the HTS layer are noticeably higher than in the other layers,
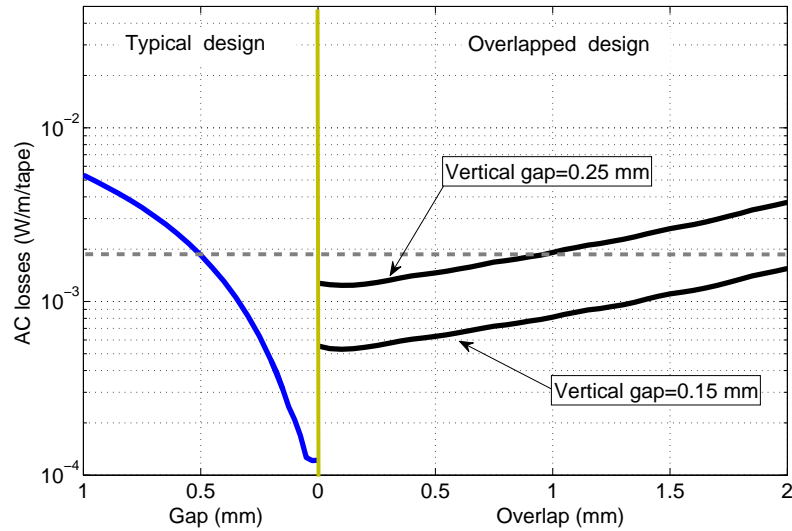
Figure 5.11 AC losses in one tape of the cable as a function of the geometric parameters, when J_c is uniformly distributed along the tape width. The dashed line corresponds approximately to the minimum losses achievable with a typical design (gap of 0.5 mm).
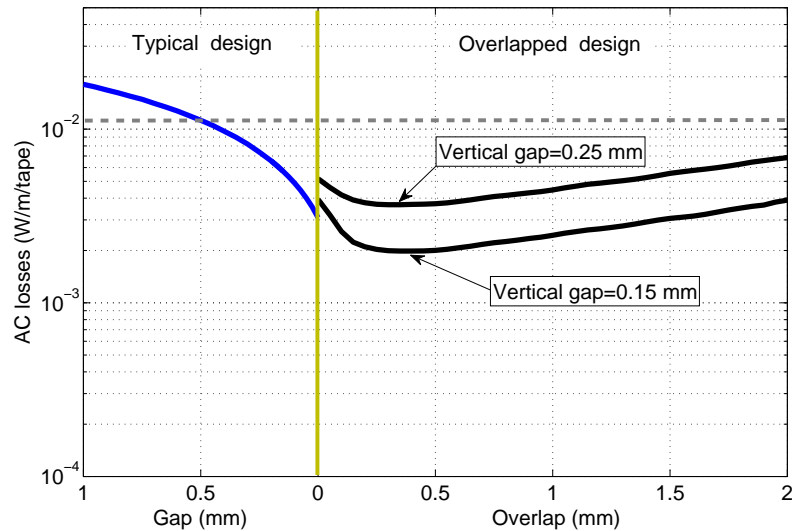
Figure 5.12 AC losses in one tape of the cable as a function of the geometrical parameters, when we considered a non-uniform J_c distribution along the tape width (see figure 5.9 for $J_c(x)$ pattern). In this case, the overlapped design always lead to lower losses than practical typical cable design (dashed line).
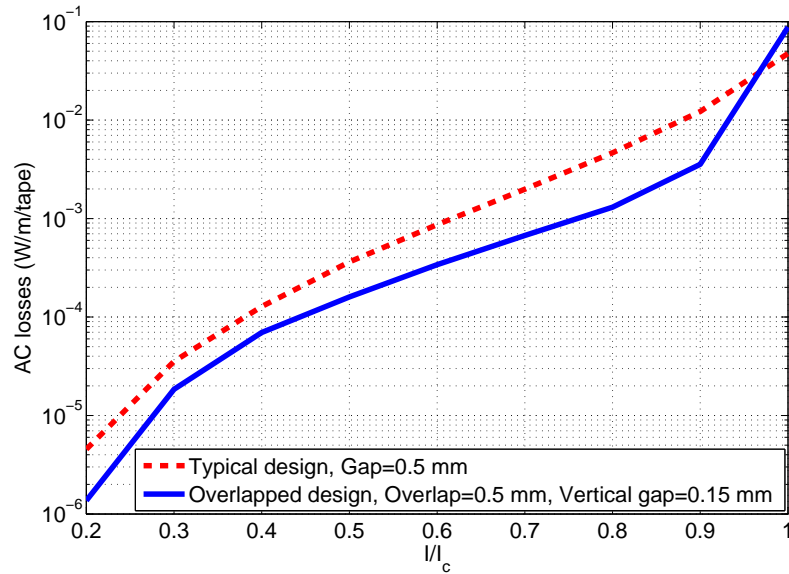
Figure 5.13 AC losses as a function of the normalized transport current, when J_c is uniform in the tapes.
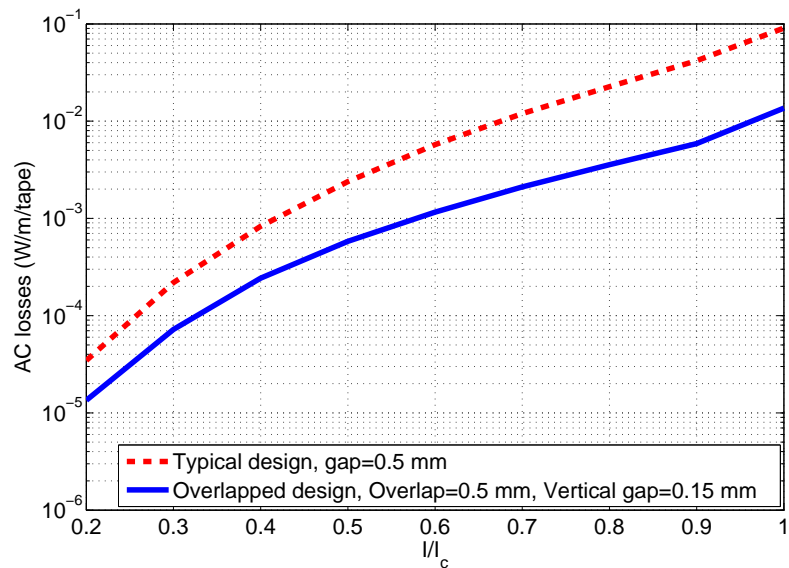
Figure 5.14 AC losses as a function of the normalized transport current, when a non-uniform distribution of J_c is considered

and one can neglect the losses in the other layers in comparison with those of the HTS layer. The agreement observed between the FEM model and the IM model in figure 5.15 and 5.16 and table 2 suggest that we can trust the results obtained by the IM method all along this paper.

5.3.4 Discussion

In order to get a better understanding of the mechanisms through which the overlapped design results in AC loss reduction over the typical design, we compared the current distribution along the width of the tapes in both cases. For the overlapped design, we chose 0.15 mm and 1 mm for the vertical gap and the overlap distance, respectively, and for the typical design, we chose a gap of 0.5 mm. To find the current profiles, the average value of J computed with the IM in the three layers shown in figure 5.5 was plotted as a function of the position along the width of the tape. These results are shown in figure 5.17.

In this figure, we clearly see that the current distribution inside the tapes is not symmetrical along their width in the case of the overlapped design. In particular, in the overlapped edge (rightmost part of the curve), the current density is very low (or even zero). In the case of a uniformly distributed J_c, this region is even almost empty of current. Another important observation is that, the current penetration in the overlapped design is also slightly lower in comparison with the typical design. Therefore, it can be deduced that, current in the overlapped design tends to flow with higher density in the middle part of the tapes.

This behavior can be explained as follows. Because of the overlap between the neighboring tapes, the system behaves almost as a continuous layer, resulting in a mostly tangential field aligned with the circumference of the cable. In the overlap region though, the top edge will still see a perpendicular field component, as shown in figure 5.18, whereas the bottom edge sees no field at all (thus no field gradient), which explains the absence of current density in that region, since $\vec{J} = \nabla \times \vec{H}$. In the typical design, the current distribution behaves symmetrically, and a perpendicular component of $\vec{H}$ (as well as a steep gradient of this perpendicular component) is seen both on the left and on the right edges of the tapes, producing a large current density in this region. These currents are responsible for the well known "edge losses".

Table 5.2 AC losses in one of the tapes of the cable

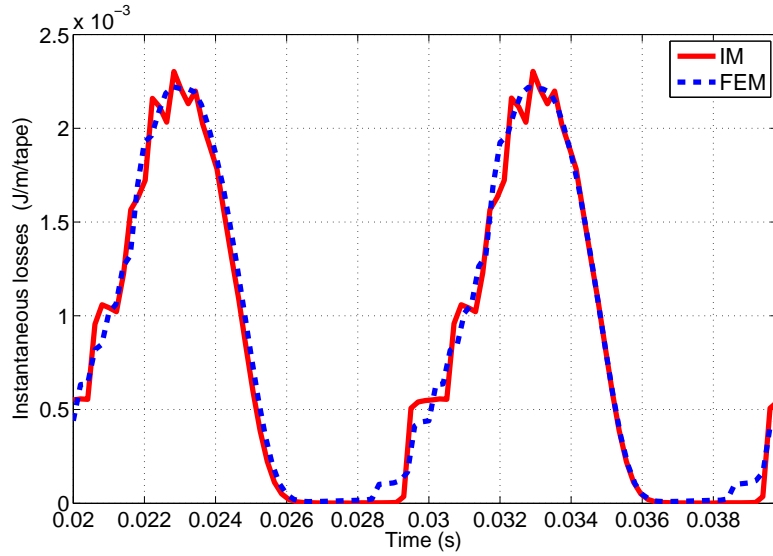|	FEM results (W/m)					IM results (W/m)
	Substrate	Upper stabilizer	Bottom stabilizer	Silver overlayer	HTS layer	HTS layer
Uniform J_c	2.14×10^{-10}	7.22×10^{-6}	2.43×10^{-8}	1.03×10^{-8}	8.27×10^{-4}	8.12×10^{-4}
$J_c(x)$	2.17×10^{-9}	1.62×10^{-6}	2.44×10^{-7}	9.28×10^{-8}	2.39×10^{-3}	2.44×10^{-3}

Figure 5.15 Instantaneous losses obtained with the IM and FEM methods, when J_c is uniform in the tapes.
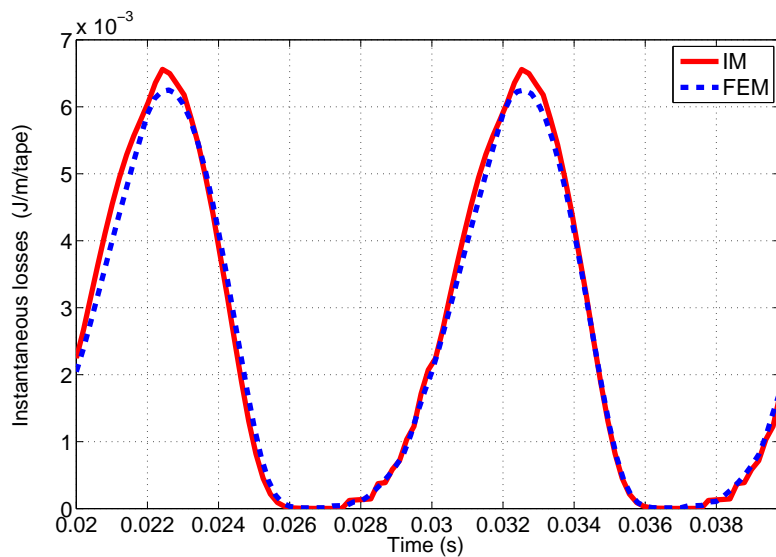

Figure 5.16 Instantaneous losses obtained with the IM and FEM methods, when a non-uniform distribution of J_c is considered.

At first sight, it might appear disadvantageous not to use the whole tape to carry the transport current, although it ends up being highly advantageous for two reasons :

1. The current that doesn't flow in the overlapped edge and also the reduced current at the overlapping edge, must flow somewhere else, and it happens that it is redistributed evenly all along the tape's width

2. The losses in coated conductors are known to be dominated by the "edge losses", and in the overlapped design, we reduce these losses since only half of the edges actually carry a current with even lower density.

These advantages are general and do not depend on the exact $J_c(x)$ distribution in the tapes, although as soon as there is a significant reduction of J_c at the edges of the tapes (for instance due to manufacturing processes), these advantages of the overlapped design over the typical design become significant.

5.4   Conclusion

In this paper, we introduced a new design scheme for HTS power transmission cables made of coated conductors. This so-called "overlapped design" was developed with the aim of reducing the level of AC losses encountered in more "classical" HTS power transmission cables, i.e. when a small gap is present between adjacent tapes. The major difference between the typical and the overlapped designs is that the adjacent tapes are allowed to overlap each other up to a certain distance from their edges, typically 1 or 2 mm.

With the help of numerical simulations, it was shown that the new overlapped design leads to a significant reduction of AC losses, typically 2 to 5 times lower than the best practical configurations of typically design cables (i.e. cables with a gap between the tape at its minimum size of 0.5 mm or so). In particular, when we consider a reduced current density at the edges of the tapes, due to the slitting effect or other any manufacturing process, the AC loss reduction is even more effective.

The validity of the simulations used to draw the above conclusions (based on integral equations) was verified through the use of a second numerical technique (finite element method). The very good agreement between the results obtained either way suggests that the conclusions are reliable.

Despite these promising results, future work will have to explore the impact of the actual helical configuration of the tapes (the current conclusions are based on straight tapes), as well as how this AC loss reduction trend extrapolates to multi-layer and three-phase cables. Also, the results could be significantly different if we considered coated conductors with a ferromagnetic substrate. The practical limitations of the various geometric parameters involved
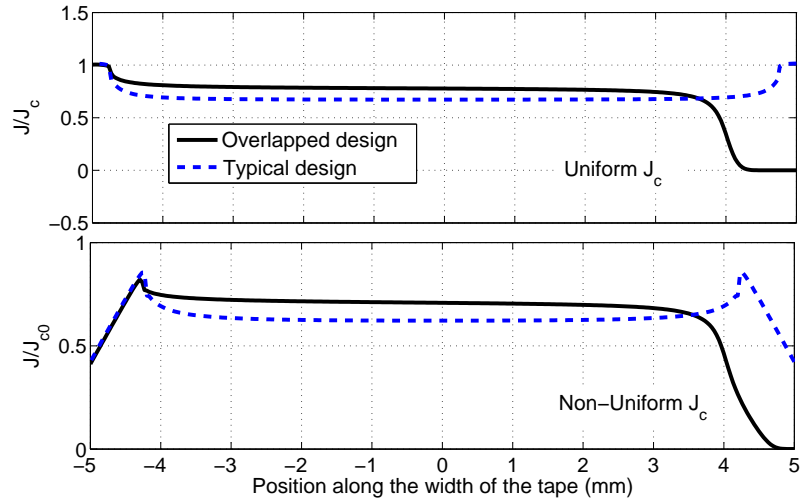
Figure 5.17 Normalized current distribution along the width of the tapes.
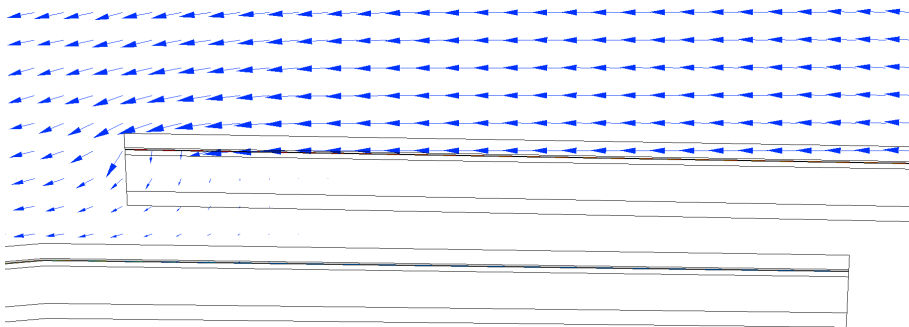
Figure 5.18 Magnetic flux density in the overlapped region.

in a cable design should also be determined with the help of HTS cable manufacturers.

5.5   Acknowledgment

CHAPTER 6

ASSESSMENT OF ALTERNATIVE DESIGN SCHEMES TO REDUCE THE EDGES LOSSES IN HTS POWER TRANSMISSION CABLES MADE OF COATED CONDUCTORS

Majid Siahrang[*], Frédéric Sirois[*], Doan N. Nguyen[+], and Stephen P. Ashworth[+]

[*]École Polytechnique de Montréal
[+]Superconductivity Technology Center, Los Alamos National Laboratory

Abstract

In this paper, we investigate the effectiveness of alternative designs to reduce the AC losses of HTS power transmission cables. The idea behind these designs is to undermine the edge effect, which is one of the main factors contributing to AC losses in HTS power cables made of coated tapes. The edge effect, which arises from the presence of gaps between the tapes, results in large normal components of magnetic field near the edges of the tapes and in turns leads to a current distribution with higher density near the edges. To perform our investigation we use a numerical technique developed in our previous work, which allows us to consider the helical configuration of the tapes. Through numerical simulations we asses the effectiveness of two overlapped designs, i.e. cyclic overalpped design and anticyclic overalpped design in reduction of AC losses in single-layer HTS power cables made of coated tapes. Simulation results show that AC losses can be reduced by about 70 % as compared with a typical single-layer cable.

6.1 Introduction

With lower AC losses, the initial and the operational costs of HTS power cables can be remarkably reduced, and this allows them to be in a better position in the competition with conventional power cables. Therefore, the reduction of AC losses is one of the most important factors to determine the level of the commercial application of HTS power cables in the future of the power transmission industry.

In general, AC losses in HTS cables include all the losses that occur in the conductors of the cable. These losses can be divided into two categories ; *classical electromagnetic losses* and *superconducting losses*. Classical electromagnetic losses in the conductors of HTS power cables made of coated conductors include the Ohmic and eddy current losses in the stabilizer layer (copper and/or silver) of the tapes and the ferromagnetic losses occurring in the substrate layer of the tapes. Ferromagnetic losses exist only when the substrate layer of the tapes is made of ferromagnetic materials, as in the case of RABiTS tape. If these magnetic substrates are exposed to AC magnetic fields, the ferromagnetic losses will correspond to the area of the hysteresis loop of the substrate B –H curve. Under normal working conditions, Ohmic and eddy current losses are quite negligible compared to the total AC losses. On the other hand, In HTS cables, the ferromagnetic losses dominate at low transport currents (below $40 - 50$ % of the critical current of the cable) and at higher transport currents, these losses become less important compared to the total AC losses of the cable [25, 26, 60].

The mechanism through which losses occur in HTS material is quite different from classical electric and ferromagnetic losses. The superconducting losses are developed when HTS materials carry time varying currents or are exposed to time varying magnetic fields, e.g. AC currents and fields. These losses are derived from the magnetic field distribution inside and on the surface boundaries of the conductors. Therefore, the geometry of the conductors (e.g. tapes in the case of HTS power cables) and their relative positioning change the field distribution and consequently affect the AC losses.

To provide a more intuitive insight into the superconducting loss mechanisms in HTS power cables made of coated tapes, it is useful to categorize these losses into different types. This categorization is very useful to give us a better conceptual understanding of the AC losses and can be used to provide helpful hints for the loss minimization task. In what follows we start from work done in [84] by Clem and Malozemoff to categorize the losses.

The first loss mechanism called "*surface Bean losses*" is responsible for the losses resulting from the field penetration from the wide faces of the tapes. These losses which are also referred to as "*top/bottom losses*" [85] can also be interpreted as the result of the variation of current distribution across the thickness of the tapes. The existence of these losses in the HTS coated tapes is not yet obvious. Based on physical assumptions that the vortex line dimension is larger than the thickness of the coated conductors (or at least they are in the same dimensions) and is not enough to build a critical state and move the flux lines [86] such losses might simply not exist in coated tapes. Even if such losses exist, their value can only be very low since the HTS layer of coated conductors is extremely thin, and therefore the surface Bean losses are likely to be negligible in HTS power cables.

The edge effect is another loss mechanism which makes a dominant contribution to the

AC losses in the tapes of HTS cables. The associated losses with the edge effects arise from the presence of a gap between adjacent tapes, which disturbs the field distribution near the edges of the tapes. Because of these gaps, the magnetic field presents high perpendicular components near the gap region, which results in large field penetration from the edges of the tapes. As a direct consequence of this field penetration, tapes carry more current near their edges which results in higher losses.

Another loss mechanism which is considered in most of AC loss analysis of HTS power cable comes from the polygonal configuration of the tapes in the 2D cross-section of a cable (see figure 6.1). Such a polygonal configuration disturbs the circumferential magnetic field along the width of the tapes and contributes to magnify the perpendicular components of the magnetic field wihtin the tapes.

In multilayer HTS cables, there is another loss mechanism which arises when the transport current of each phase is not equally shared between the layers. However, because of the helical configuration of the tapes in HTS power cables and since this current sharing highly depends on the mutual inductance between the layers, it is easy to choose proper winding angles to insure equal current sharing between the layers.

In addition to the above mentioned mechanisms, there is another loss mechanism which is called *"flux-cutting loss"*. These losses are rooted in the collision of flux fronts form orientations [87]. This loss mechanism is not well understood and is not expected to be large in HTS power cables [84] or at least not distinguishable from the other loss mechanisms.

In the typical design of HTS power transmission cables, HTS tapes are helically wound around cylindrical formers. As shown in figure 6.2, when thin tape conductors are helically wound around a cylindrical former, their wide face must be conformed to the former. As a consequence, in the cross-section of the cable, the tapes must have a bent shape conformed to the former (as shown on the right side of figure 6.2) . Therefore, there should be no losses due to the polygonal configuration of the tapes as shown in figure 6.1, as long as the HTS cable is made of helically wound tapes. This means that in the case of single-layer HTS power cable made of tapes with non-ferromagnetic substrates, and by neglecting the top/bottom losses (should they exist), the only important AC loss mechanism is the edge effect. As explained, the edge losses arise from the presence of the small gaps between the adjacent tapes (shown in figure 2). Therefore, the minimum AC losses with a typical design of single-layer HTS cables is achieved when these gaps are completely closed [33, 71]. But due to mechanical considerations, there is a minimum size for the gap $(.6 - .8 \text{ mm})$[33].

In an attempt to undermine the gap effect and reduce the perpendicular components of the magnetic fields near the edge of the tapes, an alternative overlapped design has been already proposed by SuperPower [69]. In our previous work [72], neglecting the helical configuration of
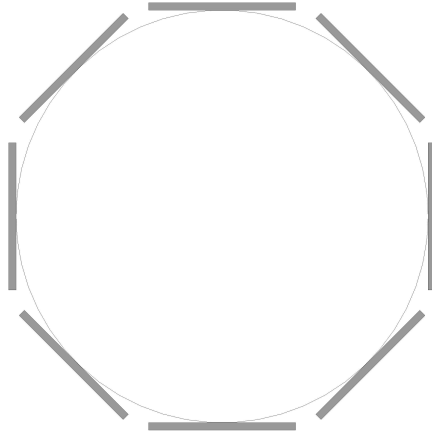
Figure 6.1 Polygonal arrangement of the tape in the 2-D cross-section of the cable, when tapes are not conformed to the cable former.
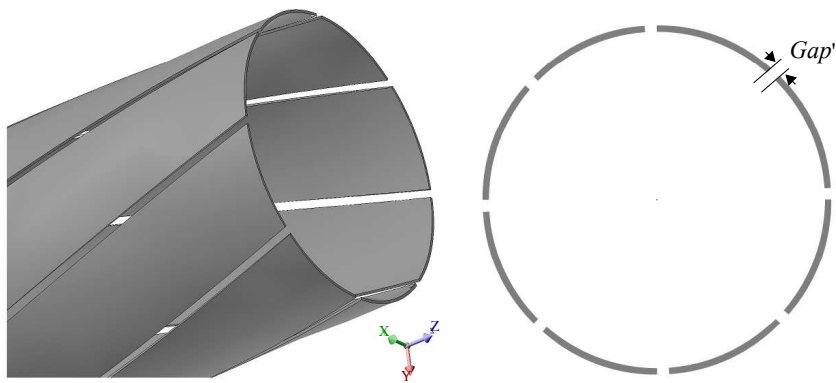
Figure 6.2 Typical design of one layer of a HTS power cable. In this design, there is a small gap between two adjacent tapes. The Gap' is the projection of the gap onto the 2-D cross-section of the cable, i.e, $Gap' = \frac{Gap}{\cos(w_a)}$, where Gap is the physical gap between the tapes and w_a is the winding angle of the tapes.

the tapes, we investigated the AC loss behavior of this design. With this design, the adjacent tapes of the cable periodically overlap each other up to a certain distance. In this previous work [72], we showed that by overlapping the tapes, AC losses can be reduced up to 5 times compare with the typical design. The reason that this new design leads to reduced losses is due to an advantageous redistribution of the current inside the tapes, so that near the overlapped edges, tapes do not carry much current and practically there were no edge effects in the overlapped edges (bottom edges).

In this paper, for the same number of tapes with the same characteristics used in [72], we investigate the impact of the helical configuration of the tapes on the AC loss behavior of the idea of overlapping the tapes. To consider the helical configuration of the tapes, we use a numerical model developed in our previous work [70, 71] to find current distribution and AC losses in helically wound thin tape conductors. In addition to the previously introduced overlapped design (which here is renamed as cyclic overlapped design) we propose two other alternative overlap designs to reduce the edge losses in HTS power cable. Through parametric numerical simulations, we assess the effectiveness of these designs to reduce the AC losses in HTS power transmission cables made of coated tapes with non-ferromagnetic substrates.

6.2   Numerical model

To perform the simulations we used an integral-type numerical model developed for the electromagnetic analysis of single-layer assemblies of helically wound thin conductors. In this method, which is a point collocation method (Brandt-like formulation[63]), the integral relationship between the current density and the magnetic vector potential, i.e. the Biot-Savart integral, is used to formulated the eddy current equation over a descretized 1-D geometry along the width of a conductor of the cable. With this model, the non-linear resistivity of superconductors can be easily incorporated in the form of a classical power law model, i.e.,

$$\rho = \frac{E_c}{J_c} \left| \frac{J}{J_c} \right|^{k-1},$$
(6.1)

where E_c is the electric field criterion (1×10^{-4} V/m), J_c is the critical current density of the HTS material, and k is the power law index. The vector of current density is assumed to be tangential to the helical trajectory of the tapes. In this model, we do not consider the non-superconducting layers of the tapes, and the superconductor layer is modelled as an infinitely thin current sheet. This method is explained in detail in [70] and its accuracy has been verified by comparisions with experiments [70].

6.3   Cyclic overlapped design

In an alternative design scheme, which has been proposed in a patent by SuperPower [69], the adjacent tapes of the cable are allowed to periodically overlap each other up to a certain distance ($1 - 2$ mm). As shown in figure 6.3, two new geometric parameters are introduced in this design, i.e. *the overlap distance* and *the vertical gap.*

In our previous work [72], the helical configuration of the cable was neglected and by numerical simulations we showed that this design can effectively reduce the AC losses in single-layer HTS cables. In the current paper, we investigate the effect of the helical configuration of the tapes on the AC loss behavior of this design scheme. By varying the different simulation parameters presented in table 6.1, we performed a parametric study on the AC loss behavior of a single-layer cable consisting of eight identical IBAD coated conductors, each 10 mm wide. Keeping fixed the number of the tapes, the radius of the cable is determined by its winding angle and the gap (in a typical design) or the vertical gap and the overlap distance (in an cyclic overlapped design). Therefore in each case, the cables have a different radius.

Figure 6.4 represents the AC losses in one tape of the cable for different winding angles as functions of the gap (typical design) or the overlap distance (cyclic overlapped design with a vertical gap of 0.15 mm). In this figure, the AC losses are expressed per unit length of the tapes, rather than per unit length of the cable. This allows us to remove the effect of different lengths of the tapes per unit length of the cable for different winding angles. Therefore in this figure, the current distribution inside the tapes is the only responsible for the AC loss behavior of the cable.

According to the left-hand side of figure 6.4, as it was already known [33, 71] , with the typical design the AC losses decrease as the size of the gap decreases. In this figure, it is

Table 6.1 Simulation parameters used in numerical simulations

Critical current of the tapes (A)	266
Critical current of the cable (A)	8×266
Peak of the imposed current (A)	186
Width of the tape (mm)	10
Power law index (k)	50
Frequency (Hz)	50
Gap (typical design) (mm)	1-0
Overlap distance (mm)	0-2
Vertical gap (mm)	0.1-0.5
Winding angle (deg)	0-75
Thickness of the HTS layer of the tapes (μm)	1
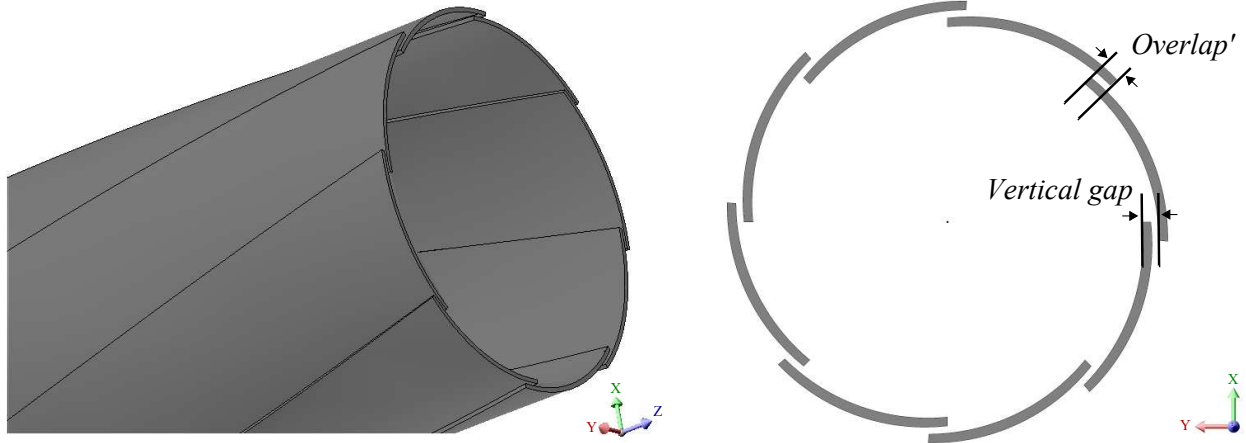
Figure 6.3 cyclic overlapped design of single-layer HTS power cables. The *Vertical gap* is the vertical distance between the adjacent tapes over the overlapped region, and the overlap is defined as the distance along which the tapes overlap each other. The $Overlap'$ is the projection of the overlap distance onto the 2-D cross-section of the cable, i.e. $Overlap' = \frac{Overlap}{\cos(w_a)}$.
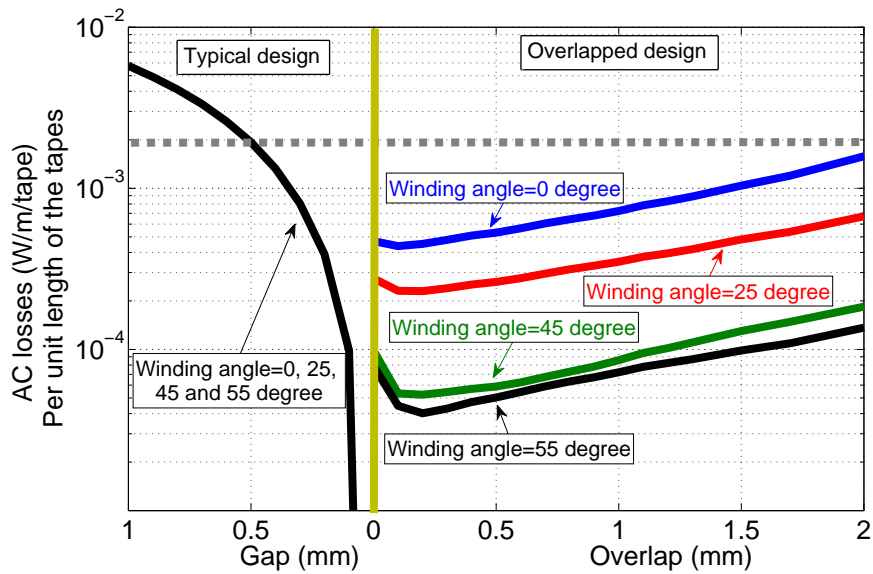
Figure 6.4 AC losses in one tape of the cable at a peak of its transport current $(.7I_c)$ as functions of its the geometric parameters. For the overlapped design the value of the vertical gap is .15 mm. The dashed line corresponds approximately to the minimum losses achievable with the typical design (gap of 0.5 mm).

observed that, for a given gap, the AC losses remain the same regardless of the winding angle of the cable. This means that with the typical design, the current distribution inside the tapes is independent of the winding angle and is solely determined by the gap. Since for a given gap, with different winding angles the cable has different radius, it can be also concluded that, the radius of the cable does not affect the current distribution inside the tapes. In figure 6.4, we have used a horizontal dashed line to represent the value of AC losses when the gap is 0.5 mm, i.e. an optimistic lower limit. Therefore, the dashed lines represent the minimum possible AC losses that can be achieved with the typical design.

The right sides of figure 6.4 represents the AC loss behavior of the cyclic overlapped design (with a vertical gap of .15 mm) as functions of the overlap distance for different winding angles. If one compares the AC losses of cyclic overlapped design with the dashed lines, it is observed that with this design the AC losses of the cable are lower than the minimum possible losses that can be achived with the typical design. Figure 6.4 reveals that, as opposed to the typical design, the AC loss behavior of the cyclic overlapped design is highly dependent on the winding angle of the tapes so that with higher winding angle, this design shows a quite better performance in reducing AC losses.

Figure 6.5 shows the AC loss behavior of the cable as a function of its winding angle, when the overlap distance is 1 mm and the vertical gap is 0.15 mm. This figure shows that there is an optimum winding angle at which the AC losses are minimum. For the simulated cable, this optimum winding angle is around 55 degree. In other words, by increasing the winding angle, the AC losses decrease and reach a minimum value when the winding angle is around 55. By further increasing the winding angle the AC losses increase, but remain lower than the AC losses with zero winding angle.

Figure 6.6 shows the AC loss behavior of the cable as a function of the vertical gap, when the overlap distance is 1 mm and the winding angle is 45 degree. In this figure one can see that with smaller vertical gaps, we can design cables with lower AC losses. The minimum possible vertical gap is equal to the thickness of the tapes (0.1 to 0.15 mm for the IBAD tapes manufactured by Superpower), but due to mechanical considerations the minimum achievable vertical gap will be larger than this value.

As mentioned, since the AC losses in figure 6.4 are expressed per unit length of the tape, the only responsible for the difference in losses is the current distribution inside the tapes. Therefore, with the cyclic overlapped design, where the AC losses are highly dependent on the winding angle, the way that current is distributed inside the tapes must be a function of the winding angle.

Figure 6.7 shows the current distribution along the width of the tapes for different winding angles when the overlap distance and the vertical gap are kept fixed at 1 and 0.15 mm

Figure 6.5 AC loss behavior of the cable as a function of its winding angle, while the overlap and the vertical gap are 1 and 0.15 mm respectively and J_c is assumed to be uniform inside the tapes. The peak of the transport current is $0.7I_c$.
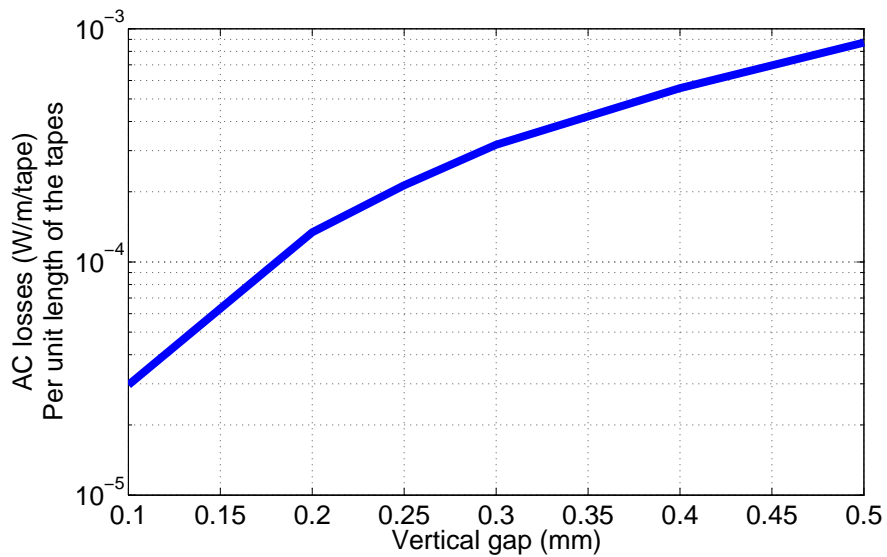
Figure 6.6 AC losses behavior of the cable as a function of the vertical gap when the overlap is 1 mm and the winding angle is 45 degree while the peak of the transport current is $0.7Ic$.

respectively. These current profiles are plotted at the peak of the transport current $(0.7I_c)$. In these figures, one can see that for straight tapes, i.e. zero winding angle, the current density near the overlapped edge (bottom edge) is very low, while the overlapping edge (top edge) experiences the maximum current density. This behavior has been already observed in [72] and was interpreted as the reason for the favorable behavior of the cycilc overlapped design in terms of AC loss reduction for single-layer cables composed of non-twisted tapes (reduction by a factor of 5 when compared to the minimum possible losses with typical design cables).

As observed in figure 6.7, by increasing the winding angle, the current density at the bottom edge starts to increase and at the same time, the current density at the top edge start to decrease. When the winding angle is around 55 degree, the current distribution inside the tape is almost symmetrical, i.e., the value of the current density at the top and the bottom edges are the same, and they are at their minimum values. Therefore as already observed in figure 5, this situation corresponds to minimum AC losses. By further increasing the winding angle, the bottom edges experience more current density than the top edges and AC losses start to increase. Therefore it seems that with combination of the overlapped design and the helical configuration of the tapes the edges effects near both edges tapes can be undermined so that the middle part of the tapes carries more current than the edges. In turn this leads to a better performance of the cyclic overlapped design in AC loss reduction. For instance in the case of the simulated cable in this research, with the optimum wining angle, i.e 55 degree, the vertical gap of 0.15 mm and the overlap of 1 mm, when the cable transports 70% of its critical current, the cyclic overlapped design leads to around 30 times less AC losses when compared to the minimum possible value of AC losses with the typical design.

Unfortunately, despite the interesting electromagnetic performance of the cyclic overlapped design, it has a big mechanical drawback. With this design each point along the width of the tapes is located at a different distance from the center of the cable. Therefore, if the tapes are wound along a helical path, the radius of the helix gradually increases from the bottom edge to the top edge along their width. As a consequence, for a given winding angle, the local pitch length along the cross-section of the tapes is not the same and must gradually increase from the bottom edges to the top edges. Therefore, with typical coated tapes whose wide face are rectangular (the top tape in figure 6.8) it is not possible to have the cyclic overlapped design and a helical configuration at the same time. To realize the cyclic overlapped design with helically wound tapes, the wide face of the tapes must has a bent shape such as the lower tape presented in figure 6.8. The arc radius of such bent tapes is a function of the geometrical parameters of the cable, for instance for the case of a cyclic overlapped design when 8 tapes overlap each other up to 1 mm with the vertical gap of 0.15 mm, the bending
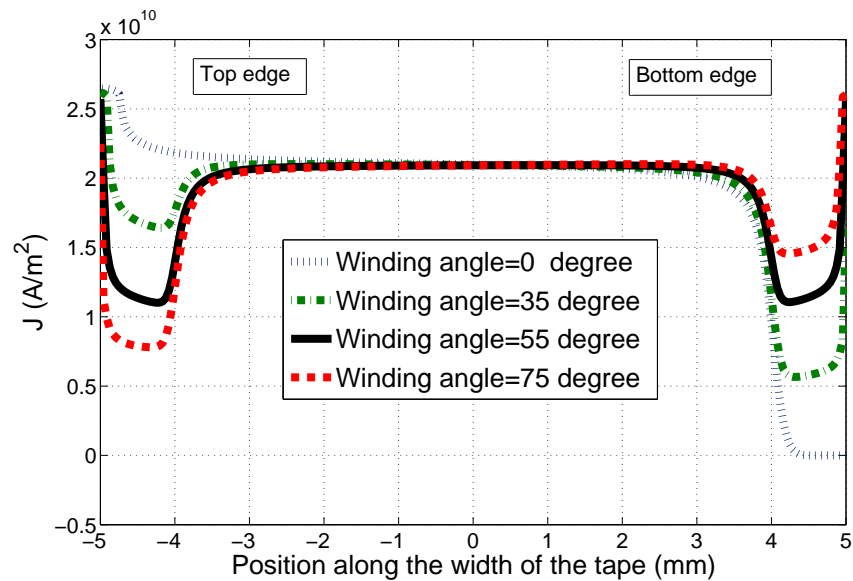
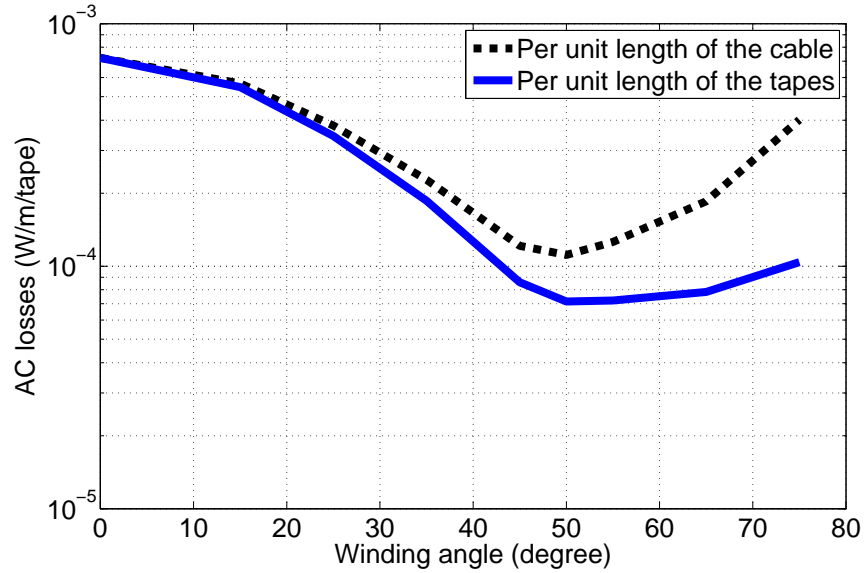Figure 6.7 Current distribution along the width of the tape for different values of winding angle while the overlap and the vertical gap are 1 and 0.15 mm respectively and J_c is assumed to be uniform inside the tapes. The peak of the transport current is $0.7I_c$.

radius of the wide face of the tapes must be 1.19 m. In figure 6.8 such a tape with a bent wide face is compared with a regular tape.

6.4   Anticyclic overlapped design

As another alternative overlapped configuration (shown in figure 6.9) the adjacent tapes can be alternatively arranged so that both edges of one tape overlap its adjacent tapes and therefore the edges of the next tape are overlapped by the edges of the two adjacent tapes. Similar to the cyclic overlapped design, the vertical gap and the overlapped distance must be defined as shown in figure 6.9. With this design, which we named it the anticyclic overlapped design, any points within the tapes have the same winding radius, therefore it can easily be realized with regular HTS tapes.

Figure 6.10 shows the AC loss behavior of this design scheme as a function of the overlap distance for a vertical gap of 0.15 mm, when the peak of the transport current of the cable is 70 % of its critical current. Compared with the minimum possible AC losses that can be achieved with the typical design (the dashed line represents the AC losses of the typical design with a gap of 0.5 mm), figure 6.10 shows that similar to the cyclic overlapped design, the anticyclic overlapped design is also effective to reduce the AC losses in single layer HTS cables. The AC losses in this figure are presented per unit length of the tapes. Both for the
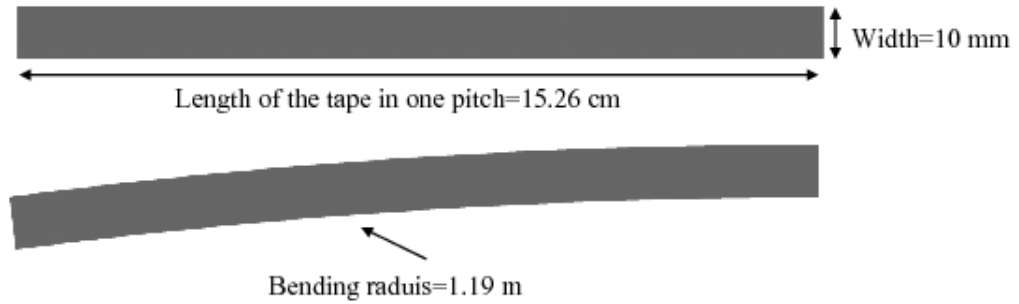
Figure 6.8 Top : The wide face view of the typical HTS coated tapes. Bottom : The wide face view of required HTS tapes to realized the cyclic overlapped design with 8 tapes when the winding angle is 55 degree and the overlap and the vertical gap are 1 mm and 15 mm respectively.
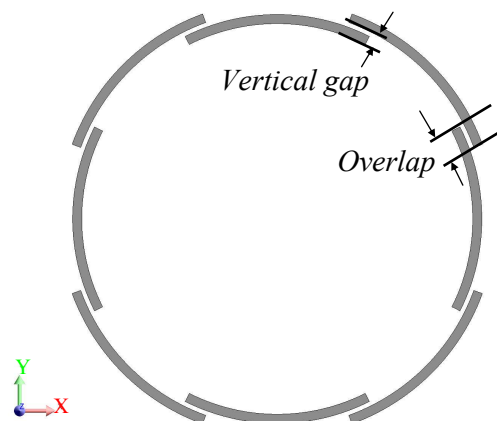
Figure 6.9 Anticyclic overlapped design ; with this design both edges of one tape overlap its adjacent tapes and the edges of the next tape are overlapped by the edges of its two adjacent tapes.

typical design and the anticyclic overlapped design the losses are independent of the winding angle of the tapes. Therefore, as opposed to the cyclic overlapped design, it seems that the winding angle does not have any effect on the current distribution inside the tapes.

Figure 6.11 compares the AC loss behavior of the typical design (gap=0.5 mm) with that of the anticyclic overlapped design (overlap=0.5 mm, vertical gap=0.15 mm) as a function of the transport current. It is observed that for the whole current range, it is possible to achieve lower AC losses with the anticyclic overlapped design compared to the minimum possible losses of the typical design.

Figure 6.12 represents the current distribution inside the tapes at a peak value of the transport currents of 0.75 I_c for both designs. As it can be observed, no edge effect can be observed in the bottom tapes (overlapped tapes), and the edge effect in the top tapes (overlapping tapes) are slightly undermined compared with the case of a typical design (dashed curve).

6.5   Typical design with cushion tapes

As another attempt to undermine the edge effect, we investigated the idea of putting narrow HTS tapes bellow the main tapes under the gap regions. As shown in figure 6.13, with this design narrow tapes symmetrically cover the gap regions under the main tapes. It is expected that the current flowing in the narrow tapes will undermine the perpendicular components of the magnetic field near the edges of the main tapes. Since the narrow tapes act as magnetic cushions for the main tapes, we called them cushion tapes. By adding the cushion tapes the critical current of the cable, and in turn, the nominal current rating of the cable, are increased.

Figure 6.14 shows the AC losses of this design as a function of the gap between the main tapes, when the width of the cushion tapes is 2 mm, and the vertical gap is 0.15 mm. As it is observed, in the presence of the cushion tapes, larger gaps between the main tapes result in lower AC losses. The reason for such a behavior can be explained as follows. To keep the configuration shown in figure 6.13 along the whole length of the cable, both the main and cushion tapes must be wound with the same winding angle. Therefore, the current share of the cushion tapes can not be adjusted by a proper winding angle. In such a two layer configuration, the current tends to flow in the tapes which are wound with larger radius, i.e. main tapes. Therefore, it is expected that just bellow the gap region the current flows in the cushion tapes. With larger gaps more current can flow in the cushion tapes and the current capacity of the these tapes is used more effectively. Therefore, when the size of the gap is in the range of the cushion tapes, the cable is expected to show a better AC loss performance.
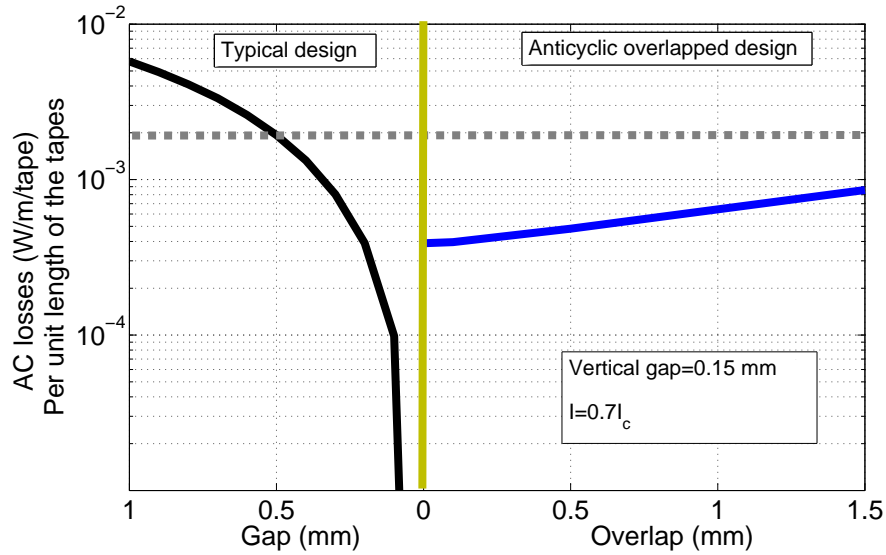
Figure 6.10 Comparison between the AC loss behavior of typical design and the anticyclic overlapped design as the function of the gap and the overlap when the vertical gap is .15 mm.
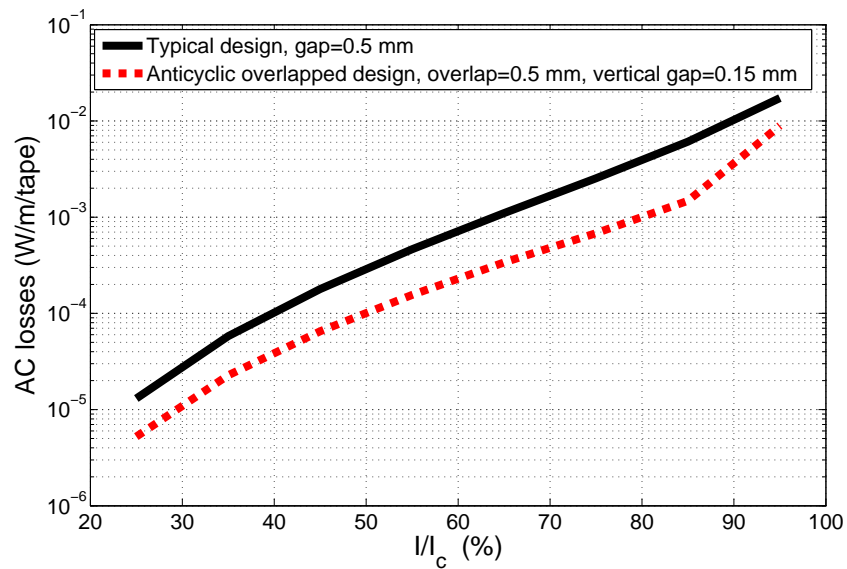
Figure 6.11 AC losses of the cables (typical design and the anticyclic overlapped design) as a function of the transport current.
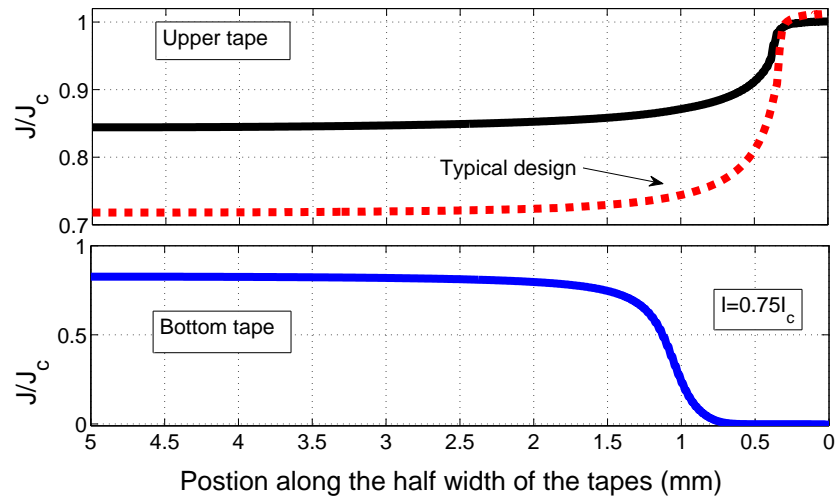
Figure 6.12 Current distribution inside the tapes in the typical and anticyclic overlapped design at a peak of the transport current $(.75I_c)$. The gap is 0.5 mm in the case of the typical design and the overlap distance and the vertical gap are respectively 0.5 and 0.15 mm in the anticyclic overlapped design.
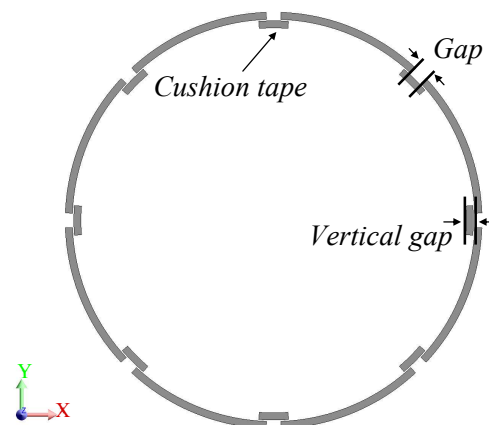
Figure 6.13 Typical design with cushions tapes
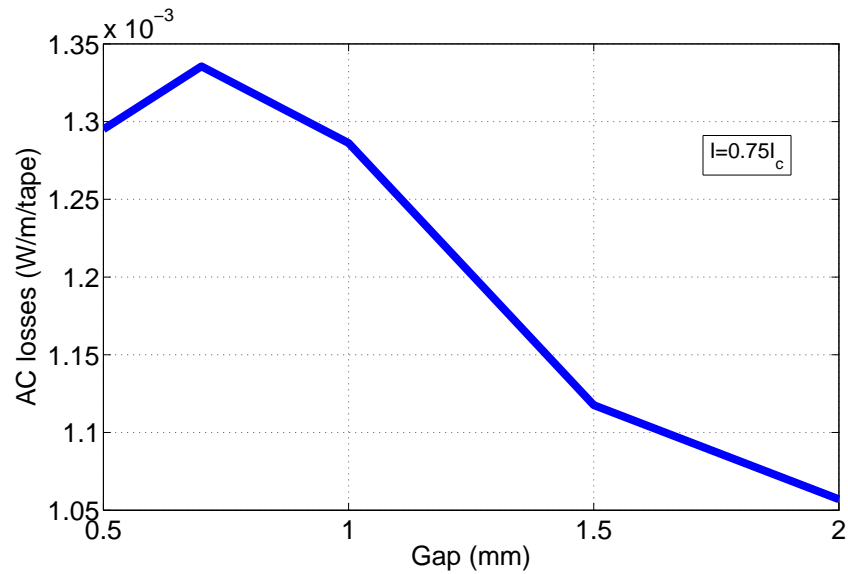
Figure 6.14 AC loss behavior of the typical design with the cushion tape as a function of the gap between the main tapes. The width of the main and the cushion tapes are 10and 2 mm respectively.

In figure 6.15 we compare the AC loss behavior of the cable with and without the cushion tapes, as function of the transport current. For the typical case, the gap size is 0.5 mm, and for the cable with cushion tapes the gap size is 2 mm, the vertical gap between the cushion and main tapes is 0.15 mm and the width of the cushion tapes is 2 mm. As it is observed, despite the fact that the cable with the cushion tapes carries 20 % more current (assuming the same J_c for the main and cushion tapes), its AC losses is lower than the cable without cushion tapes.

Figure 6.16 represents the current distribution inside the main and cushion tapes (gap=1 mm, vertical gap=0.15 mm) at the peak value of the transport current $(0.75I_c)$. On the right side of figure 6.16, the current distribution in the main tape is compared with the current distribution in the tapes of the cable without cushion tapes (gap=0.5 mm).As it is observed, because of the presence of the cushion tapes, the current penetration at the edge of the main tapes is slightly lower than the current penetration in the tapes of the cable without cushion tapes. It is also observed that, with the cushion tapes, the current tends to flow with more density in the middle parts of the main tapes.

The left side of figure 6.16 shows the current distribution inside the cushion tapes. As it can be observed, the current flows in the middle part of the cushion tapes, and almost half of the cushion tapes (near to the edges) is empty of current. As one can observes, at the $I/I_c = 0.75$ the maximum current density in the cushion tapes is less than 65 % of its critical
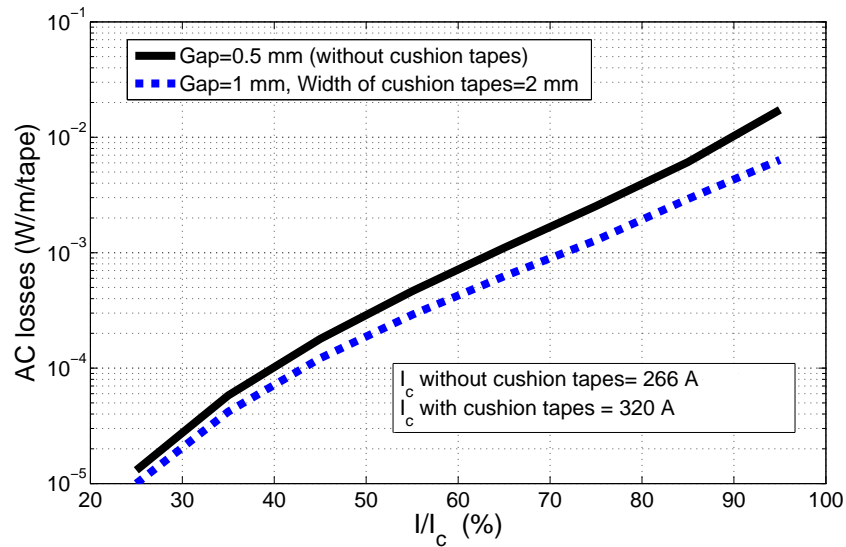
Figure 6.15 AC losses of the cables (with and without suchions tapes) as a function of the transport current

current density.

6.6   Conclusion

In this paper, through parametric numerical simulations, we compared the AC loss be-havior of a single-layer HTS power cable when its tapes are wound according to a typical design against three alternative designs in which the gap regions are covered by the adjacent tapes or additional ones. In this research, we took into consideration the helical configuration of the tapes. Simulation results revealed that, except for the case where the adjacent tapes periodically overlapped each other (the cyclic overlapped design), regardless of the winding angle for a given geometrical parameters the current distribution inside the tapes remain unchanged. On the other hand, with the cyclic overlapped design the current distribution inside the tapes, and in consequence the AC losses of the cable are highly dependent on the winding angle of the cable so that with a proper winding angle the edge effect in the edges of each tape can be remarkably undermined. This advantageous behavior results in lower AC losses compared with the minimum possible losses that can be achieved with the typical design (up to 30 times lower). Unfortunately, since with the cyclic overlpped design the winding radius of the tapes is not constant along their cross-section, this design requires HTS tapes with a bent wide face and is not feasible with regular HTS tapes. However, the anticyclic overlapped design and the idea of adding narrow tapes bellow the gap regions are practically feasible with rgular HTS tapes. Simulation results showed that, these two latter
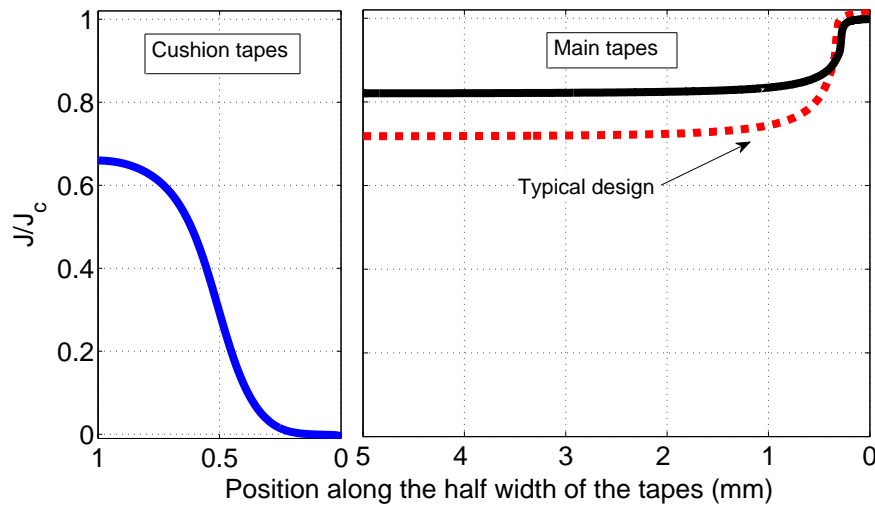
Figure 6.16 Current distribution inside main and cushion tapes at a peak of the transport current $(0.75I_c)$. Width of the main and cushion tapes are 10 and 2 mm respectively. The size of the gap is 0.5 mm with the typical design and 1 mm with the cushion tape design.

designs are also effective to reduce the edge losses in HTS power cables so that the AC losses can be reduced by more than 70 % compared with the minimum losses with a typical design.

6.7   Acknowledgment

CHAPTER 7

GENERAL DISCUSSION

Within the framework of the first phase of this thesis, a numerical tool to solve the electromagnetic problem of helically wound thin conductors was developed. The main application of this model is to find current distributions and AC losses in HTS coils and cables. The performance of the developed model, in terms of computational time and accuracy, is superior to the previously proposed models. Using this model, which its accuracy has been validated by experiments, can provide researchers and engineers with a useful tool to study the electromagnetic behavior of superconducting coils and cables. In this context, the model can be used to find optimal design parameters with respect to desired objectives, e.g. minimum AC losses.

The proposed model is developed for the case of cables made of HTS tapes with non-ferromagnetic substrates. Extending the method for cables made of HTS tapes with magnetic substrates can be proposed as the further developments of the current work. In this case, the study domain of the problem must be extended to consider the effect of magnetization in magnetic substrates. This model will be helpful to assess the effectiveness of the overlapped designs in the AC loss behavior of HTS cables made of tapes with magnetic substrates

The developed model can be applied to coils and cables consisting of HTS tapes wound along helical paths with the same winding angle. This implies that, the method can be applied for AC loss analysis of multi-layer cables as long as all the layers have a same wining angle. In practice, to reach a optimum current sharing between the layers, each layer is wound with a different winding angle. The only practical configuration for a multi-layer HTS cable whose layers have the same wining angle, could happened in a three-phase cable with three layers (each phase has a one layer). In this case since the imposed current is directly applied to the tapes of each layer, the total current share of each layer is equal to the phase currents which is almost independent of the wining angle of the tapes. Therefore, layers can have the same winding angle.

The model can be extended to consider HTS cables with two different winding angles. In this case, instead of a 1-D study domain, problem must be formulated in 2-D study domains defined over sufficient portions of the wide face of tapes. In this case, the assumption that the current density has only one component which is aligned with the helical trajectory of the tapes, is no longer valid and the current of tapes can deviate from the helical path of the tapes.

The second objective of this thesis was to use this model to examine the performance of alternative design schemes proposed to reduce the AC losses in HTS cables. In these designs the adjacent tapes of the cable overlap each other up to a certain distance from their edges. The results of the effectiveness study on the performance of the idea of overlapping the tapes have been published in [72, 73] which are inserted as Chapter 5 and Chapter 6. According to the obtained results, these design are effective to reduce the AC losses of single-layer HTS cables. The reason behind this loss reduction is to undermine the current penetration near the edges of the tapes. In this case, the edge effect, which is the dominant loss mechanism in single-layer cable is undermined near the overlapped edges.

Although the results of our study confirm the effectiveness of overlapping the tapes in single-layer cables, the performance of overlapping the tapes in the case of multi-layer cable has not yet been studied. In the case of multi-layer cables, tapes of each layer are subjected to the field produced by the current of inner layers. With the typical design, i.e. tapes do not overlap each other and their wide face are conformed with cylindrical formers, the magnetic field produced by inner layers are mostly parallel to the wide face of the outer layers. According to the picture that, overlapping a layer other than the most inner layer, may expose the tapes of that layer to magnetic fields with normal components (produced by the inner layers) to their wide face and this could lead to increase of AC losses in the tapes of that layer, it can be concluded that the idea of overlapping the tape should be applied only to the first layer of the cable.

CHAPTER 8

CONCLUSION

This thesis had two phases. The objective of the first phase was to develop a numerical approach to solve the electromagnetic problem of helically wound thin tape conductors in single layer coaxial arrangements. The main application of this model was to find current and field distributions, and AC losses in single layer HTS power transmission cables. To achieve this goal, an integral-type numerical method was developed. In this method, the inherent geometrical symmetry of the problem is used to formulate the electric voltage equation along the cross-section of one of the conductors of the cables.

The proposed model is faithful to the real helical geometry of each conductor and the only simplifying approximation in the hypothesis of the model is neglecting the thickness of the tapes, so that they are approximated as infinitely thin current sheets. Because of the very high aspect ratio of the HTS coated tapes, this approximation seems to be quite accurate and is not expected to influence the final solution. The accuracy of the developed model was validated through some experimental trials. The experimental measurements were carried out by the collaborators of the project at the Los Alamos National Laboratory in the Unites States.

The second phase of this research work was defined with the objective of assessing alternative design schemes to reduce the AC losses of HTS power transmission cables. In this phase, the effectiveness of three alternative design schemes proposed to reduce the edge losses in single layer HTS cables were investigated. In these designs, aimed at undermining the edge effect, the gap regions are covered by the overlap of the adjacent tapes or by inserting narrow tapes below the main tapes. Through extensive parametric numerical simulations, it was observed that these new designs are effective in reducing the AC losses in single layer cables. When considering realistic design parameters, the AC losses in HTS cables can be reduced by up to $30 - 70$ % compared with minimum possible losses that can be achieved by the typical design.

BIBLIOGRAPHY

[1] H. K. Onnes, "Further experiments with liquid helium. d. on the change of electrical resistance of pure metals at very low temperatures, etc. v. the disappearance of the resistance of mercury," *Proceedings Koninklijke Akademie van Wetenschappen te Amsterdam*, vol. 14, pp. 113–115, 1911.

[2] H. Kamerlingh Onnes, "Resistance of mercury near absolute zero," *Proceedings Koninklijke Akademie van Wetenschappen te Amsterdam*, vol. 14, pp. 818 – 821, 1912/02/22.

[3] W. Meissner and R. Ochsenfeld, "Ein neuer effekt bei entritt der supraleitfahigkeit. die naturwissenschaften," *Die Naturwissenschaften*, vol. 21, p. 787, 1933.

[4] F. London and H. London, "Electromagnetic equations of supraconductor," *Proceedings the Royal Society of Edinburgh*, vol. 149, no. 866, pp. 71–88, 1935.

[5] V. Ginzburg and L. Landau, "On the theory of superconductivity," *hurnal Experimentalnoi i Theoreticheskoi Fisiki*, vol. 20, p. 1064, 1950.

[6] J. Bardeen, L. N. Cooper, and J. R. Schrieffer, "Theory of superconductivity," *Phys. Rev.*, vol. 108, pp. 1175–1204, Dec 1957. [Online]. Available : http://link.aps.org/doi/10.1103/PhysRev.108.1175

[7] C. Bean, "Magnetization of hard superconductors," *Physical Review Letters*, vol. 8, no. 6, pp. 250 – 253, 1962/03/15. [Online]. Available : http://dx.doi.org/10.1103/PhysRevLett.8.250

[8] ——, "Magnetization of high-field superconductors," vol. 36, no. 1, 1964/01/, pp. 31 – 39. [Online]. Available : http://dx.doi.org/10.1103/RevModPhys.36.31

[9] J. Rhyner, "Magnetic properties and ac-losses of superconductors with power law current-voltage characteristics," *Physica C : Superconductivity and its Applications*, vol. 212, no. 3-4, pp. 292 – 300, 1993, aC losses ;Critical current density ;Critical state model ;Power law current-voltage characteristics ;. [Online]. Available : http://dx.doi.org/10.1016/0921-4534(93)90592-E

[10] J. Nagamatsu, N. Nakagawa, T. Muranaka, Y. Zenitani, and J. Akimitsu, "Superconductivity at 39 k in magnesium diboride," *Nature*, vol. 410, no. 6824, pp. 63 – 4, 2001/03/01, superconductivity ;magnesium diboride ;transition temperature ;magnetization ;resistivity ;39 K ;MgB$_2$;. [Online]. Available : http://dx.doi.org/10.1038/35065039

[11] *Design Concepts for a Superconducting Cable.* EPRI, Palo Alto, CA : 1994. TR-103631.

[12] *Superconducting Power Equipment : Technology Watch 2010.* EPRI, Palo Alto, CA : 2010. 1019995.

[13] W. V. Hassenzahl, D. W. Hazelton, B. K. Johnson, P. Komarek, M. Noe, and C. T. Reis, "Electric power applications of superconductivity," *Proceedings of the IEEE*, vol. 92, no. 10, pp. 1655 – 1674, 2004. [Online]. Available : http://dx.doi.org/10.1109/JPROC.2004.833674

[14] *Superconducting Power Cables : Technology Watch 2009.* EPRI, Palo Alto, CA : 2009. 1017799.

[15] C. Cantoni and A. Goyal, *High-Tc superconducting thin- and tick-film based coated conductors for energy applications. Thin-film metal-oxides : fundamentals and applications in electronics and energy.* Ney-York, N.Y. : Springer, 2010.

[16] *Superconducting Power Cables : Technology Watch 2006.* EPRI, Palo Alto, CA : 2006. 1012430.

[17] *Program on Technology Innovation : a Superconducting DC Cable.* EPRI, Palo Alto, CA : 2009. 1020458.

[18] P. M. Anderson, *Power System Protection.* IEEE Press, 1999.

[19] T. Janowski, B. Glowacki, G. Wojtasiewicz, S. Kozak, J. Kozak, B. Kondratowicz-Kucewicz, M. Majka, and M. Wozniak, "Fault current limitation in power network by the superconducting transformers made of 2g hts," *IEEE Transactions on Applied Superconductivity*, vol. 21, no. 3 PART 2, pp. 1413 – 1416, 2011. [Online]. Available : http://dx.doi.org/10.1109/TASC.2011.2112325

[20] N. Hayakawa, H. Kojima, M. Hanai, and H. Okubo, "Progress in development of superconducting fault current limiting transformer (sfclt)," *IEEE Transactions on Applied Superconductivity*, vol. 21, no. 3 PART 2, pp. 1397 – 1400, 2011. [Online]. Available : http://dx.doi.org/10.1109/TASC.2010.2089412

[21] J. Pyrhonen, *Design of Rotating Electrical Machines.* John Wiley & Sons, 2008.

[22] P. Kundur, *Power System Stability and Control.* McGraw-Hill, 1994.

[23] S. S. Kalsi, D. Madura, and M. Ingram, "Superconductor synchronous condenser for reactive power support in an electric grid," vol. 15, no. 2 PART II, 2005, pp. 2146 – 2150. [Online]. Available : http://dx.doi.org/10.1109/TASC.2005.849481

[24] S. D. Umans, "Transient performance of a high-temperature-superconducting generator," Miami, FL, United states, 2009, pp. 451 – 457. [Online]. Available : http://dx.doi.org/10.1109/IEMDC.2009.5075245

[25] V. Vysotsky, K. Shutov, A. Nosov, N. Polyakova, S. Fetisov, V. Zubko, V. Sytnikov, W. Carter, S. Fleshler, A. Malozemoff, and G. Snitchler, "Ac loss of a model 5m 2g hts power cable using wires with niw substrates," vol. 234, no. PART 3, Dresden, Germany, 2010. [Online]. Available : http://dx.doi.org/10.1088/1742-6596/234/3/032061

[26] V. V. Zubko, A. A. Nosov, N. V. Polyakova, S. S. Fetisov, and V. V. Vysotsky, "Hysteresis loss in power cables made of 2g hts wires with niw alloy substrate," *IEEE Transactions on Applied Superconductivity*, vol. 21, no. 3 PART 2, pp. 988 – 990, 2011. [Online]. Available : http://dx.doi.org/10.1109/TASC.2010.2089773

[27] S. Fukui, J. Ogawa, N. Suzuki, T. Oka, T. Sato, O. Tsukamoto, and T. Takao, "Numerical analysis of ac loss characteristics of multi-layer hts cable assembled by coated conductors," vol. 19, no. 3, 2009, pp. 1714 – 1717. [Online]. Available : http://dx.doi.org/10.1109/TASC.2009.2018050

[28] N. Amemiya, Z. Jiang, M. Nakahata, M. Yagi, S. Mukoyama, N. Kashima, S. Nagaya, and Y. Shiohara, "Ac loss reduction of superconducting power transmission cables composed of coated conductors," vol. 17, no. 2, 445 Hoes Lane / P.O. Box 1331, Piscataway, NJ 08855-1331, United States, 2007, pp. 1712 – 1717, coated conductors;Power transmission cables;Three-layer conductors;. [Online]. Available : http://dx.doi.org/10.1109/TASC.2007.898442

[29] A. Malozemoff, G. Snitchler, and Y. Mawatari, "Tape-width dependence of ac losses in hts cables," vol. 19, no. 3, 445 Hoes Lane / P.O. Box 1331, Piscataway, NJ 08855-1331, United States, 2009, pp. 3115 – 3118. [Online]. Available : http://dx.doi.org/10.1109/TASC.2009.2017726

[30] N. Banno and N. Amemiya, "Theoretical model of twisted high tc superconducting tapes for numerical alternating-current loss calculations," *Journal of Applied Physics*, vol. 85, no. 8 I, pp. 4243 – 4249, 1999.

[31] W. Norris, "Calculation of hysteresis losses in hard superconductors : polygonal- section conductors," *Journal of Physics D (Applied Physics)*, vol. 4, no. 9, pp. 1358 – 64, Sept. 1971. [Online]. Available : http://dx.doi.org/10.1088/0022-3727/4/9/316

[32] ——, "Calculation of hysteresis losses in hard super-conductors carrying ac : isolated conductors and edges of thin sheets," *Journal of Physics D (Applied Physics)*, vol. 3, no. 4, pp. 489 – 507, 1970/04/. [Online]. Available : http: //dx.doi.org/10.1088/0022-3727/3/4/308

[33] Y. Mawatari, A. P. Malozemoff, T. Izumi, K. Tanabe, N. Fujiwara, and Y. Shiohara, "Hysteretic ac losses in power transmission cables with superconducting tapes : Effect of tape shape," *Superconductor Science and Technology*, vol. 23, no. 2,

2010, aC loss ;Cross section ;Power transmission cables ;. [Online]. Available : http://dx.doi.org/10.1088/0953-2048/23/2/025031

[34] G. Vellego and P. Metra, "An analysis of the transport losses measured on htsc single-phase conductor prototypes," *Superconductor Science & Technology*, vol. 8, no. 6, pp. 476 – 83, 1995/06/. [Online]. Available : http://dx.doi.org/10.1088/0953-2048/8/6/014

[35] W. Carr Jr., "ac loss from the combined action of transport current and applied field." vol. MAG-15, no. 1, pp. 240 – 243, 1978.

[36] A. Ozcivan, S. Soeda, N. Hu, T. Yagai, M. Tsuda, and T. Hamajima, "Investigation on ac loss of a high temperature superconducting tri-axial cable depending on twist pitches," *Cryogenics*, vol. 49, no. 12, pp. 714 – 718, 2009. [Online]. Available : http://dx.doi.org/10.1016/j.cryogenics.2009.08.009

[37] T. Hamajima, M. Tsuda, T. Yagai, S. Monma, H. Satoh, and K. Shimoyama, "Analysis of ac losses in a tri-axial superconducting cable," vol. 17, no. 2, 445 Hoes Lane / P.O. Box 1331, Piscataway, NJ 08855-1331, United States, 2007, pp. 1692 – 1695, axial fields ;Balanced three phase currents ;Current distributions ;External out-of-phase field ;Triaxial cables ;. [Online]. Available : http://dx.doi.org/10.1109/TASC.2007.898338

[38] A. Ozcivan, M. Toda, N. Hu, K. Hoshino, T. Yagai, M. Tsuda, and T. Hamajima, "Ac loss of a multi-layer per phase tri-axial hts cable withbalanced current distribution," *Journal of Superconductivity and Novel Magnetism*, pp. 1 – 6, 2010.

[39] H. Noji, "Ac loss of a high-tc superconducting power-cable conductor," *Superconductor Science and Technology*, vol. 10, no. 8, pp. 552 – 556, 1997. [Online]. Available : http://dx.doi.org/10.1088/0953-2048/10/8/004

[40] M. Tsuda, T. Fujisawa, T. Hiraoka, N. Harada, T. Yagai, and T. Hamajima, "The effective current and magnetic field distributions for reducing ac losses in coaxial multi-layer hts transmission cable," vol. 16, no. 2, 2006, pp. 1594 – 1597, aC loss ;Coaxial multi-layer HTS transmission cable ;Current distribution ;Magnetic field distribution ;. [Online]. Available : http://dx.doi.org/10.1109/TASC.2005.864319

[41] H. Noji, "Numerical analysis of the ac losses of 500-m hts power cable in super-ace project," *Cryogenics*, vol. 47, no. 2, pp. 94 – 100, 2007, alternating current loss ;Axial field ;Electric-circuit model ;Ohmic loss ;. [Online]. Available : http://dx.doi.org/10.1016/j.cryogenics.2006.09.009

[42] H. Noji, K. Ikeda, K. Uto, and T. Hamada, "Calculation of the total ac loss of high-tc superconducting transmission cable," *Physica C : Superconductivity and its Applications*, vol. 445-448, no. 1-2, pp. 1066 – 1068, 2006.

[43] L. Rostila, J. Lehtonen, M. Masti, and R. Mikkonen, "Circuit analysis model for ac losses of superconducting ybco cable," *Cryogenics*, vol. 46, no. 4, pp. 245 – 251, 2006. [Online]. Available : http://dx.doi.org/10.1016/j.cryogenics.2005.07.006

[44] R. Inada, Y. Nakamura, and A. Oota, "Evaluation of ac losses in cable conductors using thin superconducting tapes with non-uniform jc distribution," *Physica C : Superconductivity and its Applications*, vol. 442, no. 2, pp. 139 – 144, 2006. [Online]. Available : http://dx.doi.org/10.1016/j.physc.2006.04.099

[45] J. Lee and G. Cha, "Ac loss calculation of a multi-layer hts transmission cable considering the twist of each layer," vol. 11, no. 1 II, 2001, pp. 2433 – 2436, alternating current loss ;Current sharing ;Superconducting transmission cable ;. [Online]. Available : http://dx.doi.org/10.1109/77.920354

[46] T. Fukunaga, R. Inada, and A. Oota, "Current distributions and ac losses in self-fields for superconductor tapes and cables," *IEEE Transactions on Applied Superconductivity*, vol. 9, no. 2 I, pp. 1057 – 1060, 1999, alternating current losses ;Superconductor tapes ;. [Online]. Available : http://dx.doi.org/10.1109/77.783479

[47] M. Daumling, "Electromagnetic behavior and ac loss in a multi-layer superconducting power cable," *Cryogenics*, vol. 41, no. 2, pp. 111 – 115, 2001, decay constants ;. [Online]. Available : http://dx.doi.org/10.1016/S0011-2275(01)00056-X

[48] L. Rostila, S. Suuriniemi, J. Lehtonen, and G. Grasso, "Numerical minimization of ac losses in coaxial coated conductor cables," *Physica C : Superconductivity and its Applications*, vol. 470, no. 3, pp. 212 – 217, 2010.

[49] N. Amemiya and M. Nakahata, "Numerical study on ac loss characteristics of superconducting power transmission cables comprising coated conductors with magnetic substrates," *Physica C : Superconductivity and its Applications*, vol. 463-465, no. SUPPL., pp. 775 – 780, 2007. [Online]. Available : http://dx.doi.org/10.1016/j.physc.2007.04.265

[50] M. Nakahata and N. Amemiya, "Electromagnetic field analyses of two-layer power transmission cables consisting of coated conductors with magnetic and non-magnetic substrates and ac losses in their superconductor layers," *Superconductor Science and Technology*, vol. 21, no. 1, 2008. [Online]. Available : http://dx.doi.org/10.1088/0953-2048/21/01/015007

[51] Z. Jiang, N. Amemiya, and M. Nakahata, "Numerical calculation of ac losses in multi-layer superconducting cables composed of coated conductors," *Superconductor Science and Technology*, vol. 21, no. 2, 2008. [Online]. Available : http://dx.doi.org/10.1088/0953-2048/21/2/025013

[52] M. Nakahata and N. Amemiya, "Electromagnetic field analyses of two-layer power transmission cables consisting of coated conductors with magnetic and non-magnetic substrates and ac losses in their superconductor layers," *Superconductor Science and Technology*, vol. 21, no. 1, 2008, electromagnetic field analysis ;Magnetic substrates ;Nonmagnetic substrates ;. [Online]. Available : http://dx.doi.org/10.1088/ 0953-2048/21/01/015007

[53] F. Grilli, "Numerical modelling of high temperature superconducting tapes and cables," Ph.D. dissertation, École Polytechnique Fédérale de Lausanne, Jun. 2004.

[54] S. Kim, K. Sim, J. Cho, H.-M. Jang, and M. Park, "Ac loss analysis of hts power cable with rabits coated conductor," vol. 20, no. 3, 445 Hoes Lane / P.O. Box 1331, Piscataway, NJ 08855-1331, United States, 2010, pp. 2130 – 2133. [Online]. Available : http://dx.doi.org/10.1109/TASC.2010.2041439

[55] S. Mezani, B. Douine, and J. A. Leveque, "Finite element ac-losses computation in multi-layer hts cable using complex representation of the electromagnetic field," vol. 19, no. 3, 2009, pp. 3348 – 3351.

[56] F. Grilli, R. Brambilla, and L. Martini, "Modeling high-temperature superconducting tapes by means of edge finite elements," vol. 17, no. 2, 2007, pp. 3155 – 3158. [Online]. Available : http://dx.doi.org/10.1109/TASC.2007.902144

[57] R. Brambilla, F. Grilli, and L. Martini, "Development of an edge-element model for ac loss computation of high-temperature superconductors," *Superconductor Science and Technology*, vol. 20, no. 1, pp. 16 – 24, 2007. [Online]. Available : http://dx.doi.org/10.1088/0953-2048/20/1/004

[58] Z. Hong and T. Coombs, "Numerical modelling of ac loss in coated conductors by finite element software using h formulation," *Journal of Superconductivity and Novel Magnetism*, vol. 23, no. 8, pp. 1551 – 1562, 2010, aC loss ;Coated conductors ;Critical state ;Finite element modelling ;H formulation ;. [Online]. Available : http://dx.doi.org/10.1007/s10948-010-0812-y

[59] A. Stenvall and T. Tarhasaari, "Programming finite element method based hysteresis loss computation software using non-linear superconductor resistivity and t - formulation," *Superconductor Science Technology*, vol. 23, no. 7, pp. 075 010 (9 pp.) –, 2010/07/. [Online]. Available : http://dx.doi.org/10.1088/0953-2048/23/7/075010

[60] D. N. Nguyen, S. P. Ashworth, J. O. Willis, F. Sirois, and F. Grilli, "A new finite-element method simulation model for computing ac loss in roll assisted biaxially textured substrate ybco tapes," *Superconductor Science and Technology*, vol. 23, no. 2, 2010.

[61] S. Sato and N. Amemiya, "Electromagnetic field analysis of ybco coated conductors in multi-layer hts cables," vol. 16, no. 2, 2006, pp. 127 – 130, aC losses;Electromagnetic analysis;HTS cables;Multilayer high Tc superconducting (HTS) cables;. [Online]. Available : http://dx.doi.org/10.1109/TASC.2006.870813

[62] S. Honjo, N. Hobara, Y. Takahashi, H. Hashimoto, K. Narita, and T. Yamada, "Efficient finite element analysis of electromagnetic properties in multi-layer superconducting power cables," vol. 13, no. 2, USA, 2003/06/, pp. 1894 – 7. [Online]. Available : http://dx.doi.org/10.1109/TASC.2003.812937

[63] E. H. Brandt, "Superconductors of finite thickness in a perpendicular magnetic field : Strips and slabs," *Physical Review B : Condensed Matter*, vol. 54, no. 6/PT2, pp. 4246 – 4246, 1996. [Online]. Available : http://dx.doi.org/10.1103/PhysRevB.54.4246

[64] F. Sirois, F. Roy, and B. Dutoit, "Assessment of the computational performances of the semi-analytical method (sam) for computing 2-d current distributions in superconductors," vol. 19, no. 3, 2009, pp. 3600 – 3604. [Online]. Available : http://dx.doi.org/10.1109/TASC.2009.2019582

[65] S. Fukui, R. Kojima, J. Ogawa, M. Yamaguchi, T. Sato, and O. Tsukamoto, "Numerical analysis of ac loss characteristics of cable conductor assembled by hts tapes in polygonal arrangement," vol. 16, no. 2, 2006, pp. 143 – 146. [Online]. Available : http://dx.doi.org/10.1109/TASC.2006.870818

[66] T. Tominaka, "Current and field distributions of a superconducting power transmission cable composed of helical tape conductors," *Superconductor Science and Technology*, vol. 22, no. 12, 2009. [Online]. Available : http://dx.doi.org/10.1088/0953-2048/22/12/125025

[67] E. Pardo, F. Gomory, J. ouc, and J. Ceballos, "Current distribution and ac loss for a superconducting rectangular strip with in-phase alternating current and applied field," *Superconductor Science and Technology*, vol. 20, no. 4, pp. 351 – 364, 2007, alternating current;Current distribution;Finite thickness;Fitting parameters;Superconducting rectangular strip;. [Online]. Available : http://dx.doi.org/10.1088/0953-2048/20/4/009

[68] E. Pardo, "Modeling of coated conductor pancake coils with a large number of turns," *Superconductor Science and Technology*, vol. 21, no. 6, 2008, coated conductor pancake coils;Critical state models;Longitudinal striation;Magnetic interaction;. [Online]. Available : http://dx.doi.org/10.1088/0953-2048/21/6/065014

[69] C. T. Reis and WALKER, "Low alternating current (ac) loss superconducting cable," Patent US WO200 227 735-A, 04 4, 2002. [Online]. Available : http://www.freepatentsonline.com/7109425.html

[70] M. Siahrang, F. Sirois, D. N. Nguyen, S. Babic, and S. P. Ashworth, "Fast numerical computation of current distribution and ac losses in helically wound thin tape conductors : Single-layer coaxial arrangement," *IEEE Transactions on Applied Superconductivity*, vol. 20, no. 6, pp. 2381 – 2389, 2010. [Online]. Available : http://dx.doi.org/10.1109/TASC.2010.2078813

[71] M. Siahrang, F. Sirois, F. Grilli, S. Babic, and S. Brault, "A new numerical approach to find current distribution and ac losses in coaxial assembly of twisted hts tapes in single layer arrangement," vol. 234, no. PART 2, Dresden, Germany, 2010. [Online]. Available : http://dx.doi.org/10.1088/1742-6596/234/2/022034

[72] M. Siahrang and F. Sirois, "Reduction of ac losses in hts power transmission cables made of coated conductors by overlapping the tapes," *Superconductor Science and Technology*, vol. 24, no. 1, 2011. [Online]. Available : http://dx.doi.org/10.1088/0953-2048/24/1/015004

[73] M. Siahrang, F. Sirois, D. N. Nguyen, and S. P. Ashworth, "Assessment of alternative design schemes to reduce the edge losses in hts power transmission cables made of coated conductors," *Accepted to be published in a focus issue on superconducting power systems Superconductor Science and Technology.*

[74] S. Fukui, T. Noguchi, J. Ogawa, M. Yamaguchi, T. Sato, and O. Tsukamoto, "Analysis of ac loss and current distribution in multi-layer tri-axial three-phase hts cable," *Physica C : Superconductivity and its Applications*, vol. 426-431, no. II, pp. 1374 – 1379, 2005. [Online]. Available : http://dx.doi.org/10.1016/j.physc.2005.03.055

[75] ——, "Analysis of ac loss and current distribution characteristics of multi-layer triaxial hts cable for 3-phase ac power transmission," *IEEE Transactions on Applied Superconductivity*, vol. 16, no. 2, pp. 135 – 138, 2006. [Online]. Available : http://dx.doi.org/10.1109/TASC.2006.870817

[76] F. Sirois and F. Roy, "Computation of 2-d current distribution in superconductors of arbitrary shapes using a new semi-analytical method," *IEEE Transactions on Applied Superconductivity*, vol. 17, no. 3, pp. 3836 – 3845, 2007. [Online]. Available : http://dx.doi.org/10.1109/TASC.2007.902117

[77] *The Mathworks inc. http ://www.mathworks.com.f.*

[78] L. Petzold, "A description of dassl : a differential/algebraic system solve," 1982, pp. 430 – 432.

[79] S. C. K. Brenan and L. Petzold, *Numerical Solution of Initial-Value Problems in Differential-Algebraic Equations.* Ney-York, N.Y. : Elsevier, 1989.

[80] *SUite of Nonlinear and DIfferential/ALgebraic equation Solvers (SUNDIALS) https ://computation.llnl.gov/casc/sundials.*

[81] L. Urankar, "Vector potential and magnetic field of current-carrying finite arc segment in analytical form. ii. thin sheet approximation," *IEEE Transactions on Magnetics*, vol. MAG-18, no. 3, pp. 911 – 17, 1982/05/.

[82] D. N. Nguyen, F. Grilli, S. P. Ashworth, and J. O. Willis, "Ac loss study of antiparallel connected ybco coated conductors," *Superconductor Science and Technology*, vol. 22, no. 5, 2009. [Online]. Available : http://dx.doi.org/10.1088/0953-2048/22/5/055014

[83] F. Roy, B. Dutoit, F. Grilli, and F. Sirois, "Magneto-thermal modeling of second-generation hts for resistive fault current limiter design purposes," *IEEE Transactions on Applied Superconductivity*, vol. 18, no. 1, pp. 29 – 35, 2008. [Online]. Available : http://dx.doi.org/10.1109/TASC.2008.917576

[84] J. Clem and A. Malozemoff, "Theory of ac loss in power transmission cables with second generation high temperature superconductor wires," *Superconductor Science and Technology*, vol. 23, no. 3, 2010. [Online]. Available : http: //dx.doi.org/10.1088/0953-2048/23/3/034014

[85] F. Grilli, F. Sirois, S. Brault, R. Brambilla, L. Martini, D. N. Nguyen, and W. Goldacker, "Edge and top/bottom losses in non-inductive coated conductor coils with small separation between tapes," *Superconductor Science and Technology*, vol. 23, no. 3, 2010. [Online]. Available : http://dx.doi.org/10.1088/0953-2048/23/3/034017

[86] *Archie Campbell, pers. comm. May 2010.*

[87] J. Clem, "Flux-line-cutting losses type-ii superconductors," *Physical Review B (Condensed Matter)*, vol. 26, no. 5, pp. 2463 – 73, 1 Sept. 1982. [Online]. Available : http://dx.doi.org/10.1103/PhysRevB.26.2463

APPENDIX A

Derivation of equation (4.3)

Referring to figure 4.1, we can define a tangential vector to the helical trajectory $\vec{c}$ of the tape as follows :

$$\mathrm{d}\vec{\ell} = \frac{\mathrm{d}\vec{\mathbf{c}}}{\mathrm{d}u}\,\mathrm{d}u = [-2\pi R\sin(2\pi u\,\hat{\mathbf{x}} + 2\pi R\cos(2\pi u)\,\hat{\mathbf{y}} + L\,\hat{\mathbf{z}}]\,\mathrm{d}u\,,$$

where $\vec{\mathbf{c}}$, u, R and L are defined in (4.1) and the paragraph below, and where ϕ_0 has been set to 0 to shorten the expressions. From $\mathrm{d}\vec{\ell}$, we define a unit vector $\hat{\mathbf{u}}$ that is tangential to $\vec{\mathbf{c}}$, i.e. $\hat{\mathbf{u}} = \mathrm{d}\vec{\ell}/|\mathrm{d}\vec{\ell}|$, where $|\mathrm{d}\vec{\ell}| \equiv \ell = \sqrt{(2\pi R)^2 + L^2}$ (ℓ is actually the length of tape required to wind a full pitch). We therefore obtain

$$\hat{\mathbf{u}} = \frac{2\pi R}{\ell}\left[-\sin\left(2\pi u\right)\hat{\mathbf{x}} + \cos\left(2\pi u\right)\hat{\mathbf{y}} + \frac{L}{2\pi R}\,\hat{\mathbf{z}}\right]. \qquad (\mathrm{A.1})$$

We can also define a unit vector $\hat{\mathbf{n}}$ normal to the face of the strip as

$$\hat{\mathbf{n}} = \cos\left(2\pi u\right)\hat{\mathbf{x}} + \sin\left(2\pi u\right)\hat{\mathbf{y}}\,, \qquad (\mathrm{A.2})$$

which allows us to define a third unit vector, i.e. $\hat{\mathbf{v}}$, that is parallel to the cross-section of the strip, i.e. $\hat{\mathbf{v}} = \hat{\mathbf{n}} \times \hat{\mathbf{u}}$. After some algebra, we obtain

$$\hat{\mathbf{v}} = \frac{L}{\ell}\left[\sin\left(2\pi u\right)\hat{\mathbf{x}} - \cos\left(2\pi u\right)\hat{\mathbf{y}} + \frac{2\pi R}{L}\,\hat{\mathbf{z}}\right]. \qquad (\mathrm{A.3})$$

Assuming that the tape surface is not curved (which is strictly true only if its width tends towards 0, but almost true when we considered narrow sections, such as in the discretized problem), the $\hat{\mathbf{u}}$ and $\hat{\mathbf{v}}$ vectors allow us to parameterize the strip surface in a 3-D space. Let's denote as $\vec{\mathbf{r}}'$ any point belonging to the strip surface. According to the above notation, we can write

$$\vec{\mathbf{r}}' = \vec{\mathbf{c}}(u) + a\,v\,\hat{\mathbf{v}}\,, \qquad (\mathrm{A.4})$$

where a is the strip half-width, and u and v are the parameters defining the strip surface. As written above, one must have $-1 \leq v \leq 1$. In the case of u, its value is proportional to the number of twist pitches (n_p) of the tape.

Let's consider $\vec{\mathbf{r}} = (x, y, z)$ as the observation point at which we want to evaluate the

vector potential $\vec{\mathbf{A}}(\vec{\mathbf{r}})$, and let's use the potential version of the Biot-Savart law, i.e.

$$\vec{\mathbf{A}}(\vec{\mathbf{r}}) = \frac{\mu_0}{4\pi} \int_{\Omega} \frac{\vec{\mathbf{j}}}{|\vec{\mathbf{r}} - \vec{\mathbf{r}}'|} \, \mathrm{d}\Omega \,, \tag{A.5}$$

in which $\vec{\mathbf{j}} = j \, \hat{\mathbf{u}}$, and $\mathrm{d}\Omega = (\ell \, \mathrm{d}u)(a \, \mathrm{d}v)$. After some algebra, we can express $|\vec{\mathbf{r}} - \vec{\mathbf{r}}'|$ as

$$|\vec{\mathbf{r}} - \vec{\mathbf{r}}'| = \sqrt{d_x^2 + d_y^2 + d_z^2} \,, \tag{A.6}$$

where d_x, d_y and d_z were defined in (4.4). After inserting the above developments in (A.5), we obtain

$$\vec{\mathbf{A}}(x, y, z) = \frac{\mu_0 a \ell j}{4\pi} \int_{-n_p/2}^{n_p/2} \mathrm{d}u \, \hat{\mathbf{u}} \int_{-1}^{1} \frac{\mathrm{d}v}{\sqrt{d_x^2 + d_y^2 + d_z^2}} \,, \tag{A.7}$$

which is the final form of equation (4.3).

APPENDIX B

Analytic expressions relating $\vec{B}$ and $\vec{J}$ for rectangular strips

Using the analytic expressions developed in [81], the components of the flux density generated by a rectangular sheet current as that shown in figure 4.3 at any observation point $\vec{r} = (x, y, z)$ of the local system of coordinates can be evaluated, i.e.,

$$
B_x = \frac{\mu_0 j}{4\pi} \sum_{i=1}^{2} \sum_{j=1}^{2} (-1)^{i+j+1} \arctan\left(\frac{\gamma_i \lambda_j}{y \, r_{ij}}\right),
$$

$$
B_y = \frac{\mu_0 j}{4\pi} \sum_{i=1}^{2} \sum_{j=1}^{2} (-1)^{i+j} \sinh^{-1}\left(\frac{\lambda_j}{\alpha_i}\right), \tag{B.1}
$$

where

$$
\gamma_{1,2} = \mp\frac{w}{2} - x,
$$

$$
\lambda_{1,2} = \mp\frac{h}{2} - z,
$$

$$
r_{ij} = \sqrt{\gamma_i^2 + y^2 + \lambda_j^2},
$$

$$
\alpha_i = \sqrt{\gamma_i^2 + y^2}. \tag{B.2}
$$

The arctan function should be bounded between $-\pi/2$ and $\pi/2$, so the classical "atan" function of *Matlab* can be used without any concern.

APPENDIX C

A new numerical approach to find current distribution and AC losses in coaxial assembly of twisted HTS tapes in single layer arrangement

A new numerical approach to find current distribution and AC losses in coaxial assembly of twisted HTS tapes in single layer arrangement

Majid Siahrang[1], Frédéric Sirois[1], Francesco Grilli[2], Slobodan Babic[1] and Simon Brault[1]

[1] École Polytechnique de Montréal, Montréal, QC, H3C 3A7, Canada

[2] Forschungszentrum Karlsruhe GmbH, Hermann-von-Helmholtz-Platz 1, D-76344 Eggenstein-Leopoldshafen, Germany

E-mail: `majid.siahrang@polymtl.ca`

Abstract. This paper presents a novel technique for evaluating AC losses and current distribution in single layer assemblies of coaxially wound thin conductors, such as YBCO coated conductors. The proposed approach takes into account the twisted geometry of the individual superconducting tapes by considering the integral relation between the magnetic vector potential and the current density in the tapes (Biot-Savart formula). The integrals are solved numerically and semi-analytically, and the results are used to generate a discretized system of equations based on the magnetic flux diffusion equation (eddy current problem). The latter is solved using an efficient time transient solver (DASPK). It is assumed that, due to the helical symmetry of the problem, it is sufficient to solve for the current distribution in half of a single tape cross-section, even if many tapes are present, which allows a drastic reduction of the 3-D problem to a simple 1-D domain. The method was used to evaluate the AC losses of a HTS cable made of coated conductors, and it was observed that for a given radius of the former and number of tapes, twisted tapes with smaller pitch have lower AC losses.

1. Introduction

Numerical computation of AC losses is an important technical issue for commercial application of second generation high-temperature superconductor (HTS) cables and it has been the subject of numerous research works in the area of applied superconductivity. In addition to the strongly nonlinear resistivity inherent to HTS materials, the complex geometry of the cable (involving twisted tapes with very high aspect ratio assembled in multi-layer arrangement) adds more difficulties to the accurate computation of AC losses [1].

In order to make the problem easier to solve, the numerical techniques used to investigate the behavior of HTS cables usually do not take into account the real geometry. Several 2D methods neglecting the twisted configuration have been proposed for computing AC losses in HTS cables [1-4]. While providing useful information on the AC losses, these methods cannot be used for designing purposes, where finding the optimal twist design is an important issue.

---

[1] The paper investigates the behavior of coated conductor HTS cables. For sake of simplicity, in the paper we use the term "HTS cable" to refer to cables made of coated conductor

Other methods simulating the cable as a HTS cylinder and using an anisotropic conductivity to take the twist into account have been developed, both with FEM (finite-element method) and non-FEM techniques [5, 6]. Although the twisted geometry is considered by these methods, the tape-to-tape gaps in each layer are omitted; it has been reported that this approximation leads to an underestimation of the AC losses [5].

In this paper, we propose a new and efficient technique for computing AC losses and current distribution in HTS cables. The technique is based on the formulation of the eddy current equation, it uses the integral relationship between current density and vector potential, and can directly take into account twisted geometries.

The paper is organized as follows. Firstly, we describe the mathematical formulation of the method; secondly, we compare the results with those obtained with a FEM model for the case of straight tapes; then we apply the method to the case of single-layer HTS cable with twisted tapes and we discuss the influence of the twist pitch on the current distribution and AC losses; finally, we summarize our results in the conclusion.

2. Numerical Method

The model proposed in this paper, which we call IM (Integral Method) hereafter, is based on the solution of eddy current equations discretized over a proper study domain in a 2D cross section of the cable. With this formulation, the state variable, current density J is related to the magnetic vector potential A by means of Biot-Savart law. Due to the use of this integral relation and the absence of any magnetic material, the study domain of the problem is confined to the current carrying superconducting layer of the tapes. This drastically decreases the number of degrees of freedom (DOF) of the problem compared to FEM simulations, where the area surrounding the tapes has to be considered and meshed. As a consequence, our method is more efficient in terms of memory requirements and computation time than classical FEM methods.

For sufficiently long cables, due to the symmetry of the helically wound tapes, knowing the current distribution over any 2D cross section of the cable is sufficient to accurately determine the AC losses. In addition, if the tapes are assembled in a symmetrical arrangement around the circumference of the former cylinder (as is the case of HTS cables), the study domain can be reduced to half of one tape. Finally, due to the high aspect ratio of the superconducting layer of the YBCO tapes, the study domain can be even more reduced and assimilated to a 1D straight line. These study domain reduction steps, from the real 3D geometry to a straight discretized line are shown in figure 1.

Once the study domain is established in the form of finite interconnected straight lines (figure 1d), the eddy current equation is formulated for each element i as $E_i = -\partial A_i/\partial t - \nabla V$, where E and A are the electric field and the magnetic vector potential, respectively. ∇V represents the potential gradient, which is constant over the tape cross-section. Using $E = \rho J$ as constitutive equation, the electric field is substituted with a function of the current density. In the case of HTS tapes, the power-law model $\rho = E_c/J_c|J/J_c|^{n-1}$ was used to define the nonlinear resistivity of the HTS material. Based on the symmetry arguments specific to this kind of geometry, it is intuitive that the current flowing inside the tapes can not deviate from the helical path along which the tapes are wound. Therefore, the current density (which is assumed to be constant within each elements) is aligned with the helical trajectory of the tapes. The relation between J and A is addressed by introducing an k by k matrix as $[A]_{k \times 1} = [M]_{k \times k}[J]_{k \times 1}$, where k is the number of discretized elements, which determines number of DOFs of the problem.

Although the governing equation of the problem is formulated over a reduced 1D study domain, the exact 3D twisted geometry of each individual tape is taken into account to establish the M matrix. Each entry of M is obtained from the solution of the 3D Biot-Savart potential integral applied to helically wound strips. The width of each elementary strip is $2 \times k$ times smaller than the width of an individual tape and carries a sheet current density of 1 A/m.
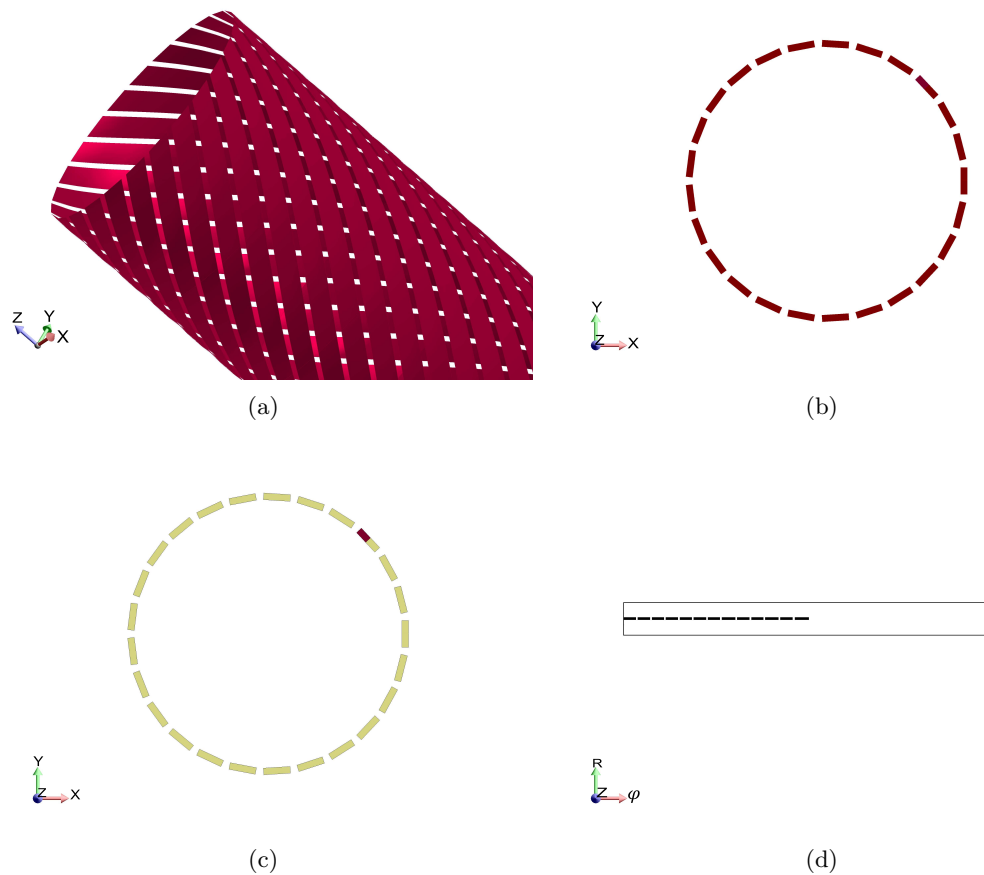
Figure 1. Successive reduction of study domain in the proposed hypothesis (tapes dimensions not drawn to scale). (a) Real 3D geometry, (b) 2D cross-section of the tapes, (c) Reduction of study domain to half of a tape, (d) Final study domain in the form of discretized interconnected 1D strips (straight lines) along half width of one tape.

As mentioned earlier, the magnetic solution for A is obtained by solving the Biot-Savart integral. Like all Biot-Savart type integrations, the denominator of the integrand tends towards zero when both the source and field points are the same or are located very close to each other. This will lead to inaccurate results at these singular or near singular points if using direct numerical integration. Since computation of A in these singular points will determine the diagonal entries of the M matrix, this inaccuracy is not acceptable here.

In order to get rid of the singularity problem, we proposed an alternative semi-analytic solution to solve the Biot-Savart integration for helically wound tapes. In this approach each tape is discretized along its longitudinal helical path while being discretized along its width. Then each obtained element is approximated with a rectangular infinitely thin sheet. In other words, each tape is approximated by a series of tiny interconnected rectangular elements. Thanks to the indefinite integration tools of the *Mathematica* software, the analytical solution of the Biot-Savart integral for such a rectangular element can easily be obtained. In the semi-analytic approach, this analytical solution will be used to find A at desired observation points by superposition of the contribution of all the elements. Since an analytic expression is used as the kernel of this method, therefore no singularities will be encountered even if the observation points are located within the tapes.

Figure 2. A twisted tape constructed by interconnecting many finite rectangular elements.

To set up the M matrix, a combination of both numerical integration and this semi-analytic approach was used. The semi-analytic method, which is more accurate at singular or near singular points, is used to consider the contribution of the parts of the tapes that are close to the observation points. An adaptive numerical integration, which is faster, was employed to model the remaining portion of the tapes. To model a long cable, this integration has to be done over a long enough length of the tapes. More details about both of these methods will be provided in a forthcoming publication.

Once the governing equations of the problem are formulated in their discretized version, an adaptive time transient solver with a sophisticated error estimator is used to solve it. One of these algorithms, called DASPK was already used in our previous works [7, 8], and is used here to solve the obtained system of differential algebraic equations(DAE). Finally, after $J(t)$ is known in all the elements, AC losses are computed using the following formula

$$Q = 2fN \times \int \rho J^2 dl \tag{1}$$

where N denotes the number of tapes and f is the frequency of the transport current. This integration has to be carried out over the length of the study domain (half width of one tape).

3. Validation methodology

Since at the present time we do not have access to experimental loss data for a single-layer HTS cable, nor have we developed a fully 3D FEM model for twisted tapes, we limited the validation of our model to the case of straight tapes. Therefore, in particular, we performed a 2D FEM simulation and computed the current distribution and the AC losses in an infinitely long cable with a former radius of 12.62 mm and composed of 16 straight tapes. For the FEM simulations, we used the edge-element model described in [9]. The tape parameters are listed in table 1. In the FEM simulations, a thickness of 5 μm (instead of 1 μm) was used, in order to keep the number of DOFs at an acceptable level.

The transport current is 70% of the critical current and the frequency is 50 Hz. Considering a large value for pitch length, we launched the IM model to solve the same problem. The meshed FEM study domain is shown in figure 2. The number of DOFs in FEM simulation was 122935, against 50 only with the IM. As mentioned earlier, the large number of DOFs in the FEM model comes from the necessity of meshing a tape with a very high aspect ratio as well as the surrounding air region.

Table 1. Cable and tape properties.

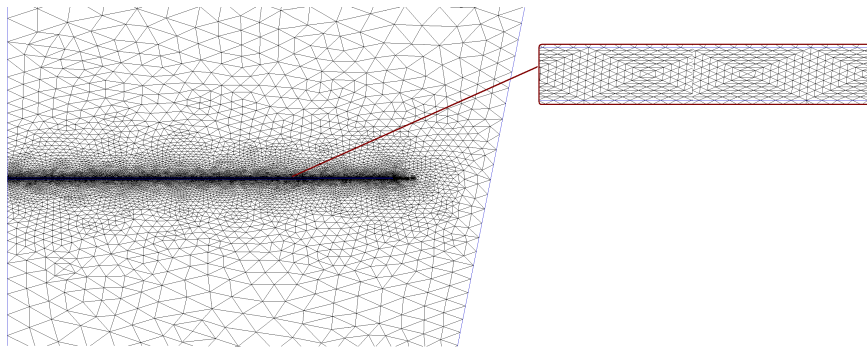|	
Tape width	4 mm
Tape thickness	1 μm
Former radius	12.7 mm
N (number of tapes	1 to 16
J_c	10^{10} A/m^2
n (power-law index)	25
Frequency	50 Hz

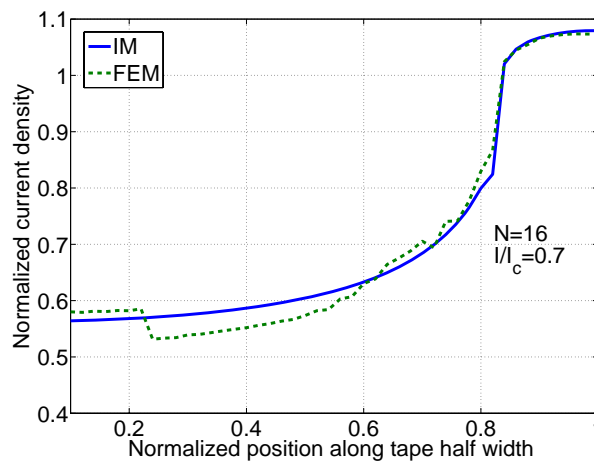**Figure 3.** Meshed study domain in FEM simulation.

Figure 4. Current density distribution along the tape width for a transport current amplitude of $0.7I_c$ and N=16 straight tapes, computed with IM and FEM.

The AC loss value computed by IM model is just 2.5% smaller than that computed by FEM. Also the computed current density distributions are very similar, as displayed in figure 4. Note that FEM simulation took more than 3 days to be solved while overall computation time of IM (included the M matrix generation) was less than an hour.

In addition, we applied the IM model to find the current distribution inside the tape in one of the cases simulated in [3] (N=8 and tape width=10 mm), and we got exactly the same results (not shown here).

4. Application of the IM to analysis of single layer twisted tapes

Since the twisted geometry of each individual tape is taken into account in the integral method proposed here, it can be applied to precisely determine the electrical performance of a single-layer arrangement of coaxially wound twisted tapes. Many geometrical parameters can be varied: in our simulations we kept the former radius fixed (12.7 mm), and we varied the number of tapes and the pitch length.

For different pitch lengths figure 5 presents the computed AC losses in each constituting tape per unit length of the cable as a function of N for a transport current equal to 70% of I_c. As expected, the AC losses decrease as the number of tapes increases. This is due to the fact that when the number of tapes increases the gap between the tapes decreases and for smaller gaps each tape experiences a magnetic field which is predominantly parallel to its width, whereas the perpendicular component near its edges tends to be smaller. The same observation has been reported in previous studies [2, 3].
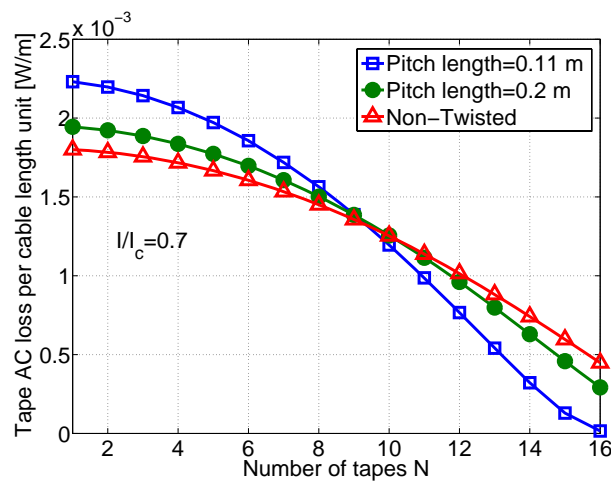
Figure 5. AC losses of a tape per cable length unit as a function of the number of tapes for different pitch lengths.
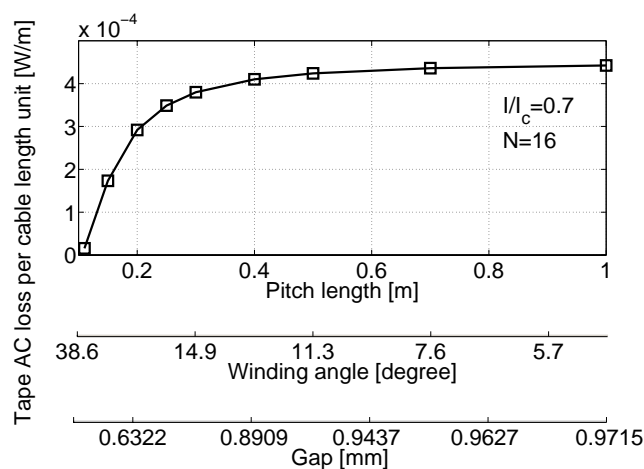
Figure 6. AC losses of a tape per cable length unit as a function of the twist pitch length.
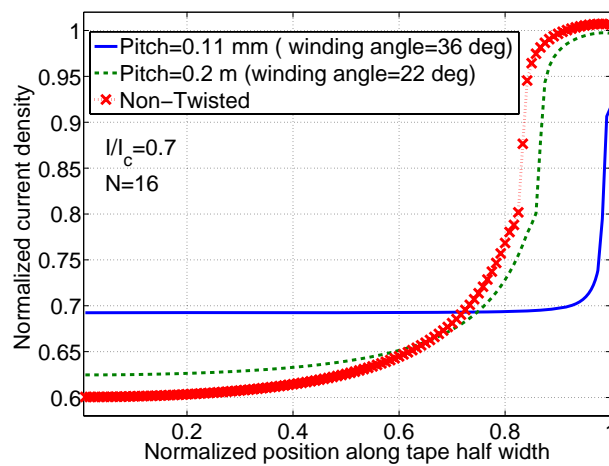
Figure 7. Current density distribution along the tape width for different twist pitch lengths.
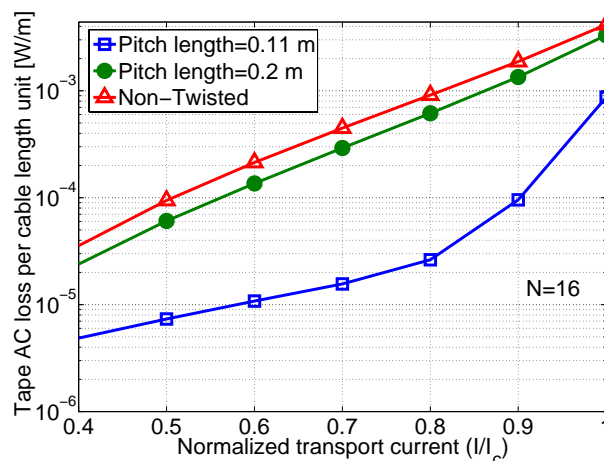

Figure 8. AC losses of a tape per cable length unit as a function of the transport current for different twist pitch lengths.

Since the former radius is fixed, for a given number of tapes N a smaller pitch length (i.e. a larger winding angle) results in a smaller tape-to-tape gap, which tends to reduce the losses, as discussed above. On the other hand, however, a smaller pitch length implies a longer tape per cable length unit, which ultimately results in higher losses. With figure 5 as reference, the following is observed:

- For N smaller than 9 tapes the tape-to-tape gap is large, so that the cancellation of most of the perpendicular field component at the tape's edge is not very effective; in this case the effect of a longer tape per cable length unit is dominant and the shorter the pitch length the higher the losses.

- For N greater than 9 tapes the tape-to-tape gap is small, the cancellation of the perpendicular field component is more effective and the consequent AC loss reduction is more important; in this case the shorter the pitch length the smaller the losses, because the loss reduction caused by placing the tapes closer to each other is more significant than the

7

loss increase caused by using a shorter pitch length.

Figure 6 shows the losses as a function of the pitch length for N=16 and I/I_c=0.7. It can be observed that as the pitch length decreases from 1 m the AC losses first decrease slowly, then more rapidly, when the tape-to-tape gaps tend to close more rapidly.

From the discussion carried out so far one can expect less current penetration inside the tapes wound with a smaller pitches. This is confirmed by figure 7, which shows (always for the case N=16 and I/I_c=0.7) the current density distribution (normalized to J_c) along the tape's width for different pitch lengths. Also current in twisted tapes tends to be more uniformly distributed inside the tapes and maximum of current density at the sides of the tapes decrease as the pitch decreases.

Figure 8 shows the AC losses as a function of the normalized transport current for three different pitch lengths. The figure extends the results mentioned above to different values of the transport currents. In addition, it can be observed that twisted tapes can transport higher current with lower losses than straight tapes. For example, the AC loss of a twisted tape with pitch length equal to 0.11 m at I/I_c=0.9 is still smaller than the loss in a straight tape at I/I_c=0.5.

5. Conclusion
A new numerical technique to solve the electromagnetic problem of a single-layer coaxial assembly of twisted thin conductors was presented in this paper. The non-linear resistivity of HTS materials can be easily inserted and it can be used to compute the electrical performance of a single-layer HTS cable made of YBCO twisted tapes. After having been tested against a FEM model for straight tapes, the proposed method was applied to find the current density distribution and the AC losses of single-layer HTS cable with different twist pitch length. Among the simulation results it was observed that, for a fixed former radius and a given number of tapes, tapes twisted with smaller pitches shows lower AC losses per cable length unit. This happens in spite of the longer effective length of the superconductor, because the suppression of the perpendicular field component caused by packing the tapes more closely is the dominant effect. The method can be extended to the case of multi-layer cables. This extension as well as the verification of the results with 3D FEM and experimental results will be the subject of a forthcoming publication.

References
[1] Nakahata M and Amemiya N 2008 *Supercond. Sci. Techn.* **21** 015007
[2] Jiang Z, Amemiya N, and Nakahata M 2008 *Supercond. Sci. Techn.* **21** 025013
[3] Fukui S *et al* 2006 *IEEE Trans. Appl. Supercond.* **16** 143-146
[4] Fukui S *et al* 2009 *IEEE Trans. Appl. Supercond.* **19** 1714-1717
[5] Honjo S *et al* 2003 *IEEE Trans. Appl. Supercond.* **13** 1894-1897
[6] Fukui S *et al* 2006 *IEEE Trans. Appl. Supercond.* **16** 135-138
[7] Sirois F and Roy F 2007 *IEEE Trans. Appl. Supercond.* **17** 3836-45
[8] Sirois F, Roy F, and Dutoit B 2009 *IEEE Trans. Appl. Supercond.* **19** 3600-3604
[9] Brambilla R, Grilli F and Martini L 2007 *Supercond. Sci. Techn.* **20** 16-24